Università degli Studi di Napoli "Federico II"

Facoltà di Ingegneria

Dipartimento di Ingegneria Chimica, dei Materiali e della Produzione Industriale

PhD in

Industrial Product and Engineering

XXXII cycle

Intrinsic Self-healing Thermoset: from design to industrial applications

Stefania Dello Iacono

Tutor: Prof. Giuseppe Mensitieri

PhD Coordinator: Prof. Giuseppe Mensitieri

Co-Tutor: Dr. Eugenio Amendola

2020

Abstract

The development of self-healing materials is a very attractive approach to provide long-lasting and efficient protection against micro damages. Great attention from numerous research groups has been paid to polymers, composites, and coatings, which exhibit self-healing behavior at different dimensional scales.

Through this thesis, the overall design flow for achieving hybrid epoxy systems containing covalent thermo-reversible bonds and the preparation and evaluation of selected examples is detailed. This work underlines that the concurring presence of thermo-reversible covalent bonds and high molecular mobility are essential requirements to develop self-healing systems.

The most effective structural modification has been pursued by adjustment of the several features: average functionality of reacting precursor mixture and cross-linking density and thermosetting network and concentration of self-healing reversible bonds. Several Diels-Alder adducts have been synthesized and introduced in hybrid architecture systems, where stable bonds and thermoreversible bonds coexist.

The resin formulation aimed at reaching a compromise between the mending capability of cured material and its dimensional stability at high temperatures, required during healing cycles. The Self-Healing ability were assessed by means of morphological, mechanical and spectroscopic characterization.

The multiple healing feature of the system was proved: the hybrid epoxy resin was able to recover damages, still exhibiting the pristine stiffness.

Satisfactory morphological and mechanical recovery results suggested that synthetic thermoreversible epoxy can envisage a new route in development of maintenance and repair strategies of structural and semi-structural components during their operative life. Furthermore, the availability of dynamic epoxies has allowed the development of smart materials, such as protective coating and re-engineered FRP. Finally, a more comprehensive approach was proposed for fiber-reinforced composites: the development and integration of an active interface, able to recover adhesive damage.

Table of Contents

List of Figures

1. Self-healing phenomenology in polymers

Synthetic polymers are lightweight structural materials that have revolutionized many industries, including transportation, aviation, and biomedicine. Traditionally, the main goal of materials development was to improve them by enhancing their properties and optimizing their manufacturing process. Although materials with extraordinary properties have been developed, even smallest defects are not avoidable. Furthermore, these materials are susceptible to ulterior damage induced by mechanical, chemical, thermal, UV radiation, or a combination of these factors [1].

That leads to the need of periodical inspections and repairs which are highly time-consuming and expensive. Nowadays, the long-term durability, high performance and reliability are major challenges for polymeric architecture. Thus, the development of breaks and microcracks, leading to catastrophic failures in industrial components, remains a significant issue for these widely used materials.

In theory, ideal repair methods are ones that can be executed quickly and effectively directly on damaged site, eliminating thereby the need to remove a component for repair. Actually, when polymer materials become damaged, there are only a few methods available to attempt to extend their functional lifetime.

One of the earlier healing methods for fractured surfaces was hot-plate welding, where polymer pieces were brought into contact above the glass transition temperature of the material, and this contact was maintained long enough for interdiffusion across the crack face to occur and restore strength to the material. It has been shown, however, that the location of the weld remains the weakest point in the material and thus the favourite site for future damage to occur [2]. For laminate composites, resin injection is often employed to repair damage in the form of delamination, even if it can be problematic when the crack is not easily accessible for such an injection. For fiber breakage in a laminate composite, a reinforcing patch is often used to restore some of the strength to the material. None of these methods of repair is an ideal solution to damage in a structural composite material. These are temporary solutions to prolong the lifetime of the material, and each of these repair strategies still requires monitoring of the damage and manual intervention to further the repair. This greatly increases the cost of the material by requiring regular maintenance and service.

Alternative healing strategies are therefore of great interest, inasmuch as these conventional repair methods are not effective, for example, for healing invisible microcracks within the structure during its service life.

In response, the concept of self-healing polymeric materials was proposed in the 1980s as a means of healing invisible microcracks for extending the working life and safety of the polymeric components [3]. The publication in the topic by White and Sottos in 2001 [4], of which an explanatory scheme is shown in Figure 1-1, further inspired world interests in these materials.
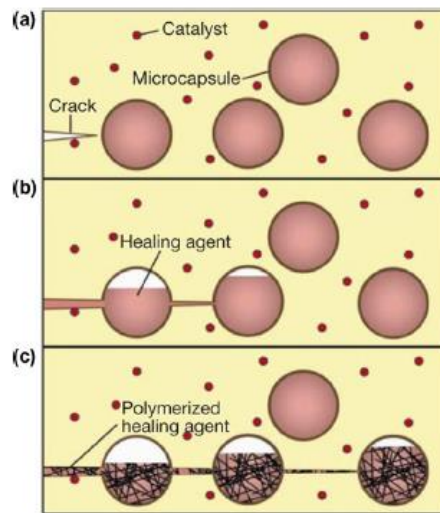
Figure 1-1. Capsule based self-healing composite (White *et al.*, 2001 [4])

In summary therefore, the target is a further step towards the development of nature-inspired synthetic polymers that can self-heal failures, such as delamination, or aesthetic damage, improving maintenance and repair procedures and significantly extending the lifetimes of these industrial materials, according to the scheme in Figure 1-2 [5].
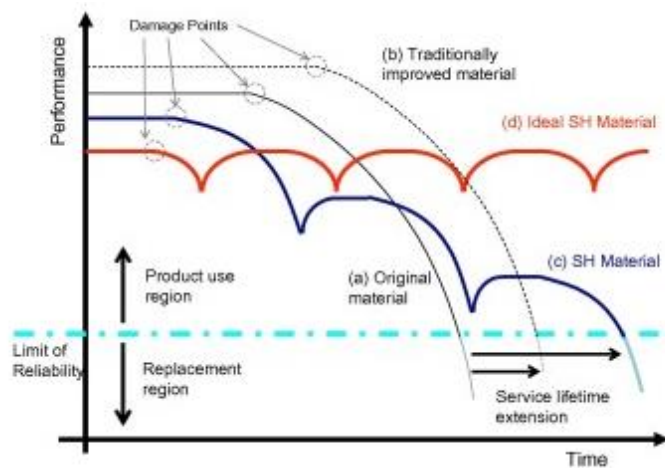
Figure 1-2. Lifetime extension of engineered materials by implementation of self-healing principle (Garcia, 2014 [5])

1.1. Classification

Current self-healing polymers can be sorted in two main groups depending on the need of an external trigger to initiate the healing process: non-autonomic and autonomic. Non-autonomic self-healing materials require an external stimulus, like heat or light. Contrariwise, autonomic materials use the own damage as starter of the healing action.

A second way, most cited, of categorising self-healing composites is represented by the healing strategy: extrinsic and intrinsic healing [6].

1.1.1. Extrinsic Self-healing

The extrinsic healing process is based on the use of a healing agent contained in the matrix as a separate phase. The healing agent is usually in the liquid state, placed into reservoirs which may be microcapsules or hollow fibers or microvascular network. In most approaches, the healing agent is used with a catalyst, which can also be encapsulated or dissolved in the matrix. In some cases, the catalyst is not required to initiate the healing process; the healing agent can also react with itself. The extrinsic healing concept is based on the response after or at the onset of damage. Current research is concerned with the improvement of healing agents in terms of compatibility and catalyst-free system with some new encapsulation techniques.

Microcapsule embedment

The basic principle of encapsulation strategy is healing by incorporated healing functionality or reactive constituents into capsules followed by chemical reactions. These reactions take place by various mechanisms including ring opening metathesis polymerization (ROMP) [4], cycloreversion [7], cycloaddition [8], cross-linking reactions [9], or a mechanochemical catalytic activation [10]. Damage acts as a stimulus to initiate the healing process: it ruptures the microcapsule, and subsequent release of the healing agent occurs. The healing

precursor reaches the damage site by capillary action and spreads itself over the two fracture surfaces due to the surface tension. White *et al.* [4] designed a dicyclopentadiene (DCPD) Grubbs' system, based on capsule healing, achieving 75% recovery of virgin fracture toughness.

There are different ways to achieve capsule healing: the encapsulated liquid agent can be combined with a dispersed catalyst; both the healing agent and the catalyst can be embedded in different capsules; the healing agent can also directly react with a functionality of the matrix under an external stimulus; the healing agent and the catalyst can be placed in the matrix as a separate phase.

The encapsulation strategy is mainly focused on meltable dispersion and *in situ* and interfacial encapsulation techniques for capsules. Meltable dispersion consists in dispersing the curative agent in a melted polymer to form the capsules by solidifying of the polymer [11]. In interfacial and *in situ* techniques, the shell is developed by polymerization at the interface between healing agent droplets and oil-in-water emulsion. Different microencapsulation methods are optimized such as physical methods, chemical methods, and physicochemical methods. Robust, in terms of mechanically and thermally stable, microcapsules with healing precursor have been synthesized for self-healing polyurethane matrix [12]. Triethylenetetramine (TETA) microcapsules for wear-resistant polymer composites [13] and poly(methyl methacrylate) microcapsules with high storage and thermal stability [14] have been manufactured and implemented. Polydimethylsiloxane-based self-healing elastomers also are reported [15]. Dual component self-healing epoxy system containing epoxy (DGEBA) and different variants of hardener microcapsules are investigated [16].

However, this type of self-healing is limited by processing difficulties and inhomogeneous distributions of the two components: reduction of mechanical properties is common following the introduction of external chemicals.

Moreover, the major drawback of encapsulation techniques is that self-repair can only occur once at each site.

Hollow fiber embedment

Hollow fibers are used to deliver a larger amount of liquid healing agent. These are embedded within either glass fiber-reinforced plastic (GFRP) or carbon fiber-reinforced plastic (CFRP) composites. Liquid-filled hollow fibers based self-healing systems are shown Figure 1-3 [17]. Healing-agent-filled hollow fibers are introduced into the matrix by the vacuum-assisted resin transfer molding (VARTM) process. Extending the 1D vascular concept of liquid-filled hollow fibers, 2D and 3D networks have also been developed [18,19]. Its invasiveness must be minimized so that its effect does not undermine the polymer mechanical properties. Therefore, its structure and the healing agent characteristics, such as fluidity and stability, should be carefully selected.
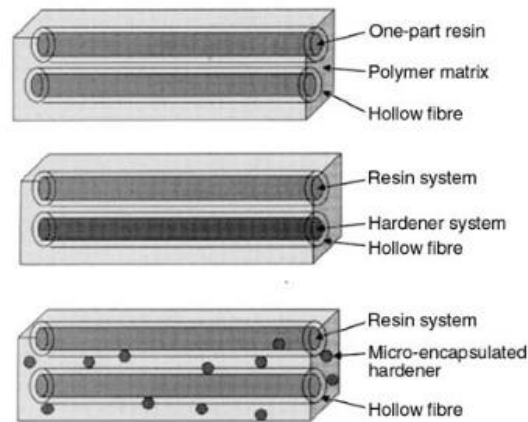
Figure 1-3. Schematic diagram for hollow fiber repair (Bleay *et al.*, 2001 [17])

Resin-filled hollow glass fibers impart healing capability on low-velocity impact damage in CFRP. Large-diameter capillaries are not feasible to demonstrate damage healing. Smaller hollow glass fibers filled with resin have been also used, but they were unable to deliver the resin into the crack due to the highly viscous epoxy resins.

The fracture of hollow fibers is mandatory to release healing precursors. The low viscosity of healing agent is preferable to facilitate fiber infiltration, which is necessary. The reinforcement of hollow glass fibers into CFRP also affects the coefficient of thermal expansion so that multistep fabrication stages of the hollow fiber are another challenge. A novel hybrid multi-scale carbon fiber/epoxy composite reinforced with self-healing core-shell nanofibers at interfaces has been demonstrated [10].

The microvascular embedment

To enhance the healing efficiency, vascular method is adopted: a 3D microvascular network, inspired from the respiratory system of livings, is developed into the matrix to store the healing agents. Self-healing materials based on hollow fibers or a mesoporous network are called vascular materials. Microvascular fabrication is possible by various techniques including laser micromachining, soft lithography, electrostatic discharge, fugitive inks, and hollow glass fibers. Healing precursors are introduced into these channels either by pumping or through capillary forces. The introduction of sacrificial fibers into woven preforms enables the continuous fabrication of 3D microvascular composites that are both strong and multifunctional [19,20]. To employ damage healing in microvascular systems, functional fluids that act as a healing agent are released upon fracture of vascular network. Further, the healing agent polymerized with adjacent catalyst can form a network and restricts the growth of damage. Replacement of some reinforcement fibers of FRPs by individual hollow fibers is a well-known method to achieve microvascular composites [21]. Schematic diagram of self-healing materials with 3D microvascular networks is shown in Figure 1-4 [19].
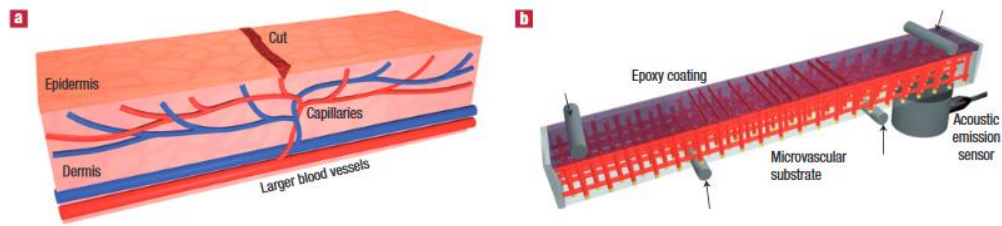
Figure 1-4. Self-healing materials with 3D microvascular networks (K. S. Toohey *et al.*, 2007 [19]**). a) Schematic diagram of a capillary network in the dermis layer of skin; b) Schematic diagram of the self-healing structure in an epoxy coating**

Vasculature-based healing allows the efficient delivery of the healing agent and additionally healed a large area. Furthermore, the incorporation of micro-channels within a polymer composite offers multiple healing, because the network may be refilled. However, the large-scale production of self-healing fiber-reinforced composites is not feasible due to complex vasculatures and lack of scalability.

1.1.2. Intrinsic self-healing methodology

Structurally dynamic polymers are a macromolecular system in which dynamic bonds are responsible for the restructuring of molecular architecture upon to external stimuli. Intrinsic healing is based on the own healing capability of the matrix material. When subjected to an external stimulus or an internal damage, the material can repair itself through the reversibility of chemical or physical bonding in the matrix phase. No external agents are needed, so they have the advantage that multiple healing events can occur. The healing is possible via temporary local mobility enhancement of polymeric chains, induced by various modes of energy, *e.g.* temperature, static load, UV.

A two-step process is needed: a softening step leading to local mobility towards the damage, followed by a hardening process leading to the restoration of the original properties. In Figure 1-5 is represented the recovery of the local viscosity after the healing trigger (temperature) is removed [5].
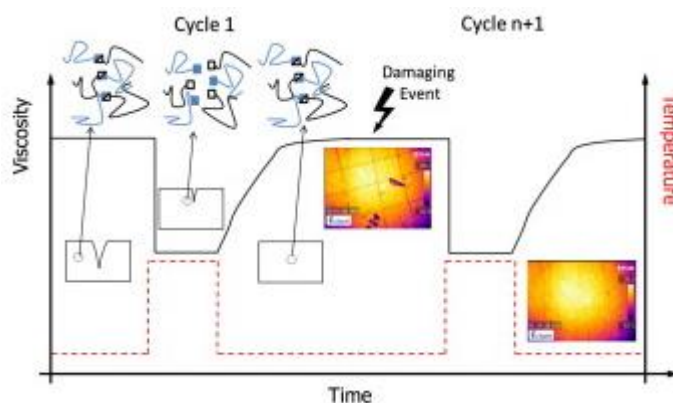
Figure 1-5. Multiple healing events with intrinsic healing: viscosity triggered by temperature (Garcia, 2014 [5])

The most significant strategies of intrinsic self-healing materials are based on reversible covalent bonds, thermoreversible physical interactions and supramolecular chemistry [22].

Supramolecular noncovalent interaction-based self-healing

To overcome the issue of poor in performance extrinsic techniques, great attention is focused on supramolecular systems which respond to damages autonomously and recover mechanical integrity without the addition of foreign reactive species and human intervention. These non-covalent interactions recover mechanical properties almost completely but take longer time. Reversible bonding can be used to design supramolecular healable polymers and composites which respond to external stimuli such as heat [23], pressure [24], water [25], or light [26]. Stimuli responsiveness [27] and a high diffusion rate of oligomeric components [28] are the main characteristic of supramolecular polymers which make them for rapid and controllable healing system. The reversible non-covalent interactions can be possible by hydrogen bonding, ionic bonding, metal-ligand bonding, and π-π stacking.

H-bonding Supramolecular chemistry

H-bonding is the most popular route to achieve supramolecular polymers. Upon heat, interactions between the polymeric chains decrease, they are reassembled

upon cooling, and finally the non-covalent cross-linking recover the strength and mechanical integrity.

However, individual supramolecular polymers are affected by low mechanical strength. The mechanical strength of supramolecular system is enhanced by an increase in the number of non-covalent interaction [29] and by reinforcement with nanofiller [30].

Metal-ligand supramolecular polymers

Reversible behavior of metal ion and ligand bond in metal ligand complexes is of great interest to design stimuli-responsive materials. These polymers can be healed upon exposure to light [26,31]. During the whole healing mechanism, supramolecular interactions and light-heat conversion happen subsequently. The temporary disentanglement of metal-ligand motifs occurs when excited electronically upon exposure to UV, and further, heat energy is released. Subsequently, the average molecular weight and viscosity of system decrease, and defects are healed. Local damages can also be recovered only after exposure to light.

Supramolecular π-π interaction-assisted self-healing

A thermally triggered reversible network is achieved based on π-π stacking interactions, in which end-capped π-electron-deficient groups interact with π-electron-rich aromatic backbone. The driving forces for producing tough, stable, healable homogeneous blend of elastomers are interpolymeric π-π stacking complexes [32]. At higher temperatures, the disengagement of the supramolecular (π-π stacking and hydrogen bonding) interactions is possible, and it leads to change in the apparent molecular weight of the homogeneous noncovalent polymer blend and further rapid change in viscosity with temperature. A polymer blend recovers the mechanical strength by refurbishing these supramolecular interactions.

Supramolecular self-healing ionomers

Ionomers are a class of thermally activated supramolecular self-healing polymers that possess the ability to self-heal several types of damage such as scratches and ballistic impact damage [33]. In ionomers, ionic metal salts are bonded to the polymer backbone creating electrostatic interactions. These interactions are capable of cluster formations that can be broken when a specific temperature is applied. Once the clusters are broken the polymer enters into a transition phase that gives rise to a certain mobility allowing sufficient polymer flow and thereby healing. Because the transition phase is initiated at a much lower temperature than the melting point of the ionomer, the polymer maintains its main mechanical properties even during the healing process. A schematic overview of a typical ionomer molecular structure is given in Figure 1-6 [34]. Here, the clustering of the charged ionic species and the final network formation are clearly indicated.
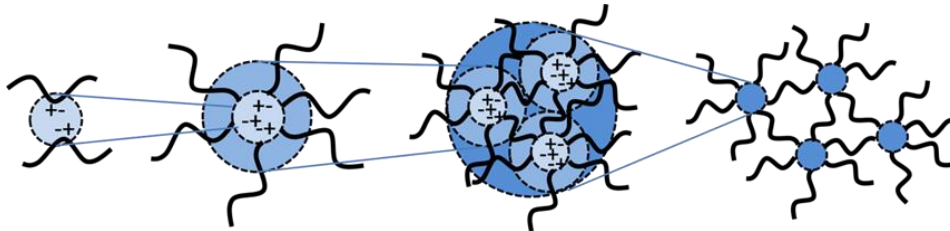
Figure 1-6. Schematic overview of the molecular structure of an ionomer polymer (Bose *et al.*, 2015 [34])

During whole mechanism free volume plays a great role which provides enough mobility to polymer chain rearrangement and interdiffusion. Besides, many other factors, such as impact energy, nature of ionic groups, and counterions, the neutralization degree, increased temperature during impact, the content of ionic groups and dielectric constant, and so on, also play a key role to make effective self-healing by ionomers. To enhance the healing efficiency of ionomers composites, conductive and magnetic fillers are added.

Dynamic Covalent Chemistry based Self-healing

Dynamic Covalent Chemistry (DCC) consists in extending the dynamic features found in supramolecular chemistry to molecular chemistry using reversible covalent bonds. DCC covers dynamers, covalent adaptable networks (CANs) and vitrimers. The first step in the development of dynamic components are dynamers, which are constitutional dynamic polymers of either supramolecular or molecular nature whose monomeric components are linked through reversible connections, which can be either non-covalent interaction or reversible covalent bonds, according to Skene and Lehn [35]. They can respond to physical and chemical stimuli by establishing reversible networks.

Stimuli-responsive systems are achieved by incorporation of some dynamic covalent functionality into matrix backbone and/or in side chains.

Typical dynamic bond chemistry is belonging to disulfide bridges [36,37], hindered urea [38], alkoxyamine [39], ester linkages [40], and Diels-Alder bonds [41,42].

Among them, Diels-Alder chemistry has been widely adopted because of its simplicity, high efficiency and repeatability through only the application of heat.

2. Diels-Alder Chemistry for Self-Healing materials

Even if the non-covalent interactions of supramolecular chemistry have long been utilized for their inherently reversible nature, they are far weaker than their covalent counterparts. It is therefore desirable when designing a structural healable polymeric material to utilize the stronger covalent bond reversibly. The most widely used and intensely studied reversible covalent bonds are found in the Diels-Alder cycloaddition reaction. The reaction involves the concerted addition of a conjugated diene with a dienophile to form a cyclohexene.

Four electrons from the conjugated diene and two electrons from the dienophile are involved in a [4+2] cycloaddition reaction. Essentially, three π bonds break and two new C-C σ bonds and one new C-C π bond are formed, as shown in Figure 2-1.
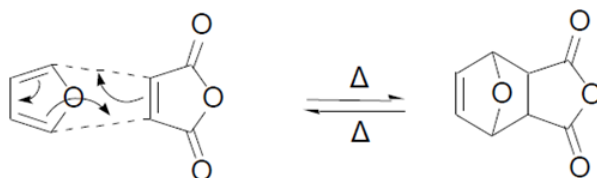
Figure 2-1. The Diels-Alder reaction mechanism

The diene and dienophile components of this reaction can be altered to incorporate almost any functionality imaginable, and thus the reaction is an extremely versatile one in organic chemistry.

The only limitation is that the diene used in the DA reaction have to be in *s-cis* conformation, which is thermodynamically less stable due to steric repulsion. Thus, cyclic diene, such as furan, cyclopentadiene and anthracene, are appropriate candidate as diene in DA reaction, since the *s-cis* conformation is already locked in their structure. In particular, the furan group is very reactive, with a r-DA reaction temperature relatively low (approximately 120°C), if compared with 250°C cleaving temperature of the anthracene group [43–45]. Similarly, in order to increase the reactivity of the dienophile, it is necessary to have one or more electron-withdrawing groups, such as a carbonyl group (C=O) or a cyano group (C≡N), attached to the C=C bond. The role of electron-withdrawing groups is to withdraw electrons from the C=C bond and to make the sp2 carbon have a partially positive charge, which helps the dienophile to be more reactive toward the diene groups. Therefore, maleimide moieties with two C=O bonds is a good dienophile candidate [46].

2.1. Diels-Alder in Self-Healing Polymers

The Diels-Alder cycloaddition reaction is thermally reversible, leading to its application in the field of healable materials as a thermal stimulus responsive material. The self-healing polymers employing the furan group as a diene and the maleimide group as a dienophile have been the most widely studied.

The first use of Diels-Alder chemistry for healable materials was in 2002 by Chen *et al*. [47], in which the furan and maleimide moieties were incorporated into the polymer backbone. Since this ground-breaking work, several Diels-Alder based thermally stimulated healable materials have been created.

The Diels-Alder healing system devised by Chen et *al*. [47] utilized the DA and r-DA reaction between furan and maleimide, according to scheme in Figure 2-2.
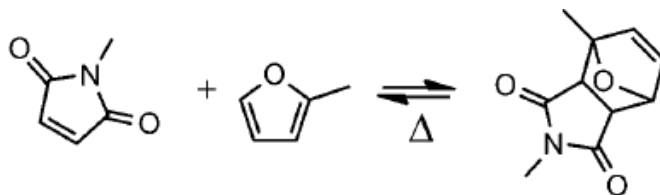
Figure 2-2. Diels-Alder reaction between a maleimide derivative and a furan derivative

The material consisted of four furan moieties and three maleimide moieties, the reaction of which led to a macromolecular network formed by reversible crosslinking covalent bonds.

The r-DA reaction was proposed as the major reason for crack propagation, as the bonds formed in the DA adduct are weaker than the other covalent bonds in the system; this also means that DA active functional groups are exposed following crack propagation, and therefore healing of the material via the re-formation of DA adducts is possible.

Moreover, the DA reaction occurs slowly at room temperature without any other external stimulus and the reaction becomes faster as the temperature increases. Thus, DA polymers can still prevent the propagation of micro-damage at room temperature. Finally, the temperatures for the r-DA reaction between furan and maleimide are low enough for prevent thermal degradation [47,48].

This material was shown to have mechanical properties akin to common structural epoxy materials, indicating their potential for use in engineering composite materials. The initial studies of these polymers showed a 57% healing efficiency upon application of a thermal stimulus (120–150°C), which is significant for a cross-linked thermoset without any additional components. The lack of total healing was due to complete specimen fracture into two separate pieces: this resulted in poor interfacial match-up between the two halves during the healing process. The most remarkable aspect of this system, however, is its inherent ability to undergo this healing process multiple times, greatly extending the functional lifetime of the material. Indeed, after two full cycles of fracture and healing, the load at fracture of the third crack was 80% that of the second crack, demonstrating the ability of this material to undergo multiple successful cycles of healing. A follow-up study by Chen *et al.* in 2003 [48] addressed some issues that arose during their initial study. Improvements include the creation of a lower melting maleimide monomer, the removal of the need for solvent during polymerization, as well as the implementation of a sample geometry that prevented complete fracture of the specimen. Indeed, this monomer allowed for a higher mobility of molecules, resulting in higher healing efficiencies of 80% on average, with the ability for the sample to undergo healing multiple times as evidenced by an average of 78% healing efficiency for the second cycle of mending. These healing cycles require a thermal stimulus to initiate the r-DA reaction and subsequent re-formation of the DA adducts, and were accomplished at temperatures ranging from 120 to 150°C.

This same furan/maleimide healable material system was revisited in 2007 by Plaisted and Nemat-Nasse [49], again utilizing sample geometry that allowed for controlled incremental crack growth. These studies were designed to further examine and quantify in a systematic manner the thermal treatment required for healing, including time and temperature necessary to regain mechanical strength

in the material. Indeed, it was found that effective healing could be achieved at 85–95°C: at 85°C visual healing occurs after only four minutes, the approximate time for the sample to reach thermal equilibrium, and further heating to the onset of the T_g at 95°C allows full recovery of mechanical strength. In addition, the healing efficiency was found to be near 100% after several cycles of fracture and healing and it was shown that the degree of healing did not increase past one-hour application of a thermal stimulus.

Unlike the polymers synthesized by Chen *et al.* with the DA reaction, there has been more research by Gheneim *et al.* on the synthesis of polymeric dienes; bearing pendant furan moieties to the main chain in a polymer, whereas the maleimide moieties are embedded as a crosslinking agent or vice versa [50]. Similarly, Amalin Kavitha and Singha investigated a polymethacrylate bearing furfuryl functionality with bismaleimide [51].

Also, Zhang *et al.* [52] has investigated the use of a remendable thermoset material based on the DA reaction between furan and malemide. Starting from a polyketone, they produced a polymer containing pendant furan groups following conversion using the Paal-Knorr reaction. Upon mixing of this furan-containing polymer with a bis-maleimide, a cross-linked network was obtained; the reversibility of this material through the DA and r-DA reactions was initially demonstrated through reversible gelation as a function of temperature. Healing is possible in this system since the free healing agents become crosslinked with the other bearing moieties. The primary benefit of having free maleimide or furan moieties is that these molecules have increased mobility and are better able to find the pair moieties when healing is initiated. The authors also fabricated polymer samples which were tested via three-point bending. However, instead of healing the fractured sample and re-testing to determine healing efficiency, as is the norm in this field, the fractured material was ground up and a new specimen fabricated. The new sample was re-tested and performed similarly to

the original, leading the authors to claim 100% healing efficiency. While the demonstration of the recyclability of these materials is quite impressive, this variation from the common testing procedure limits the comparisons that can be made to other healable materials in the field.

In 2009, Tian et al. [53] reported a healable epoxy that contained furan and malemide moieties. Traditional epoxy materials cannot be altered after they undergo curing; by incorporating DA components to the material, however, the ability to heal can be introduced to the system. The furan functionality was attached to an epoxy compound via a two-step procedure. This epoxy could then be cured as usual, leaving pendant furan groups free to react with an added bis-maleimide compound. Polymer specimens were fabricated, and the mechanical properties found to be comparable to commercial epoxy materials. The authors showed the qualitative healing of the materials at temperatures above 100°C, but did not report on the healing efficiencies of these materials.

Besides furan, a widely studied cyclic diene for DA reactions is cyclopentadiene. In addition to be a desirable diene for this reaction, cyclopentadiene can also act as a dienophile and self-react to form a DA adduct Figure 2-3.
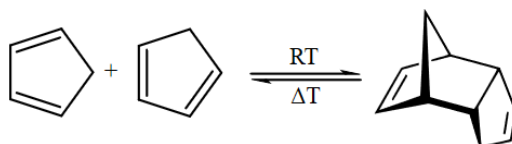
Figure 2-3. Diels-Alder cycloaddition reaction of cyclopentadiene to form dicyclopentadiene

A new healable material was prepared: a monomer containing a dicyclopentadiene core unit was synthesized and was subsequently polymerized to form a single component polymer network in which the polymer backbone consisted of thermally reversible DA adducts [54].

In addition to the formation of the adduct, it was found that dicyclopentadiene can undergo a second DA reaction, leading to trimer formation and resulting in cross-linking of the network. An advantage of this system is that the material is

created from a single crystalline component, ground up and heated neat to form the polymer network, greatly simplifying not only the preparation and processing of the material, but also the recovery of mechanical properties of the system. This material was shown to undergo healing upon exposure to a thermal stimulus, giving an average 46% healing efficiency when heated to 120°C for 20 minutes. Another approach was developed by Peterson *et al.* [55] by incorporating a secondary phase containing cross-linked furan and maleimide within a traditional epoxy–amine thermoset. This system showed about 37% recovery of initial strength. In addition, due to the reversibility of the Diels–Alder bond, both materials could be healed multiple times. An ulterior publication by Peterson *et al.* [56] showed healing of a furan-functionalized epoxy–amine thermoset through the use of a bismaleimide solution as a healing agent. Application of the healing agent solution to the fracture surface resulted in recovery of 70% of the initial polymer strength. The ability of samples to recover the load was not only attributed to the Diels–Alder reaction on the fracture surface, but also to solvent induced swelling and resulting mechanical interlocking. Additionally, the samples were able to be healed multiple times because of the reversibility of the Diels–Alder bond. In a subsequent work, Pratama *et al.* [57] studied the effects of multimaleimide (MMI) structure and solvent selection on the healing efficiency of furan functionalized epoxy networks.

2.2. Diels-Alder in Self-Healing Polymer based Composites

After the study of promising self-healing polymers with the DA reaction, further research was conducted on the self-healing FRP composites, in particular with the use of furan/maleimide based DA adducts.

By using these molecules, Park *et al.* [58] and Ghezzo *et al.* [59] fabricated self-healing CFRP composites. These self-healing CFRP composites were produced mixing all the monomers at the melting temperature and using a resin transfer mold (RTM) method. The healing performance was evaluated trough tensile strain test: as a result, around 90% of the tensile strain was recovered.

However, there are some drawbacks to these composites. First, the polymer might not be as stable as a conventionally crosslinked polymer, since currently developed polymers have been synthesized by either crosslinking only the DA monomers to form networks [47,48] or embedding free crosslinking agents in the polymers [50,51,60,61]. The former polymers can be completely cleaved by heating them above 130°C (the cleaving temperature) since the only interlinkage in these polymers is the DA intermolecular bonds, and the latter polymers can have varying properties depending on the amount of free agents in the polymers. Moreover, the chemical synthesis process of DA monomers is relatively expensive and complicated [62,63], and the strength of the matrix is not as good as some commercial epoxy resins. This could potentially hinder large-scale production of DA self-healing polymers for industrial applications.

Turkenburg and Fisher [64] developed epoxy resins functionalized with Diels-Alder based thermo-reversible crosslinks, suitable for manufacturing of composites capable of multiple self-healing repair processes. The key challenge in realizing a structural combination of conventional epoxy amine systems with furfuryl and maleimide functional groups was to achieve a high conversion in the reversible cross-linked polymer network formation, while avoiding the major side-reactions. Densely cross-linked, solvent resistant polymeric networks was

obtained, that maintain the ability to un-crosslink and thus regaining fluid behavior at elevated temperatures for at least five subsequent heat cycles. Glass fiber reinforced polymer composite films, which were fabricated using these resins, demonstrate that the thermo-reversible effect was strong enough to achieve full self-healing of a severely cracked and delaminated test specimen.

Further research has been conducted to increase the adhesion between the polymer matrix and fiber reinforcements since interface interaction affects the properties of composites by controlling the load transfer between the matrix and fibers [65,66].

As shown in Figure 2-4, Peterson *et al*. have implemented this feature by functionalising the surface of glass fibers with maleimide and an epoxy-amine thermosetting matrix with furan [65]. The GFRP composites were fabricated using functionalized fibers and matrix, and the healing performance was characterized via short beam shear (SBS) testing. In the work by Peterson *et al.*, a relatively low average healing efficiency of 41% was obtained.
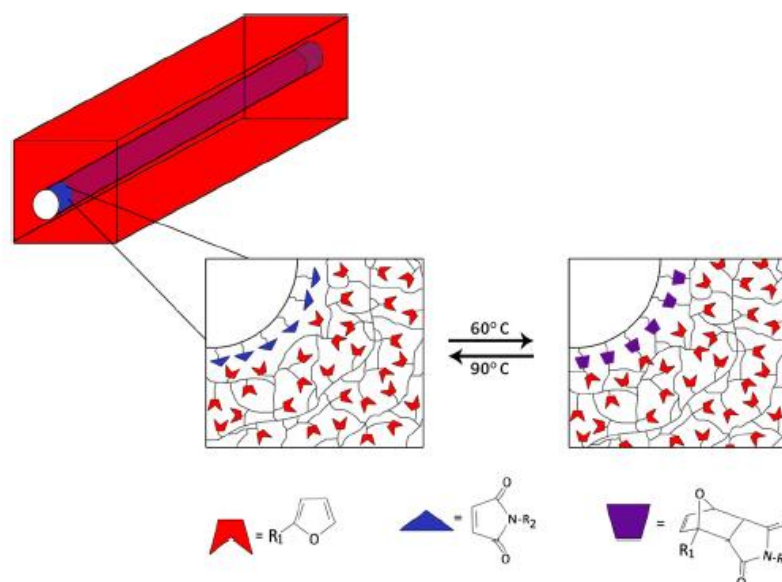
Figure 2-4. Interfacial healing concept. Maleimide functionalization (blue triangles) of glass fiber within a furan-functionalized (red notched trapezoids) polymer network will result in a thermoreversible, and healable, fiber–network interface (Peterson *et al.*, 2011 [65]**)**

Similarly, Zhang *et al.* [67] used thermo-reversible Diels-Alder bonds, formed between maleimide and furan groups, to generate an interphase between carbon fiber surface and an epoxy matrix, leading to the ability of interfacial self-healing in carbon-epoxy composite materials. The maleimide groups were grafted on an untreated T700 carbon fiber from a three step surface treatment (Figure 2-5): nitric acid oxidization, tetraethylenepentamine amination, and bismaleimide grafting.
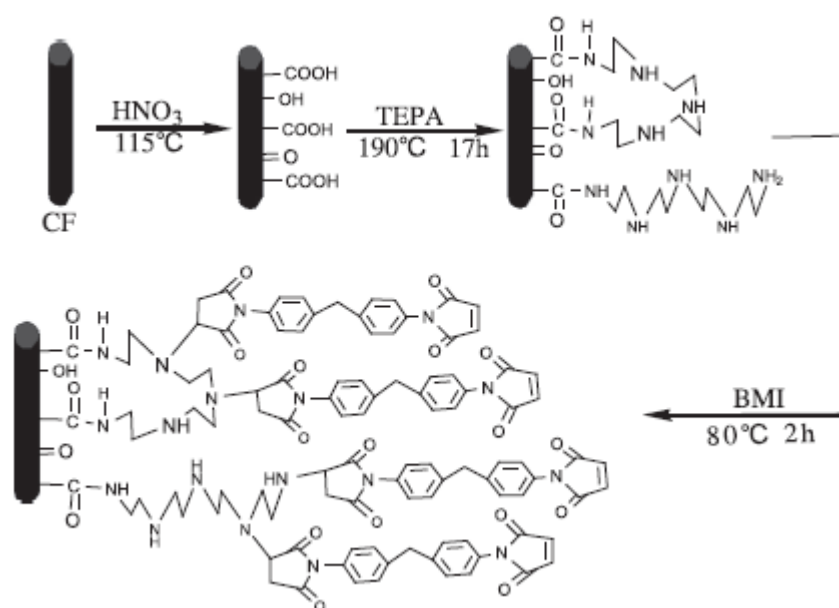
Figure 2-5. Protocol for grafting maleimide groups on T700-U carbon fiber surface (Zhang *et al.*, 2014 [67])

The furan groups were introduced in the reactive epoxy system from furfuryl glycidyl ether. The interface between untreated carbon fiber and epoxy matrix was considered as a reference. The interfacial shear strength (IFSS) was evaluated by single fiber micro-debonding test. The highest healing efficiency calculated from the debonding force was found to be about 82% more compared to the value for the reference interface. All the interphases designed with reversible DA bonds have a repeatable self-healing ability. As after the fourth healing, they can recover a relatively high healing efficiency (58% for the interphase formed by T700-BMI which is oxidized for 60 minutes during the first treatment step).

On a similar system, in a subsequent work Zhang *et al.* [68] evaluated the influence of the content of furfuryl glycidyl ether on the architecture and on the

thermomechanical properties of an epoxy network by using micro-debonding test. From this method, the debonding force and the fracture energy, G_{ic}, of the interface were determined to analyze the interfacial mechanical properties of these functional composite materials. The suitable content of FGE, with which the composite system displayed, not only high interfacial self-healing ability, but also kept significant interfacial mechanical performances, was found to be an inclusion of between 20% and 30% by weight.

3. Design strategies for Self-Healing Polymers

Diels-Alder chemistry was first described by Otto Diels and Kurt Alder in 1928 [69], and is particularly useful in synthetic organic chemistry as a reliable and clean method for introducing a 6-membered DA adducts on a wide range of organic substrates which can be end-capped by reactive functional groups, such as epoxies, acrylates, amines, isocyanates, and hydroxyls. The DA reaction is a thermally reversible cycloaddition between a conjugated diene and a dienophile resulting in a cyclohexene derivative. The crosslinked DA adducts can undergo a cleavage reverse reaction at higher temperatures [70,71].

The bond energy of the new C-C σ bonds in DA adducts was evaluated to account to 96.2 kJmol [47], while other covalent bond energies are 348 kJ/mol for C-C bonding, 293 kJ/mol for C-N [72]. Since covalent bonds are 3 to 4 times stronger than C-C σ bonds formed in DA adducts, cracks are more likely to form and propagate between the new formed bonds in DA adducts. Consequently, available diene and dienophile on the freshly generated surface increase the efficiency of the self-healing method, through the DA recombination.

While several diene-dienophile couples are available for DA reaction, to date, the most investigated precursors are furan-maleimide derivatives. A notable implication, resulting for the diene-dienophile choice, is the temperature where the self-recovery can be achieved. The range for the r-DA reaction of

furan/maleimide derivatives is approximately at temperatures higher than 115-120°C, while at lower temperatures the DA recombination is favoured.

When considering self-healing thermosets with the DA reaction, the local molecular mobility, displayed during mending cycles, is a key parameter affecting the healing efficiency. Fast and efficient damage recovery and DA bond recombination is achieved via a local and temporary increase of mobility occurring at temperatures higher than polymer glass transition temperature, but lower than r-DA cleavage temperature. In the case of DA adducts based on the furan/maleimide couple, a useful processing window can be identified between the polymer's T_g (~ 90°C) and r-DA temperature (~ 120°C).

Epoxy resins have been widely used due to their excellent heat resistance, outstanding corrosion protection, high electrical resistivity, superior mechanical properties. However, cracks might occur as a result of thermal stress and mechanical fatigues during processing and service conditions. Many papers already described epoxy resins containing DA adducts in their backbone [56,73]. Following a related concept, multi-functional epoxy precursors crosslinked with amines will be described in present work. The choice to locate the reversible DA bond on the epoxy or on the amine moieties results in structurally equivalent networks, as far as the self-healing phenomena are concerned. Nevertheless, the synthetic path to produce epoxy DA adducts is easier with respect to the preparation of DA amines, due to the added complexity of amine protection/deprotection step [74]. For the sake of simplicity, tetra functional amines were used as crosslinkers in the following, while the epoxy functionality was varied between 2 and 4, to investigate about the effect of different crosslinking density.

Indeed, a number of Diels-Alder polymers have been presented in the scientific literature up to date, but there is a lack of systematic study dealing with molecular parameters. This chapter focuses on the effects of different structural

features, such as average number of crosslinking functionality and molecular mobility of epoxy precursors, on the efficiency of healing process. The molecular design, the preparation, and the preliminarily evaluation of properties of self-healing epoxy have been discussed below.

Through the chapter, the overall design flow for achieving hybrid epoxy systems, containing covalent thermo-reversible bonds and the preparation and evaluation of selected examples were detailed. This work underlines that the concurring presence of thermo-reversible covalent bonds and high molecular mobility are essential requirements to develop self-healing systems. The most effective structural modification has been pursued by adjustment of the several features: average functionality of reacting precursor mixture, cross-linking density, thermosetting network and concentration of self-healing reversible bonds. Also, the requirements of easy and efficient self-healing were compromised with development of material properties compliant with structural and semi-structural applications.

3.1. Design for best performances

Crosslinking density and conformational stiffness of molecular fragments between adjacent crosslinks are the main parameters, which affect properties, such as T_g, mechanical stiffness and overall molecular mobility. However, accurate experimental evaluation of crosslinking density is often difficult, especially for glassy and rigid polymers. Therefore, the use of an easily defined marker as a measure of crosslinking density is strongly envisaged. In this respect, the average functionality of a mixture of monomers can be defined as the average number of functional groups per monomer molecule for all types of monomer molecules. It is defined by equation 3-1.

$$f_{avg} = \frac{\sum N_i f_i}{\sum N_i}$$ 3-1

where N_i is the number of molecules of monomer i with functionality f_i, and the summations are over all the monomers present in the system. As a rule of thumb, reactive mixture with f_{avg} strictly equal to 2 can lead to high molecular weight linear polymer, f_{avg} smaller than 2 results in low molar mass oligomers, while f_{avg} greater than 2 produces branched and crosslinked networks. In our specific case, for a system consisting of 2 mol of di-epoxy and 1 mol of tetra-functional amine f_{avg} is 2.67; for a system consisting of 1 mol of tetra-functional epoxy and 1 mol of tetra-functional amine f_{avg} is 4.00. All the intermediate values are achievable by proper adjustment of the ratio between bi-functional vs tetra-functional epoxy, stoichiometrically balanced by the amine.

In the case of conventional crosslinked networks, f_{avg} is invariant with respect to temperature, and the network cannot flow upon heating. If the network precursors include reversible bonds, such as DA, f_{avg} decreases at high temperatures, after triggering the r-DA cleavage reaction. Referring to the bi- and tetra-functional DA epoxy crosslinked with conventional tetra-functional amine,

the f_{avg} drops to 1.60 in former case, while the values is 2.67 for the latter one. Obviously, a high crosslinking density hinders molecular mobility: a value of f_{avg} higher than 2 prevents the healing phenomenon, if the condition holds true, also in the cleavage state at high temperature.

The ability to adjust the molecular mobility during the healing cycle at a desired pre-set value is an important molecular design tool, which is helpful in addressing specific application requirements. For example, if the thermosetting DA resin is intended for restoration of small impact damages or micro-delaminations, which are often encountered in the case of Barely Visible Impact Damages (BVID) of composite materials, a moderate molecular mobility is required. The sample has to retain its geometry and fibers placement, and long-range viscous flows are detrimental. This target can be achieved tailoring the cleaved state f_{avg} so as its value is close to 2. On the contrary, if thermal recycling of thermoset is sought after, a high extent of molecular mobility is required in the cleaved state to allow materials flow. While in the first case the overall materials properties closely resemble the conventional thermosets, in the latter case a dynamic thermoplastic-like state is achieved during self-healing. The epoxy mixture formulation can be properly adjusted to suits one of the previous conditions to achieve bespoke molecular mobility, measured by f_{avg}. For this purpose, crosslinking density of the cleaved stage can be pre-set to different levels, corresponding to reduced molecular mobility, by mixing bi-functional Diels-Alder epoxy with conventional epoxy, or mixing a bi- and a tetra-functional Diels-Alder epoxy. The introduction of conventional epoxy brings the added benefits of overall reduced costs because of the use of a cheaper precursor, while the introduction of tetra-functional Diels-Alder epoxy benefits the healing efficiency increasing the overall concentration of DA functional groups.

Further degree of freedom can be introduced in the molecular design if detailed precursor structure is considered. In fact, according to Figure 3-1a, a symmetrical

Diels-Alder precursor, bearing a pair of cleavable dienophile groups, can be designed. But the same structural features can be achieved using a smaller molecule, as shown in Figure 3-1b. In the former case, the formation of an unbound dienophile allows higher molecular mobility, increasing therefore the healing efficiency.
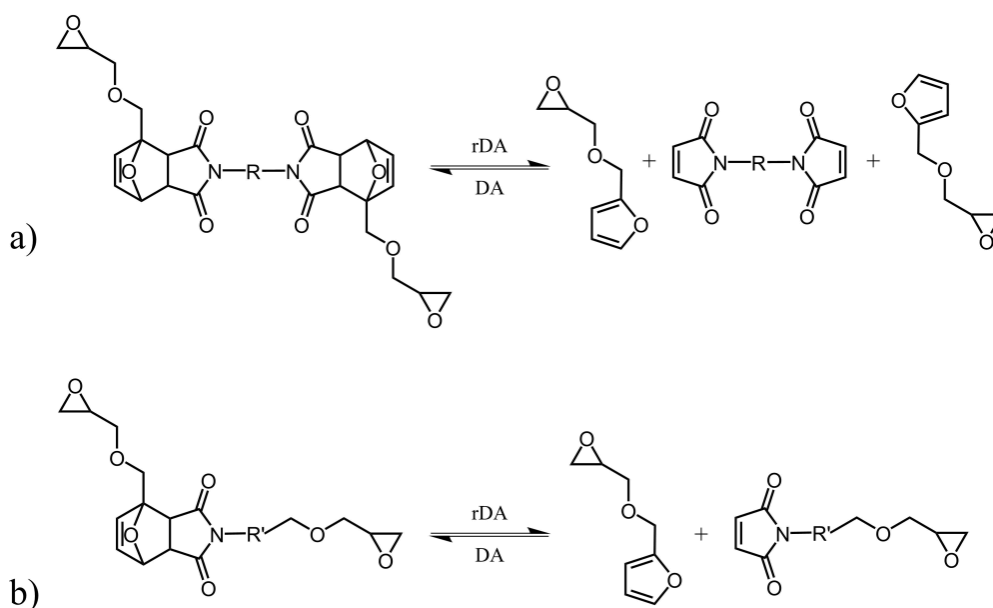
Figure 3-1. Symmetry of Diels-Alder adducts

The coexistence of a stable and a thermo-reversible polymeric network, required for the development of robust self-healing ability [5,75], is depicted in the following Figure 3-2. The hybrid polymer architecture is guaranteed by irreversible crosslinks of conventional epoxy (green oval) with tetra-functional amines (green rectangle) and reversible covalent bonds between furan derivative diene (red pincer) and bismaleimide derivative dienophile (yellow square) of a DA adduct.

The left-hand side of Figure 3-2 is representative of the crosslinked structure which prevents viscous flows. At low temperatures the material behaves like a thermoset. As the temperature is increased above the r-DA threshold trigger, the cleavage of epoxy DA activates a higher molecular mobility. Small molecular fragments, depicted in the right-hand side schematics of Figure 3-2 as result of

retro Diels-Alder reaction, symbolize distinguishing mobile state and viscous flow of thermoplastic material. Therefore, the presence of thermo-reversible chemical bonds switches the material state between thermoset-like behavior at low temperature, and thermoplastic-like flow at high temperature.
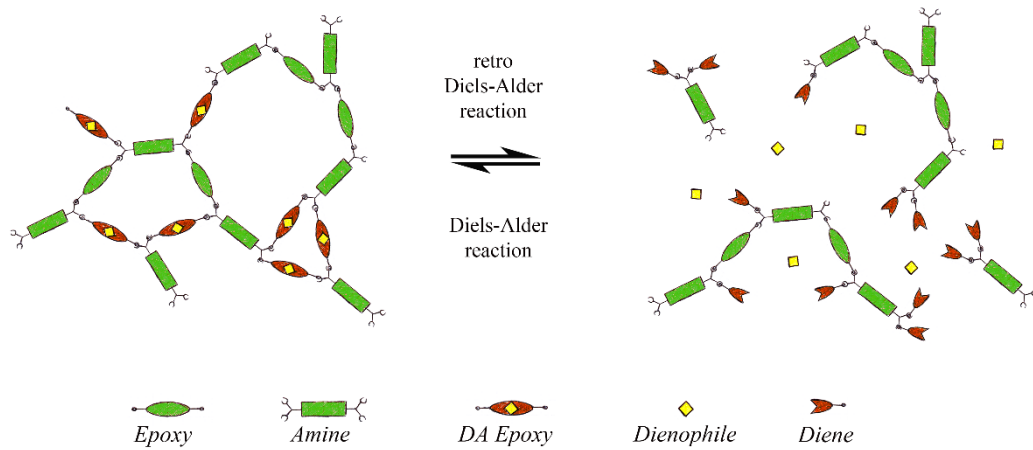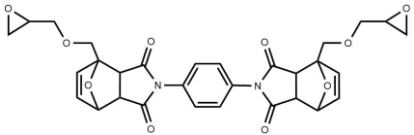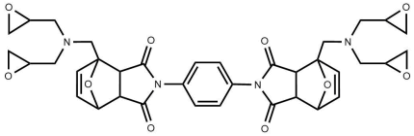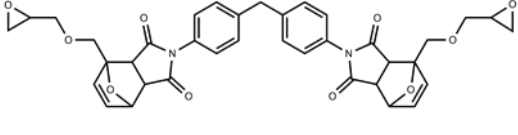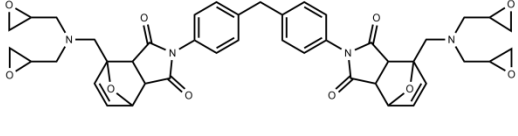
Figure 3-2. Hybrid network sheme

3.2. Synthesis of Diels-Alder precursors

A homologous family of epoxy resins containing Diels-Alder adducts was synthesized and analysed to investigate the self-healing capability of this class of thermosetting materials. The precursors were prepared with the aim to elucidate the role of main structural parameters, such as molecular stiffness and crosslinking density, on the intrinsic mending properties of cured networks.

Therefore, the epoxy precursors, reported in Table 3-1, differing for number of functional groups and flexibility of linkers between epoxy groups and central core containing DA adducts, were synthesized.

Table 3-1. Diels-Alder Epoxy prucursors

Acronym	Molecular structure	Molecular weight (gmol⁻¹)
1Ph2Epo		586.55
1Ph4Epo		696.71
2Ph2Epo		666.68
2Ph4Epo		776.84

3.2.1. Synthesis of 1Ph2Epo

*Synthesis of bis-maleimide (*Figure 3-3*)*

Maleic anhydride (544 mg, 5.6 mmol) was dissolved in acetone (15 mL). To the solution, cooled in an ice bath, was added the diamine (300 mg, 2.7 mmol) dropwise. The resulting mixture was kept under stirring, allowing the temperature to increase spontaneously. The gradual generation of an orange precipitate was observed, and after 4 hours it was filtered and washed with cold acetone. The solid residue was dried in vacuum and transferred to a round-bottom flask. It was suspended with acetic anhydride (1 mL), then sodium acetate (228 mg, 2.8 mmol) was added dropwise. The mixture was refluxed for 6.5 hours under stirring. Subsequently, the solution was cooled to room temperature and crushed ice was added to the flask. The bismaleimide was filtered, washed with cold water and dried in vacuum.
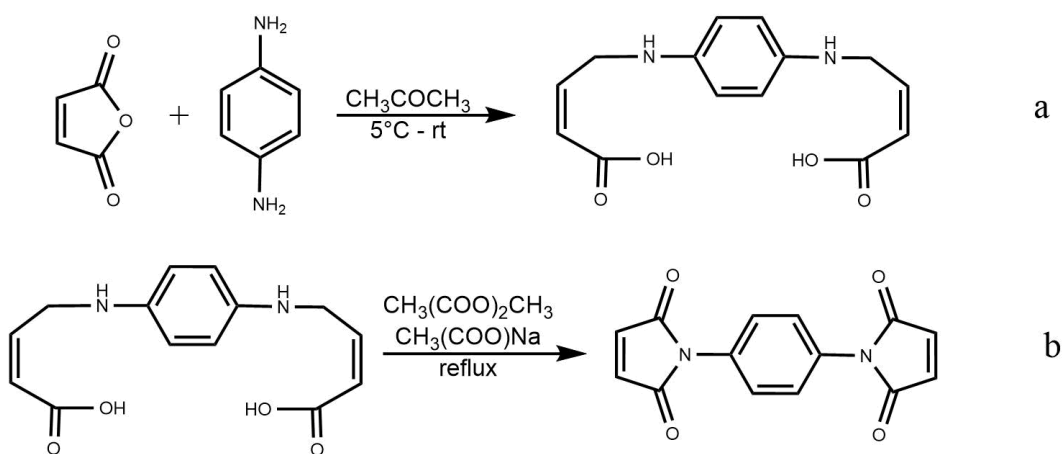
Figure 3-3. Synthetic scheme for bismaleimide from p-Phenylenediamine and maleic anhydride: formation of diamide (a) and cyclization (b)

*Synthesis of glycidyl furfuryl ethers (*Figure 3-4*)*

According to Almeida *et al.* [76], Epichlorohydrin (120 mmol) was slowly added to a cold mixture of 40% w/w aqueous sodium hydroxide (50 mL), furfuryl alcohol (30 mmol) and tetrabutylammonium bromide (1.5 mmol). The progress of the reaction was monitored by thin layer chromatography (TLC) in ethyl acetate/hexane 7/3. After completion of the reaction, the mixture was extracted

twice with ethyl acetate. The combined organic phase was dried with sodium sulphate, filtered and evaporated. The liquid was further purified by chromatography on silica gel column with ethyl acetate/hexane 7/3 as eluent: glycidyl furfuryl ether was obtained in 80% isolated yield.
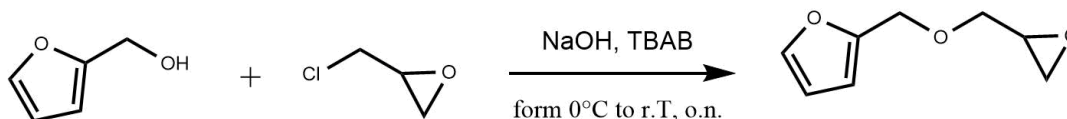
Figure 3-4. Synthetic scheme of furfuryl alcohol alkylation with epichlorohydrin

Synthesis of 1Ph2Epo (Figure 3-5)

N, N-phenylene-bismaleimide (100 mg, 0.37 mmol), was dissolved in chloroform (ca 5 mL) in a round-bottom flask, equipped with a refrigerant. Glycidyl furfuryl ether (126 mg, 0.81 mmol) was added to the solution and the flask was heated to reflux temperature. The progress of the reaction was monitored by TLC, while the reaction mixture was kept under stirring at reflux temperature for 12 hours. The product was purified by flash-chromatography on a silica gel column with 8/2 chloroform/acetonitrile mixture as eluent.
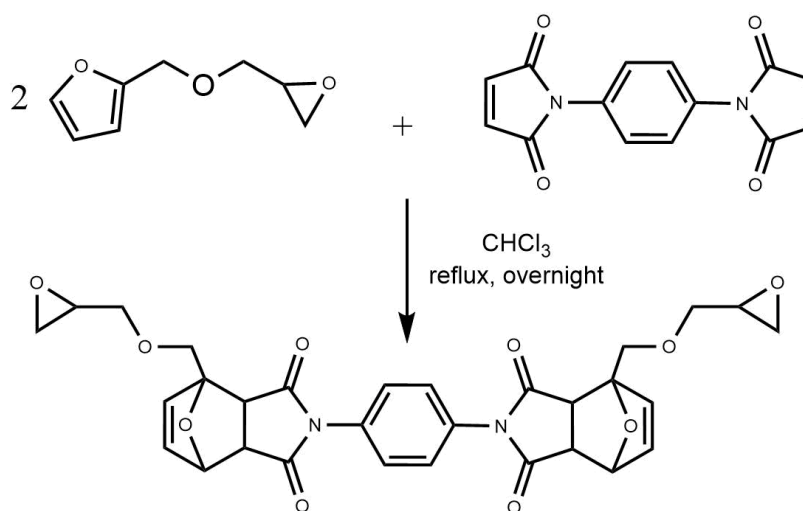
Figure 3-5. Synthetic scheme for 1Ph2Epo from *N, N*-phenylene-bismaleimide and furfuryl glycidyl ether

Synthesized epoxy adduct 1Ph2Epo was analysed by protonic nuclear magnetic resonance (^{1}HNMR), recorded in CDCl$_3$ with a Bruker 400 MHz spectrometer.

Characteristic peaks of hydrogen NMR were assigned (Figure 3-6): proton of CH in 2,5-dihydrofuran at δ (ppm) ~ 5.5 (a); protons of $CH_2=CH_2$ in furan moiety δ ~ 6.5 (b, c); protons in oxirane ring between δ ~ 2.6 e 2.8 (d, e); protons of CH_2 next to epoxy ring at δ ~ 3.3 (f); protons of C-CH_2-O δ ~ 3.6 (g); protons in C-CH-CH C=O δ ~ 3.2 (h), Ar-H at δ ~ 7.5 (i).
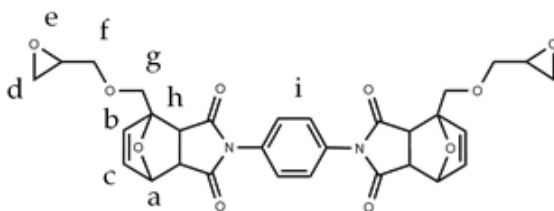
Figure 3-6. Protonic nuclear magnetic resonance peaks assignation for 1Ph2Epo adduct

3.2.2. Synthesis of 1Ph4Epo

Synthesis of diglycidyl furfuryl amine (Figure 3-7)

Epichlorohydrin (1 mol) was stirred and heated to 40°C in a 250 mL round-bottom flask equipped with a condenser. Furfuryl amine (0.5 mol) was added dropwise and the reaction mixture was stirred for 5 h at 40°C, then cooled down to room temperature. Aqueous sodium hydroxide (160 mL, 50%w/v NaOH) was added slowly. The reaction was continued for additional 12 hours at 30°C. NaCl was extracted with water from the organic phase, and the solvent evaporated under vacuum. The liquid was further purified by flash-chromatography on a silica gel column using a 7/3 chloroform/acetonitrile mixture as the eluent. Glycidyl furfuryl amine was isolated in 80% yield.
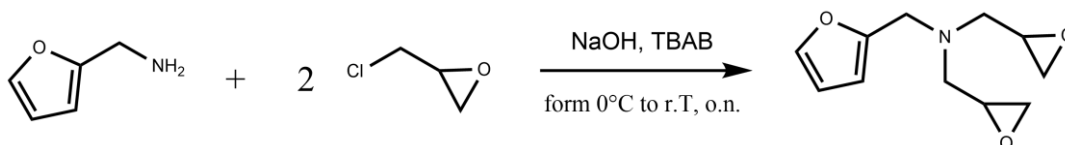
Figure 3-7. Synthetic scheme for furfuryl amine alkylation with epichlorohydrin

Synthesis of 1Ph4Epo (Figure 3-8)

N, N- phenylene-bismaleimide (184 mg, 0.68 mmol), synthetized according the scheme in Figure 3-3, was dissolved in chloroform (5 mL) in a round-bottom

flask, equipped with a refrigerant. Diglycidyl furfuryl ammine (2.2 eq, 1.5 mmol) was added to the solution and the flask was heated to reflux temperature. The progress of the reaction was monitored by TLC, while the reaction mixture was kept under stirring at reflux temperature for 12 h. The product was purified by flash-chromatography on a silica gel column with 8/2 chloroform/acetonitrile mixture as eluent.
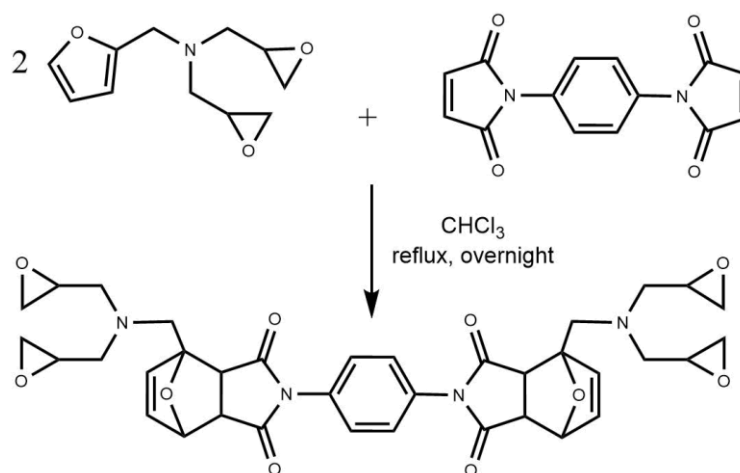
Figure 3-8. Synthetic scheme of the DA adduct 1Ph4Epo from N, N- phenylene-bismaleimide and furfuryl diglycidyl amine

Characteristic peaks of hydrogen NMR and their integration values confirm the chemical structure of 1Ph4Epo. ^{1}HNMR (CDCl3): proton of CH in 2,5-dihydrofuran at δ (ppm) ~ 5.4; protons of $CH_2=CH_2$ in furan moiety δ ~ 6.4; protons in oxirane ring between δ ~ 2.6 e 2.8; protons of CH_2 next to epoxy ring at δ ~ 3; protons of $C-CH_2-N$ δ ~ 2.9; protons in C-CH-CH C=O δ ~ 3.1; Ar-H at δ ~ 7.3.

3.2.3. Synthesis of 2Ph2Epo

1,1'methylenedi-4,1-phenylene-bismaleimmide (31.1 mmol) was dissolved in chloroform (10-12 mL) in a 250 mL round-bottom flask equipped with a refrigerant. Glycidyl furfuryl ether (2.2 eq, 68.5 mmol), according to Figure 3-4, was added to the solution and the flask was heated to reflux temperature. The progress of the reaction was monitored by TLC and the reaction mixture was

kept under stirring at reflux temperature for 12 h. The product was purified by flash-chromatography on a silica gel column using 8/2 chloroform/acetonitrile mixture as eluent.
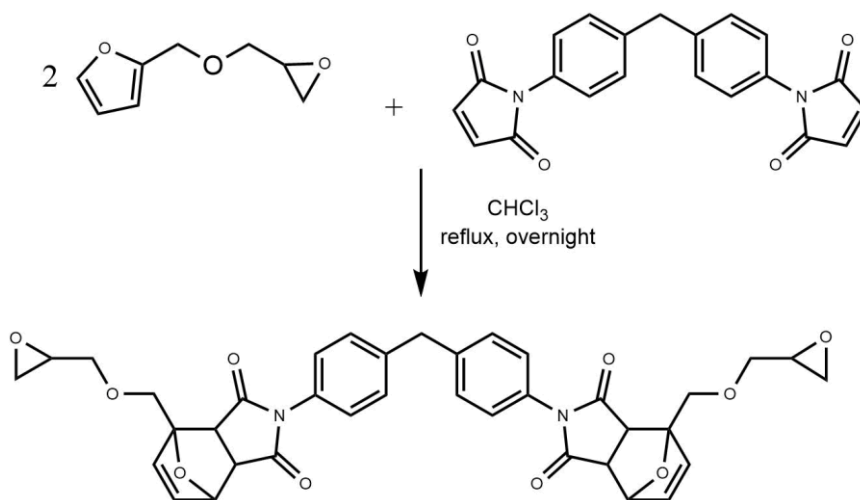
Figure 3-9. Synthesis of the DA adduct 2Ph2Epo from 1,1'methylenedi-4,1-phenylene-bismaleimide and furfuryl glycidyl ether

Analysis ^{1}HNMR recorded in d6-CDCl3 on a sample previously purified by column chromatography confirmed the product structure.

Characteristic peak of DA adduct: proton of CH in 2,5-dihydrofuran (at $\delta \sim 5.4$), where the carbon atom changes from sp2 to sp3 hybridization. A double peak slightly splits for the formation of the two stereoisomers, *endo* and *exo*, with the first overwhelming the second. Furthermore, protons of $CH_2=CH_2$ in furan moiety $\delta \sim 6.5$; protons in oxirane ring between $\delta \sim 2.6$ e 2.8; proton of CH_2 next to epoxy ring at $\delta \sim 3.2$; protons of C-CH_2-O $\delta \sim 3.8$; protons in C-CH-CH C=O $\delta \sim 3.2$; Ar-H at $\delta \sim 7.3$; protons in CH_2 between benzyls $\delta \sim 4$.

3.2.4. Synthesis of 2Ph4Epo

1,1'methylenedi-4,1-phenylene-bismaleimmide (12.3 mmol) was dissolved in chloroform (10-12 mL) in a 250 mL round-bottom flask equipped with a refrigerant. Glycidyl furfuryl ammine (2.2 eq, 27 mmol), according to scheme in Figure 3-7, was added to the solution and the flask was heated to reflux temperature. The progress of the reaction was monitored by TLC and the reaction

mixture was kept under stirring at reflux temperature for 12 h. 2Ph4Epo was purified by flash-chromatography on a silica gel column using 8/2 chloroform/acetonitrile mixture as eluent.
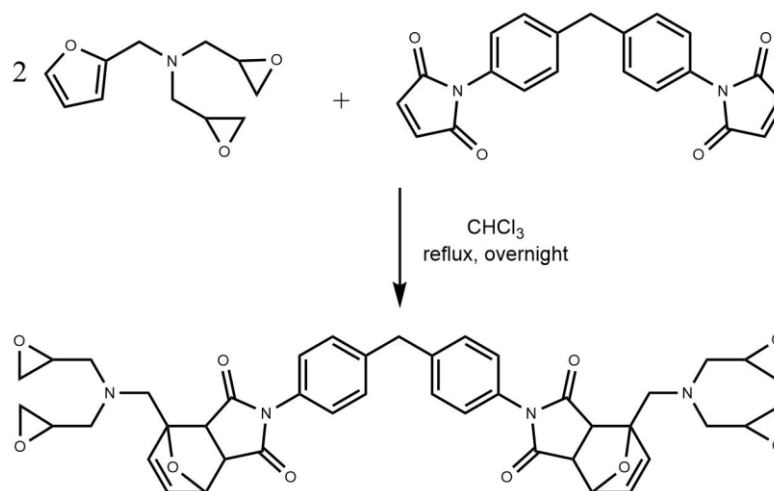

Figure 3-10. Synthesis of the DA adduct 2Ph4Epo from 1,1'methylenedi-4,1-phenylene-bismaleimide and furfuryl diglycidyl amine

^{1}HNMR recorded in d6-CDCl3: proton of CH in 2,5-dihydrofuran at δ (ppm) ~ 5.4; protons of $CH_2=CH_2$ in furan moiety δ ~ 6.5; protons in oxirane ring between δ ~ 2.5 e 2.7; protons of CH_2 next to epoxy ring at δ ~ 3; protons of C-CH_2-N δ ~ 2.9; protons in C-CH-CH C=O δ ~ 3.2; Ar-H at δ ~ 7.3; protons in CH_2 between benzyls δ ~ 4.

3.3. Selection criteria for Diels-Alder adducts

All synthesized Diels-Alder adducts are crystalline solids, but 1PhxEpo (1Ph2Epo and 1Ph4Epo) have a melting point that exceeds the onset of degradation.

Moreover, the melting points of the precursor dienophiles of 1PhxEpo and 2PhxEpo (2Ph2Epo and 2Ph4Epo) are also very different: N, N' - (1,4-phenylene) dimaleimide and 1,1 '- (methylenedi-4,1-phenylene) bismaleimide have melting points > 300°C and 158°C, respectively.

This different structural characteristic, also found in the corresponding DA adducts, implies a different propensity to Diels-Alder reaction.

In fact, the inability of the 1Ph2Epo and 1Ph4Epo adducts to reform the Diels-Alder bonds, once cleaved by r-DA reaction, even if subjected to adequate thermal stimulus, was observed by optical microscopy.

N, N' - (1,4-phenylene) dimaleimide, in the crystalline phase, tends to segregate and not react again with the furan derivative (diene in the Diels-Alder reaction). Although it was possible to mix the different maleimides (1PhXEpo and 2PhXepo) in any proportion, as a strategy to depress the crystalline phase, for the sake of simplicity it was preferred to continue the study exclusively with 2PhXEpo.

3.4. System formulation and mixture preparation

Chen *et al.* reported the occurrence of an endothermic event at temperature higher than 120°C, associated to the retro Diels-Alder reaction [47]. The pristine molecular structure can be restored by annealing at 90°C. This evidence was used to properly formulate the crosslinking mixture. In fact, the curing temperature cannot exceed the r-DA activation temperature, so as not to incur in the temporary scission of epoxy precursor. Analogously, the glass transition temperature of crosslinked resin cannot exceed curing temperature, in order to prevent vitrification during curing.
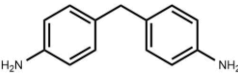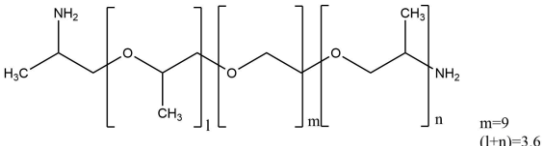
Indeed, Diels-Alder is a well-known reversible reaction [69,71]. The direct DA is predominant at temperatures lower than 90°C, while its reverse, r-DA, activates at higher temperatures. The intrinsic self-healing DA mechanism is based on temperature driven equilibrium of Diels-Alder reaction. Therefore, it is worth emphasizing that the r-DA reaction is beneficial for the occurrence of self-healing, but it is highly detrimental if it happens before crosslinking. If this were the case, splitting the epoxy adduct into its precursors would allow a side reaction, *i. e.* Michael addition between NH_2 group of amine and $CH_2=CH_2$ of imide, thus reducing the healing efficiency.

Generally, epoxy precursors react with several available nucleophiles, such as primary and secondary amines, acids and alcohols. The most widely used epoxy curing agents are amines and anhydrides. The presence of rigid and planar aromatic rings results in crosslinked resin with high glass transition temperature. The epoxy and amine groups have to be carefully stoichiometrically balanced in order to achieve high fractional conversion and a chemically stable crosslinked system. Primary aliphatic amines react more readily with epoxy resins with respect to aromatic amines. In addition, their low melting point increase even further the ability to react at low temperatures. The reaction path of anhydrides with epoxies is quite complex, because the hydroxyl groups formed by the

cleavage of oxirane rings and carboxylic acids formed by the opening of anhydrides can react with available epoxy groups. Hence, a strict stoichiometric balance between epoxy and anhydride is not required.

Therefore, a mixture of aromatic and aliphatic amines was exploited to set glass transition temperature of crosslinked resin around 90°C. In particular, 4,4′-diaminodiphenylmethane (DDM) and O, O′-bis(2-aminopropyl) polypropylene glycol-block-polyethylene glycol-block-polypropylene glycol (Jeff 500) were used, as curing agents, according to composition described in Table 3-2.

Table 3-2. Curing agent components and stoichiometric relationships

Acronym	Molecular structure	composition (% mol)
DDM		60
Jeff 500		40

In order to develop materials with robust thermo-stability and efficient self-healing ability, the coexistence of a stable polymeric network and a thermo-reversible one is required, for the formation of a hybrid polymer architecture. Diene/dienophile functionalities infer the self-healing property, while epoxy/amine bonds guarantee the three-dimensional macromolecular network in the homogeneous resin.

In order to obtain an epoxy mixture formulation with a crosslinking density of the cleaved stage corresponding to a determinate molecular mobility, Diels-Alder epoxy adduct was also mixed with conventional epoxy diglycidyl ether of bisphenol A (DGEBA) in Figure 3-11.
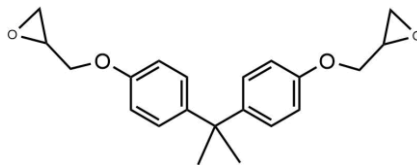
Figure 3-11. Diglycidyl ether of Bisphenol A (DGEBA)

The Diels-Alder epoxies, 2Ph2Epo, 2Ph4Epo, and their mixture with DGEBA, were stoichiometrically balanced with DDM and Jeff 500, as curing agents.

Due to the presence of solid crystalline compounds, coupled with the need to operate at low temperatures, the use of a solvent-assisted high-shear mixing procedure was required. The addition of solvent during the mixing of all the components of the mixture is of great benefit for a homogeneous dispersion. Acetonitrile, CH_3CN, was selected as the most suitable solvent, based on the solubility of the components and the low boiling temperature (82°C). The solvent, added in the minimum possible quantity (1 mL per gram of formulation) is mixed using a Thinky planetary mixer (2 min, 1000 rpm, P = 100.02 KPa); subsequently carefully evaporated with a vacuum cycle of the same mixer (5 min, 800 rpm, P ~ 0.2KPa). All the systems, whose composition is shown in Table 3-3, were treated in oven at 90°C for 24 hours (Figure 3-12).
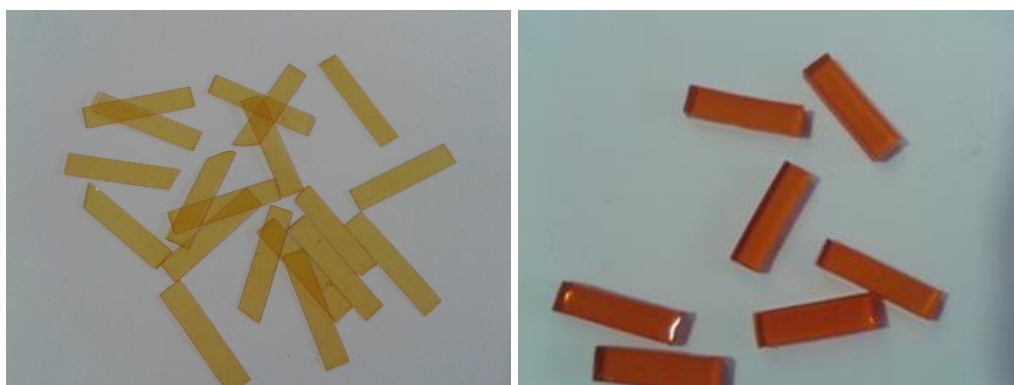
Figure 3-12. Crosslinked resin samples

Table 3-3. Crosslinked resin composition

Acronym	DA epoxy (mol)	DGEBA (mol)	DDM (mol)	Jeff 500 (mol)
2Ph2Epo100	1.00	-	0.30	0.20
2Ph2Epo65	0.65	0.35	0.30	0.20
2Ph4Epo100	1.00	-	0.60	0.40
DGEBA100	-	1.00	0.30	0.20

3.5. Case studies

A bifunctional epoxy precursor, named 2Ph2Epo, a tetrafunctional epoxy one, 2Ph4Epo, with a molecular weight of 666.68 gmol^{-1} and of 776.84 gmol^{-1} respectively, were investigated. In both cases, to induce the self-healing capability, two identical dienes (furfural derivatives) were capped on a bismaleimide dienophile, resulting in symmetrical epoxy compounds containing two Diels-Alder adducts.

The Diels-Alder epoxies 2Ph2Epo, 2Ph4Epo, and their mixture with DGEBA were crosslinked using DDM and Jeff 500 as curing agents (Table 3-3), at 90°C for 24 hours.

Hence, the work has been focused to investigate the effects of different structural features, such as average number of crosslinking functionality and molecular flexibility of epoxy precursors, on the material performances and the efficiency of healing process to recover the pristine properties after a mechanical damage. Nanoindentation was used in order to investigate the elastic modulus of cured material. The reduced elastic modulus, E_r, was calculated based on equation 3-2, taking into account the effect of non-rigid indenter column:

$$E_r = \frac{\sqrt{\pi}S}{2\beta\sqrt{A}} = \left(\frac{(1-\nu_i^2)}{E_i} + \frac{(1-\nu_s^2)}{E_s}\right)^{-1} \qquad 3\text{-}2$$

where A is the contact area, β the geometric constant (1.034 for a Berkovich indenter) and S the unloading stiffness at maximum load. E and ν are the elastic modulus and the Poisson ratio; and the subscripts "i" and "s" refer to the diamond indenter and the specimen, respectively. The E_i is 1140 GPa, ν_i is 0.07 and the ν_s is 0.35.

Nanoindentation tests were performed with Micro Materials Ltd NanoTest Platform, in load-controlled mode: ten different indentation loads ranging from 50 mN to 250 mN were carried out. Data were corrected for thermal drift and

instrument compliance and subsequently analysed with the Oliver and Pharr method [77]. Maximum depth was limited to less than 50 µm, corresponding to 10% of sample thickness, in order to avoid substrate interference to the measure. In Table 3-4 measured values of reduced modulus are reported. The values measured for the three set of samples are similar and close to those expected for a conventional epoxy thermoset. Therefore, the elastic modulus, to which the reduced modulus can be related, does not represent a discriminating element for the choice of the Self-Healing epoxy system.

Table 3-4. Nanoindentation tests for DA resins

Specimen Type	Reduced Modulus [GPa]
2Ph2Epo100	3.52±0.15
2Ph2Epo65	3.85±0.13
2Ph4Epo100	3.91±0.19

The observation of superficial scratches and their recovery is a generally accepted technique for the assessment of self-healing features. As already discussed, the self-healing capability of small fractures and BVID is related to local molecular mobility, temporarily activated by temperature increase.

For this task, a controlled mark has been produced by sharp scalpel and observed by optical microscopy (Olympus BX 51 M), applying suitable thermal stimulus by means of Linkam THM600 hot stage.

As expected, microscopy observation performed on cross-linked DGEBA resin cured with a mixture of 60/40 mol/mol of DDM and Jeff 500 amines (DGEBA100, $T_g = 90°C$) evidenced the lack of scratch recovery even at 140°C (Figure 3-13), well above sample T_g.
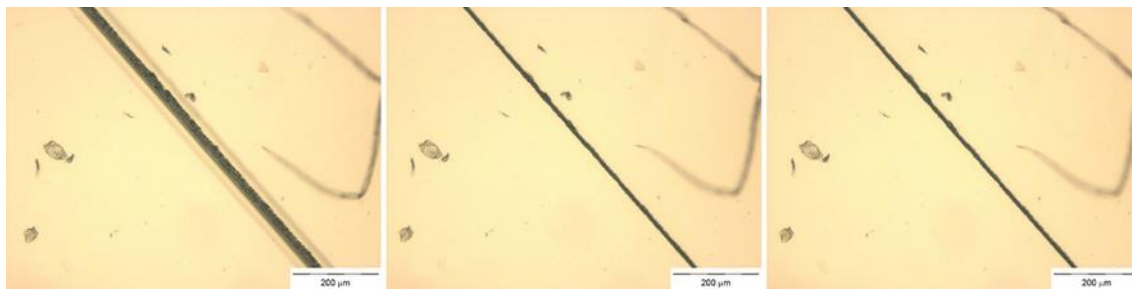
Figure 3-13. Scratch recovery for DGEBA100, 10X magnification. From left to right: at room temperature, at 140°C, after additional annealing for 20 min at 140°C

Only a minor modification of scratch width can be detected as a result of stress relaxation at temperature higher than resin T_g: self-healing is hindered by cross-links. Instead, thermal treatment at 120°C for 5 minutes completely restored the damaged surface of 2Ph2Epo100 sample, as depicted in Figure 3-14. Unfortunately, the high molecular mobility achieved in the activated stage produced sample deformation and viscous flow. In fact, due to the high concentration of reversible bonds, the cross-linking density in the cleaved stage dropped, and materials transformed into viscous thermoplastic.
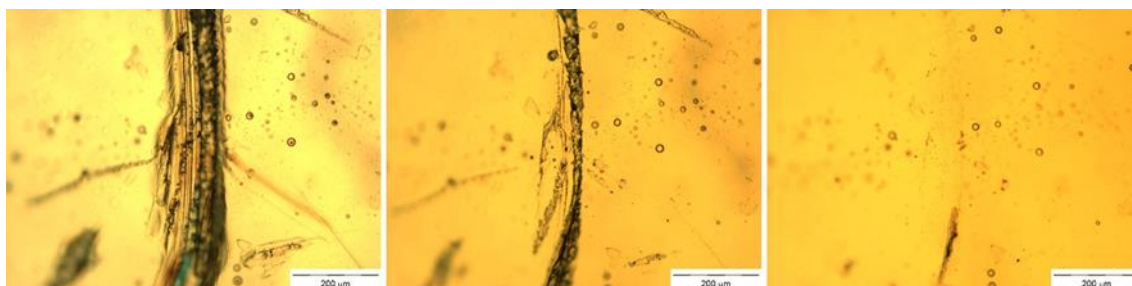
Figure 3-14. Scratch recovery for 2Ph2Epo100, 10X magnification. From left to right: at room temperature, at 120°C, after additional annealing for 5 min at 120°C

The occurrence of this phenomenon is not desirable if self-healing materials have to be used for structural application and the molecular mobility has to be reduced, either by introducing a thermally stable epoxy precursor such as DGEBA or by using a tetrafunctional DA precursor. In the first case, the 2Ph2Epo65 system, containing 65% of DA epoxy and 35% of DGEBA (Table 3-3), was prepared, with T_g of 88°C. Self-healing capability of 2Ph2Epo65 was confirmed despite of the reduction of thermo-reversible bond concentration. The

increased network stability preserved the sample shape and dimension, still allowing self-healing phenomenon, as reported in Figure 3-15. The scratch completely disappeared after 20 min at 120°C, restoring the pristine surface.
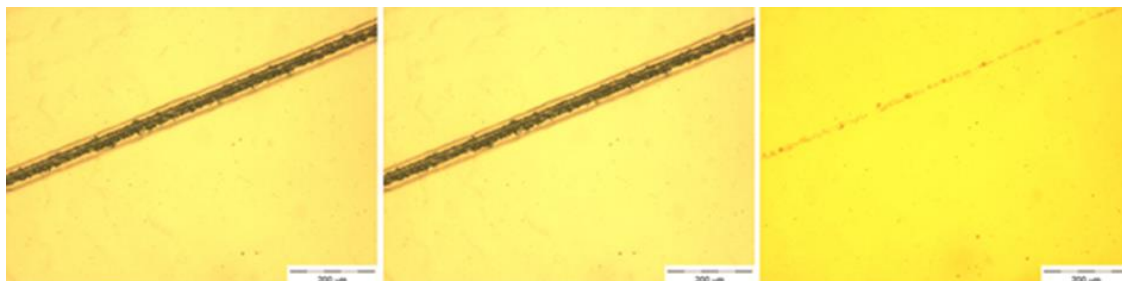
Figure 3-15. Scratch recovery for 2Ph2Epo65, 10X magnification. From left to right: at room temperature, at 120°C, after additional annealing for 20 min at 120°C

The second approach to prevent viscous flow of materials during the high-temperature stage is to use Diels-Alder epoxy adduct with functionality higher than 2. The presence of four reacting epoxy groups for each precursor molecule (2Ph4Epo) increases the cross-linking density. 2Ph4Epo100 was prepared according to Table 3-3. Crosslinked resin composition was crosslinked and fully cured at 90°C for 24 hours, reaching a T_g of 95°C. The occurrence of r-DA reaction reduces the cross-linking density at high temperature, as always happens. But the f_{avg} calculated in the cleaved state for tetrafunctional DA epoxy is 2.67 and suggests hindered molecular mobility, as already discussed. Consequently, morphological damages were not recovered for 2Ph4Epo100 (Figure 3-16).
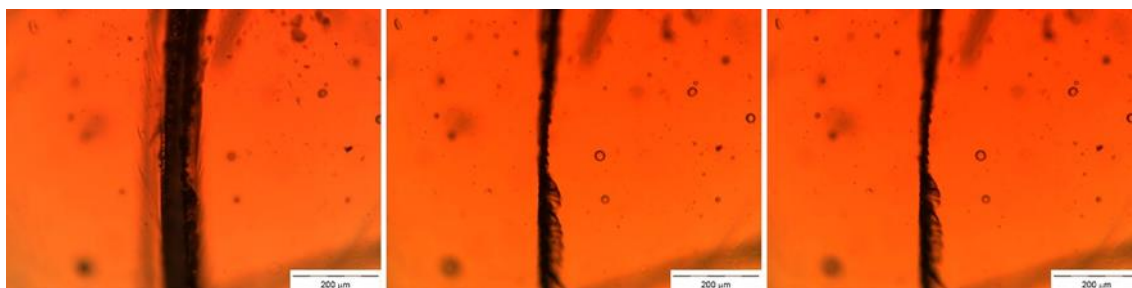
Figure 3-16. Scratch recovery for DGEBA2Ph4Epo100, 10X magnification. From left to right: at room temperature, at 120°C, after additional annealing for 20 min at 120°C

4. Synthesis and Properties of 2Ph2Epo65 thermo-reversible epoxy

As already discussed, the presence of thermo-reversible DA adducts allows healing of mechanical damages. Healing mechanism is intrinsically associated to the presence of diene and dienophile pairs, either *in-situ* spontaneously generated during damage or produced by suitable temperature treatment above the r-DA temperature.

The assembly of healable epoxy resins based on Diels-Alder chemistry requires the coexistence of both diene/dienophile and epoxy/amine reactive functionalities, where the former infer the self-healing property and the latter the three-dimensional macromolecular network. Hence, a careful balance has to be achieved during resin formulation. By selecting constituents is possible to address final properties of an epoxy-based system to fulfil specific applications, such as structural bulk materials, adhesives, waterproofing and dielectric insulation. Within this framework the insertion of DA adduct into an epoxy system could combine exceptional mechanical properties with mendable capability.

A hybrid epoxy resin with intrinsic self-healing properties has been prepared from bifunctional 2Ph2Epo Diels-Alder adduct. Indeed, the proposed 2Ph2Epo meets all the requirements and can be mixed with DGEBA in all percentages. As

already noted, if epoxy resin is 100% composed of 2Ph2Epo DA adduct, self-healing behavior is maximized, but consequently, poor thermal and mechanical stability are determined. On the other hand, if epoxy resin is 100% composed of DGEBA, the lack of DA adducts in the mixture prevents any self-healing behaviour, corresponding to a conventional formulation.

The suitable mixture, named 2Ph2Epo65, of 2Ph2Epo and DGEBA has been cured with DDM and Jeff 500 amines, according to Table 3-3. It is noteworthy to mention that the general approach described in literature consists in either the simultaneous DA formation and nucleophilic attack of amine onto epoxy [53], or preliminary reaction of amines with furfuryl glycidyl ether, followed by crosslinking with a proper bismaleimide [78]. While, according to our procedure, 2Ph2Epo adduct is first synthesized (Figure 3-9), then mixed and crosslinked with other components, in order to prevent side reactions.

In this chapter, the selected DA adduct (2Ph2Epo) has been more extensively characterized, and the most promising formulation of thermo-reversible epoxy system (2Ph2Epo65) has been discussed and experimentally investigated. Results reported a satisfactory morphological recovery: the induced damages disappear after thermal healing by treating the epoxy resin for 20 minutes at 140°C. Spectroscopic analysis, IR and Raman, revealed that the crosslinked mixtures of self-healing adduct and commercially available DGEBA kept the capability to recover damages after the crosslinking. The typical vibrational modes characterizing the presence of broken/healed molecules have been recognized in the 2Ph2Epo65 system after each heat treatment. The multiple healing feature of the system was proved by mechanical tests performed on undamaged and healed system. The hybrid epoxy resin resulted able to recover damages, still exhibiting the pristine stiffness (mean value 2.75 GPa), while the strength of the system decreases after progressing healing cycles.

4.1. 2Ph2Epo Adduct

The selected DA adduct has been more extensively characterized. Thermal analysis of the 2Ph2Epo adduct samples was performed by differential scanning calorimetry (DSC) with DSC Discovery of TA Instruments: previously melted in an aluminium pan, 2Ph2Epo has been tested at 10°C/min up to 140°C to identify the occurrence of direct and reverse DA reactions. The DSC thermogram (Figure 4-1) shows three separate phenomena at 40°C, 100°C and 125°C, respectively.
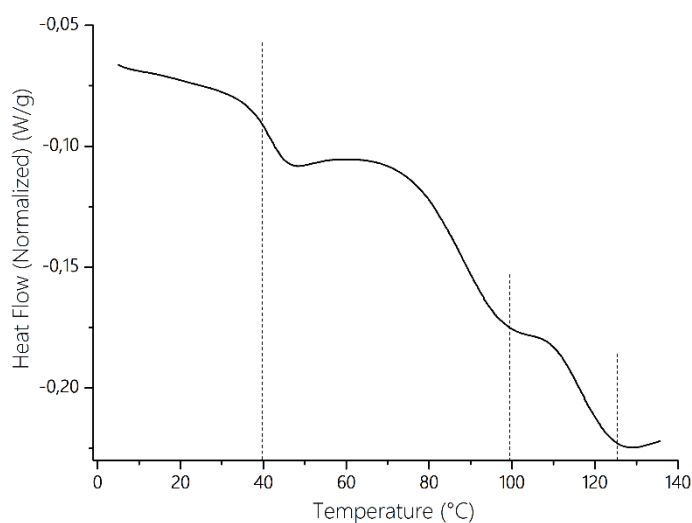
Figure 4-1. DSC analysis of the 2Ph2Epo adduct

The first was associated to the softening transition of pure 2Ph2Epo adduct. The second and third endothermic phenomena can be attributed to r-DA reactions, according to Froidevaux *et al.* [79]. The authors reported that DA reaction of furan and maleimide derivatives leads to formation of a mixture of two diastereomers: a kinetic compound, named *endo*, and a more stable thermodynamic compound, named *exo*. The *endo* compound is the first to be unblocked, fixing the onset of r-DA reactions.

NMR spectrum of 2Ph2Epo confirms the presence of two diastereomers, *exo* and *endo*, with the first overwhelming the second. Furthermore, the inversion of stereoisomers concentration after heating 2Ph2Epo at 120°C and subsequent

cooling to room temperature evidenced the occurrence of r-DA and DA recombination.

Rheology represents a suitable investigation tool to evaluate the melt state behavior based on the complex morphology exhibited by the studied materials. Linear viscoelastic measurement allows probing into the dynamics of the samples without affecting their microstructure. Rheological tests were performed using a strain-controlled rotational rheometer (AR-G2 supplied by TA Instruments) in parallel plates geometry with 25 mm diameter plates. The complex viscosity of 2Ph2Epo was monitored at frequency $\omega = 1$ Hz, while the sample was cooling from T = 120°C down to T = 90°C (–5°C/min, equilibration time 1 min). This allowed to appreciate changes in the adduct molecular weight due to the DA reactions.

Indeed, the fact that thermo-reversible bonds influence molecular mobility [80] suggests the use of rheological techniques to detect the onset of the DA reaction [81]. Figure 4-2 reports the cooling step for the 2Ph2Epo after an isothermal hold at 120°C for 20 minutes. The complex viscosity shows the expected inverse dependence on the temperature. However, the material exhibits a distinctive change of the temperature dependence of the complex viscosity during the cooling ramp. This is related to the occurrence of the direct DA reaction at 105°C, which causes a progressive change in the adduct molecular weight. In particular, the rheological behavior clearly shows two materials status: above 105°C the material is characterized by lower molecular weight because the DA bonds are completely cleaved, while below the critical 105°C temperature an higher molecular weight is achieved as an effect of the DA adduct reformation [82]. Thermo-reversible bonds allow the reconfiguration of material when the r-DA and DA reactions are triggered by thermal stimuli and, as a result, the material's fluidity increases and decreases, respectively.
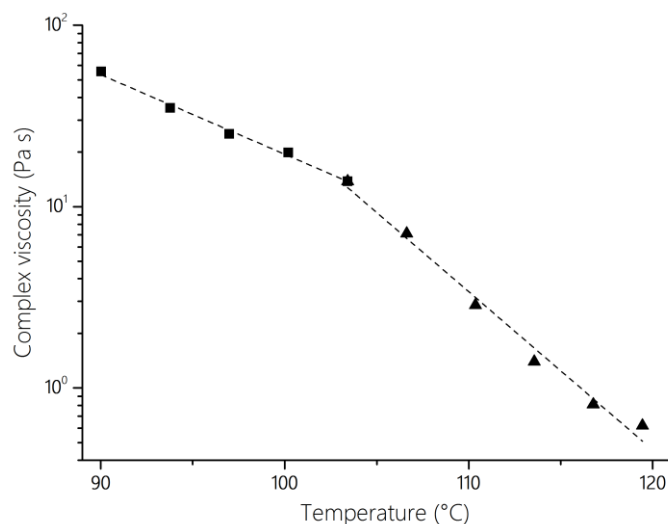
Figure 4-2. Complex viscosity (ω = 1 Hz) of the 2Ph2Epo adduct during cooling stage

Fourier Transform Infrared Spectroscopy (FT-IR) analysis was performed to identify and interpret the temperature-dependent spectral changes within the DA adduct. A Perkin Elmer Frontier spectrophotometer has been used to measure the absorbance of the materials in attenuated total reflectance (ATR) in the mid-infrared range. Figure 4-3 reports FT-IR spectra recorded on 2Ph2Epo adduct, in the pristine and cleaved configuration, as a consequence of different thermal treatments. As an invariant reference, the peak at 1700 cm^{-1} associated to C=O stretching of imide was chosen. Three signals have been selected to monitor the progress of DA and r-DA reactions: the IR absorbance signals at 688 cm^{-1} associated to C=C stretching vibration in the maleimide ring, the peak at 832 cm^{-1} related to the C–O–C stretch in furan ring, and the peak at 1146 cm^{-1} associated to C–H bond attached to C=C.

The comparison between the spectra shows the presence of bands at 1146, 832 and 688 cm^{-1} in the open configuration b, while the same absorption bands are absent in the spectrum a, related to the as prepared DA adduct.

The treatment at 120°C promotes the r-DA reaction and the intensities of these three absorption peaks increase. In fact, the DA bond cleavage leads to the formation of DA precursors, with available furan and maleimide groups.
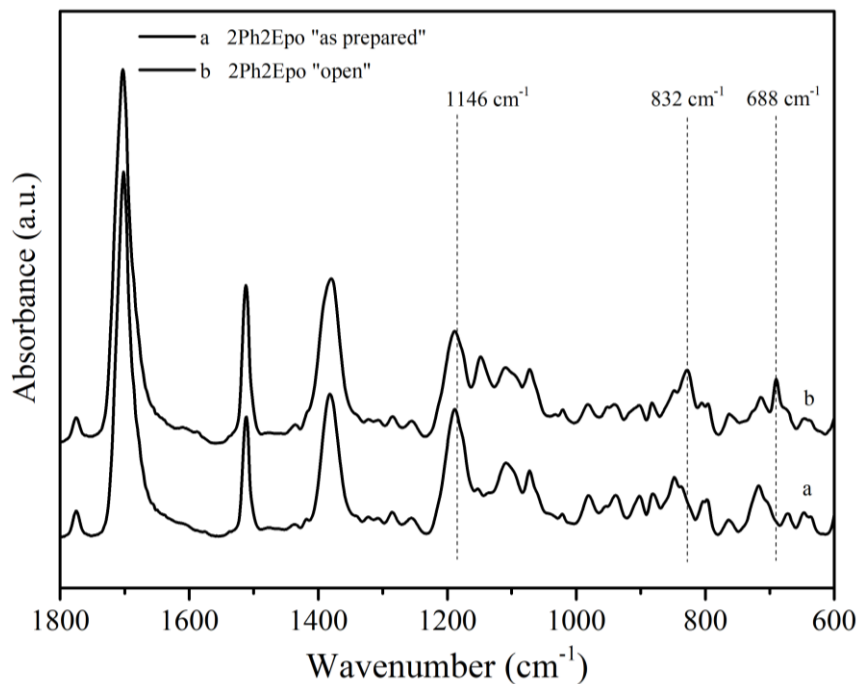
Figure 4-3. FT-IR spectra for the 2Ph2Epo adduct: (a) as prepared; (b) open (thermally treated 20 min at 120°C)

4.2. 2Ph2Epo65 system: formulation and properties

Based on the previous assumptions, the best compromise between self-healing ability and physical-chemical properties has been achieved with 2Ph2Epo-DGEBA and DDM-Jeff 500, containing an epoxy molar ratio of 65/35 between 2Ph2Epo and DGEBA.

After preliminary screening for curing agent selection, based on T_g of resulting cured resins, a mixture of DDM and Jeff 500, 60/40 by mol, has been adopted.

The 2Ph2Epo-DGEBA (65:35) + DDM-Jeff 500 (60:40) mixture has been reacted at 90°C and the extent of curing monitored by DSC. At the end of crosslinking, T_g reaches the value of 88°C and no further residual reaction is recorded during the first heating scan, as shown in Figure 4-4. At higher temperatures a broad endothermic phenomenon is observed during DSC scan at 123°C, related to occurrence of r-DA reaction [83].
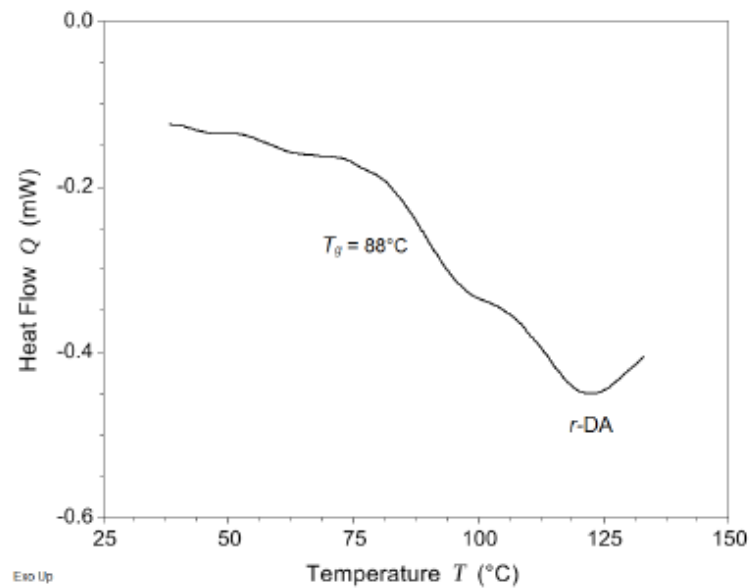
Figure 4-4. DSC thermogram of 2Ph2Epo65 resin system

A full rheological study at room temperature up to 90°C was performed to evaluate the suitability of the developed reversible resins in traditional manufacturing processes. It was found that the viscosity of hybrid epoxy system

is compatible with liquid infusion and pre-preg techniques traditionally used in the manufacturing of fiber composites.

The ulterior analysis of rheological properties during an isothermal test allowed identifying the process window for composite manufacturing, thereby defining the maximum time and temperature for handling the polymer before onset of crosslinking. Figure 4-5 shows the rheological response of the 2Ph2Epo65. The onset of crosslinking, gel point, is clearly evident as the cross-over of storage and loss moduli, in an isothermal step at 90°C.
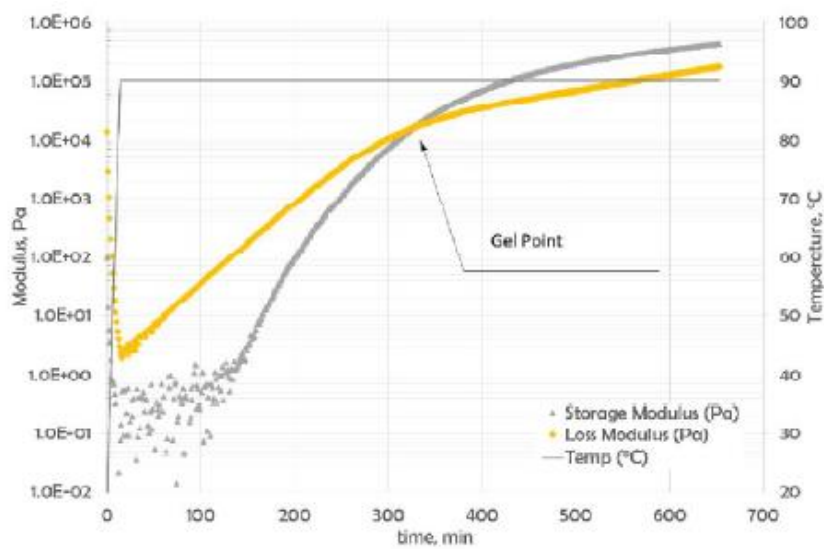
Figure 4-5. Complex viscosity of hybrid epoxy resin 2Ph2Epo65

4.3. 2Ph2Epo65 self-healing assessment by Ft-IR and Raman molecular spectroscopies

In this section, FT-IR analysis was performed to verify that the final system is able to recover damages. To simulate a failure event, the material was kept at the temperature of 120°C to promote the opening of all thermo-reversible bonds. Figure 4-6 reports FT-IR spectra of 2Ph2Epo65 crosslinked resin, as prepared, in open and in healed configurations, induced by different thermal treatments. As an invariant reference, the peak at 1700 cm^{-1}, associated to C=O stretching of maleimide, was chosen.
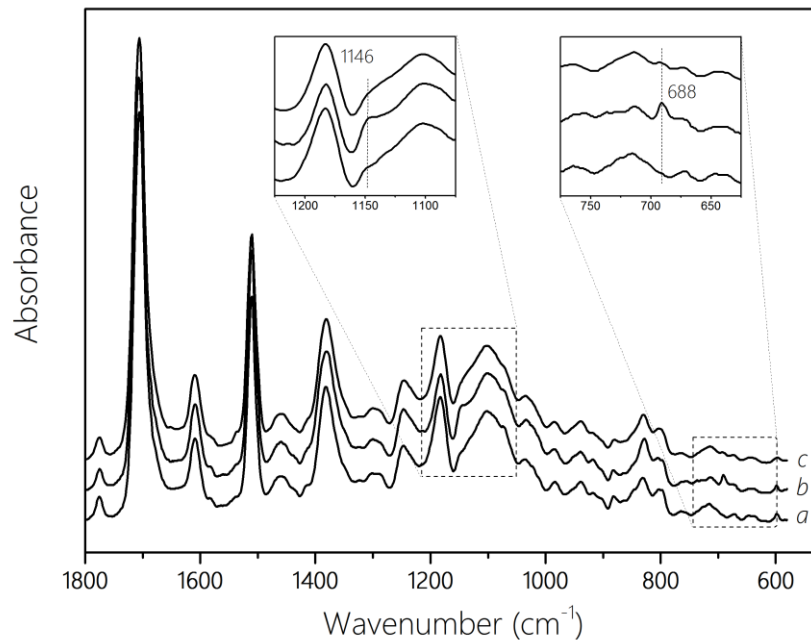
Figure 4-6. FT-IR spectra for the 2Ph2Epo65 crosslinked system: undamaged system (a); thermally treated 20 min at 120°C (b); after additional cooling to 90°C at 0.1°C/min (c)

The IR absorbance signals at 688 and 1146 cm^{-1} were selected to monitor the progress of DA and r-DA reactions. The peak at 688 cm^{-1} is related to C=C stretching vibration in the maleimide ring and the peak at 1146 cm^{-1} is associated to C–H bond attached to C=C. The spectra were recorded on the crosslinked epoxy system in three different states: (a) as prepared sample, (b) after heating at 120°C for 20 minutes and quenching at room temperature, (c) after heating at

120°C and cooling to 90°C at 0.1°C/min rate. The most accurate information can be gained observing the trend of 688 cm^{-1} peak. It can be found in the (b) sample, after thermal treatment at 120°C, while it is missing in the pristine crosslinked resin (a) and it disappears again after the complete healing cycle (c). A similar trend can be identified for the 1146 cm^{-1} band, although its observation is hindered by the presence of other complex spectrum features. After the treatment at 120°C, promoting the r-DA reaction, the intensities of these two absorption peaks increased due to DA adduct rupture. A further annealing at 90°C following the heat treatment at 120°C, strongly reduced the aforementioned peaks, resulting in a FT-IR spectrum similar to the "as prepared" sample. This is a strong evidence that annealing at reduced temperature (90°C) promoted again the formation of DA adduct, depleting the maleimide and furan groups during the DA reaction.

Similarly, Raman investigation on the reversible bonds was able to assign distinctive bands for the products of DA and r-DA reactions. This spectroscopic analysis, in fact, identifies characteristic bands for individual chemical species and allows monitoring the progress of self-healing phenomenon as function of temperature variation. Raman spectroscopy provides useful information related to molecular structures and vibrational transitions of molecules, even though band assignments are difficult in the case of polymers. Spectra were recorded in the wavenumber region between 500 and 2000 cm^{-1} at room temperature using a Renishaw inVia Reflex Raman spectrometer in backscattering configuration. An infrared laser line with 785 nm wavelength was used for excitation. Spectra were normalized to the peak at 1612 cm^{-1}, in fact, the C-C aromatic ring chain vibration is a suitable invariant peak because its intensity is not influenced by the progress of DA and r-DA reactions. Unfortunately, unlike what reported by Geitner *et al.* [84], not all the C=C stretching vibrations at 1501, 1575, 1585 and 1600 cm^{-1} bands, related to DA reaction between furan and maleimide, were clearly identified, due

to the system complexity. Only the signal at 1501 cm^{-1} was used as marker of 2Ph2Epo65 in Raman spectra reported in Figure 4-7.
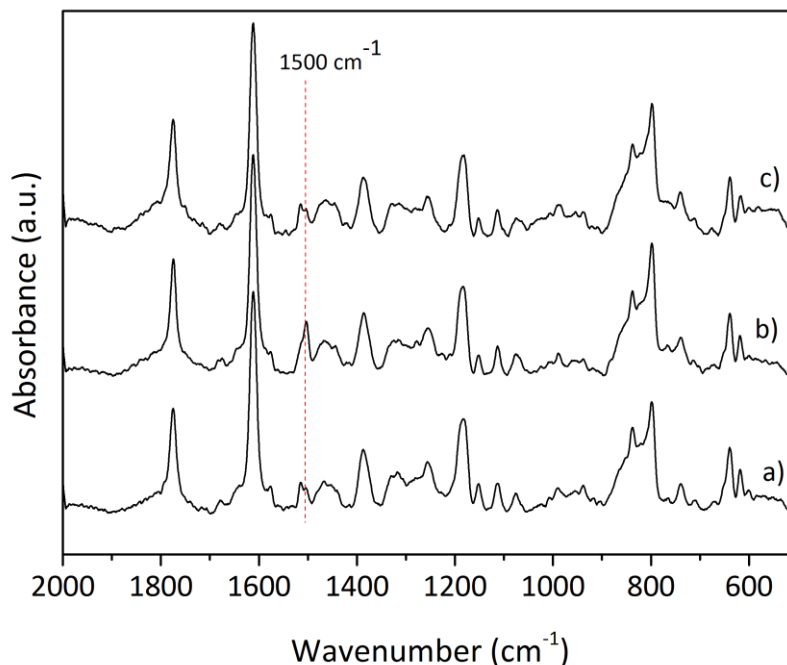
Figure 4-7. Raman spectra of self-healing resin: 2Ph2Epo65 as crosslinked (a); 2Ph2Epo65 quenched after thermal treatment at 120°C (b); 2Ph2Epo65 after further annealing at 90°C (c)

Figure 4-7 shows 2Ph2Epo65 self-healing resin in the following conditions: as crosslinked (a), after thermal treatment for 20 minutes at 120°C and quenching (b), and after a further annealing for 12 hours at 90°C (c). The peak at 1500 cm^{-1} is ascribable to C=C stretching vibration of the furan ring [85,86]. Its intensity increase (Figure 4-7b) highlights a greater amount of furan, formed as a result of the r-DA reaction occurring during the first thermal treatment at 120°C. Furthermore, this band decreases during the annealing at 90°C (Figure 4-7c), to point out that DA recombination between furan and maleimide took place. Therefore, the similarity of the peak intensity at 1500 cm^{-1} between spectra shown in Figure 4-7a and Figure 4-7c is considered an evidence of network restoration. The recovery capability has also been confirmed by means of morphological observation: scratches and fractures have been produced on a cured sample, and

morphological assessment of self-healing recovery behavior has been observed during a suitable heat treatment (Figure 4-8).
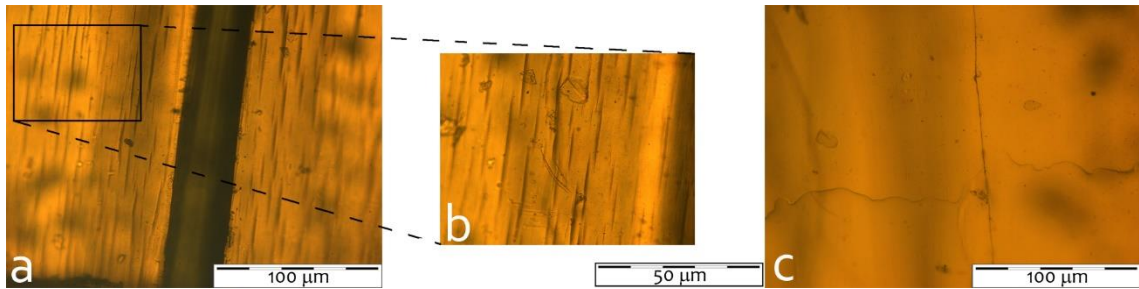
Figure 4-8. Scratch recovery upon a thermal treatment

The fracture rims (Figure 4-8a) and micro-cracks (Figure 4-8b) were evident before treatment, while the defects disappear after thermal healing induced by treating the epoxy resin for 20 minutes at 140°C (Figure 4-8c).

4.4. Quantitative evaluation of self-healing capability and multiple healing assessment by mechanical properties

However, spectroscopic analysis and optical microscopy give quick information about the capability of the material to heal without reporting a quantitative evaluation of the recovery achieved.

Moreover, the morphological recovery, obtained by a treatment at 120°C for 20 minutes, is only the first step for the complete restoration of the material. In fact, the macroscopic damage is recovered during this preliminary stage, but the resulting material is characterized by a less dense network, with reduced overall mechanical properties.

Indeed, upon sample breakage, Diels-Alder bonds are preferentially cleaved because they are weaker than other covalent bonds building up the cross-linked network. Therefore, the occurrence of mechanical damage makes diene and dienophile groups available for self-healing on the fracture surface. But molecular backbone in the close proximity of damage remains unaffected, and the overall material stiffness prevents an efficient fracture healing. For this reason, further thermal treatment at 120°C is applied to complete cleavage of DA bonds and to maximize molecular mobility. Physical healing, due to diffusion of molecular fragments in the activated stage, allows the fracture edges recombination. After the first step, a further annealing at 90°C is required to restore the pristine cross-linking density and mechanical properties by direct Diels-Alder reaction.

A preliminary evaluation of the 2Ph2Epo65 mechanical recovery ability was performed by nanoindentation tests. The sample was tested in the following conditions: "as prepared" (undamaged), after thermal treatment to replicate a damage scenario (20 minutes at 120°C) and finally healed (an additional thermal treatment of 24 hours at 90°C). For each test ten indentation loads ranging from 50 mN to 250 mN were performed. Figure 4-9 reports the final load cycle for each

condition. The elastic modulus is proportional to the slope of the unloading curve where the material recovers its initial condition; the hardness is measured as ratio of the maximum load experienced and the effective contact area [77]. The recorded force and displacement raw data were corrected with the pre-calibrated instrument compliance C_m. Then, a power-law fit was applied to the first 60% of the unloading data to derive the contact compliance C_s and the contact depth h_c (difference between the depth at maximum load and the zero load depth in the unloading), which was used to calculate a projected contact area A_c of the indents via the pre-calibrated indenter area function.
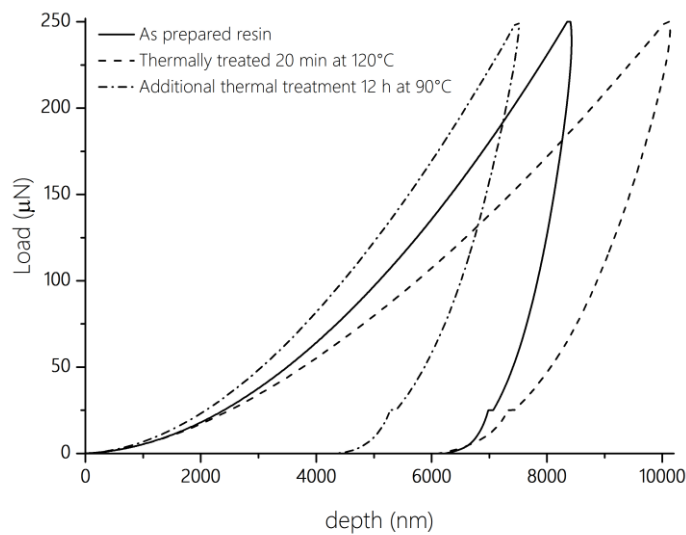
Figure 4-9. Indentation test on pristine and thermal treated samples

Table 4-1 reports the results for nanoindentation tests: reduced modulus and hardness have been estimated for each load step and averaged values have been recorded.

In particular, the hardness H was calculated as the mean pressure that the material support under load, according to equation 4-1:

$$H = \frac{P_{max}}{A} \qquad\qquad 4\text{-}1$$

where P_{max} is the peak indentation load and A is the projected area of contact at peak load. In case of Berkovich indenter, become equation 4-2.

$$H = \frac{P}{3\sqrt{3}h^2 tan\theta/cos\theta} \qquad\qquad 4\text{-}2$$

where θ is the geometric constant (65.27° for a Berkovich indenter) and h is the displacement of the indenter.

Table 4-1. Nano indentation tests on 2Ph2Epo65 resin system

Specimen Type	Nanoindentetion test	
	Reduced Modulus [GPa]	Hardness [GPa]
As prepared	3.89±0.35	0.19±0.02
Morphological healing 20′ at 120°C	2.60±0.29	0.16±0.02
Additional annealing 20′ at 120°C	3.10±0.63	0.21±0.06

Finally, the system showed a good healing efficiency by considering the material stiffness (83.8%) and the hardness have been fully recovered by the thermal treatment.

It is worth to remark that the elastic modulus calculated from reduced modulus, measured by depth sensing indentation, could be invariantly higher than tensile test by a value of 5–20% as highlighted by Zheng *et al.* [87].

In general, the experimental comparison between the loading capacity of intact and healed material can indicate the healing efficiency (equation 4-3):

$$\eta = \frac{P_{healed}}{P_{initial}} \cdot 100 \qquad\qquad 4\text{-}3$$

the subscripts refer to whether the property is measured after healing (healed) or before damage occurs (initial). In many cases, healing efficiency is defined in terms of the fracture toughness [88] or in terms of material strength [89,90], or considering the material stiffness [36].

Therefore, the mechanical recovery capacity has been evaluated through the most classic tests. Quasi-static mechanical tests were performed on specimens to evaluate the mechanical performances of the formulated resin system. The loading scheme was a three-point bending configuration, and the specimens were dramatically damaged by running the tests until breakup. To allow a perfect correspondence of the fracture surfaces, a thin layer of polyimide adhesive strip was stuck on the upper side of the specimen.

Figure 4-10 compares stress-strain curves for pristine and healed 2Ph2Epo65 samples. Broken specimens were treated according to previously described thermal cycle (120°C and 90°C) to achieve mechanical integrity. Multiple healing was studied by repeating the test three times.
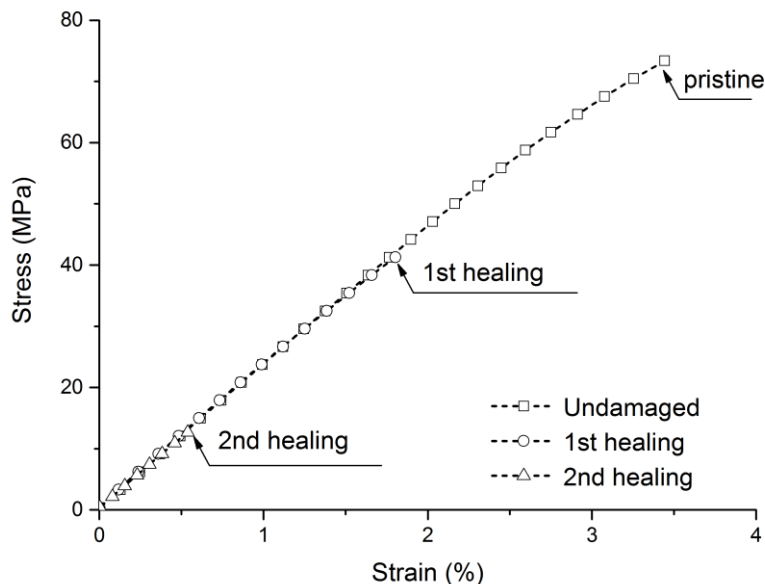
Figure 4-10. Three-point bending test on the 2Ph2Epo65 system

The mechanical data are reported in Table 4-2. The virgin sample had an elastic behavior up to 2% deformation, followed by a plastic deformation up to the breaking of the sample at the deformation of about 3.5%. The healed sample had the same stiffness (slope of the stress-strain curve), but a fragile fracture was recorded in the elastic region. The first healing led to a final strain of 1.8%, the second heat treatment led to a strain of 0.7% at break. Although the samples recovered all their original stiffness (mean value 2.75 GPa), ultimate strain decreased during further test cycles, due to micro-defects not completely restored and acting as crack initiators in subsequent mechanical tests.

Table 4-2. Quasi-static tests on 2Ph2Epo65 resin system

Specimen type	Stiffness [GPa]	Strength [MPa]	Efficiency [%]
Undamaged	2.77±0.12	73.38±4.13	-
First healing treatment	2.74±0.15	41.30±3.06	98.9±56.3
Second healing treatment	2.76±0.13	12.68±2.16	99.6±17.3

5. Self-Healing composites and coatings

Research in this field of Diels-Alder-based healable materials is still at the beginning, but the implications have already been widely recognized. These materials not only exhibit structurally desirable mechanical properties, but also allow multiple healing cycles to occur. Unlike systems that rely on the addition of a healing agent to regain mechanical strength, which guarantee a limited recovery capacity to the reserve of the healing agent, these materials have the integrated ability to restore mechanical properties numerous times. Furthermore, the structure of the healed material is identical to that of the virgin material: this eliminates potential problems involving the inclusion of multiple materials within the system.

For all these reasons, the epoxy matrix based on the Diels-Alder adduct, 2Ph2Epo65, was used for applications suitable to industrial scale-up, and subjected to the related efficiency tests.

The present thesis reports the use of a Diels Alder epoxy resin as a functional coating; the rationale for this application is the ability of 2Ph2Epo65 resin to heal small damages if exposed to proper thermal stimulus. Optical microscopy, nanoindentation and electrochemical impedance tests validated the morphological and structural recovery of the coating. Immersion test in saline solution and subsequent micro-mechanical tests revealed the complete

restoration of polymeric network and mechanical proprieties, thus of the corrosion protection for a healed sample. Furthermore, trough Electrochemical Impedance Spectroscopy (EIS), the water uptake and diffusion coefficient into the polymeric coating were evaluated by studying the capacitance evolution in virgin and healed samples. During initial exposure, there is a homogeneous diffusion of water within the coating. Both the systems, virgin and after healing treatment, showed similar trends with a beginning saturation after 25 hours of exposition, confirming that healing treatment guarantees the complete recovery of the coating functionality.

Finally, the effort to fabricate composite structural material made by Diels-Alder (DA) thermoset has been discussed. Self-healing composites, using a thermally mendable polymer (2Ph2Epo65), were manufactured and subjected to various multiple damage loads. In this thesis, traditional mechanical methods and a computed tomography scan technique to evaluate the structural recovery of the self-healing laminate structures are presented. The performances were recorded and compared at each stage of induced damage and healing cycle. The results highlight an efficient multiple self-healing in the structural recovery, with a recovery ability of 95.1% in static interlaminar strength and 81.7% in fracture toughness.

5.1. Corrosion-resistant Self-healing Coatings

The following section reports the use of a 2Ph2Epo65 DA epoxy resin as protective coating and describes its capability to heal small damages, like surface scratches and fractures, if exposed to proper thermal stimulus.

The development of systems able to prevent corrosion damages of metallic substrates is a primary issue for many applications. Active cathodic protection or anodic passivation are widely used in addition to improved physical barrier of coatings. The cathodic reduction is one of the oldest methods to re-establish and prolong as long as possible anticorrosion protection of metal structures when the coating is damaged [91]. The metal is kept at a negative potential by applying a direct low voltage, and the electrical energy consumption prevents its corrosion. Passivation is another classic method: a passive oxide layer forms on the exposed area via anodization of a metal. The use of anti-corrosive organic coatings is also common to protect a metal substrate from corrosion, for example, electroactive polyaniline coatings on the alloys imparts a form of anodic protection which stabilizes the materials in mineral acids [92]. Moreover, in the effort to increase the service life of organic coatings, different active pigments, such us zinc phosphate and zinc molybdenum phosphate modified, have been added to the primer to guide the electrochemical corrosion processes [93].

Recently, self-healing organic coatings attract attention as an effective route for corrosion protection. Self-mendable extrinsic coatings, incorporating micro-containers or nano-capsules dispersed within the polymeric layer, are able to repair small damages and to release corrosion inhibitors in case of contact with water [94] or as a response to pH variation [95].

Intrinsic self-healing polymers represents a fascinating option. These smart materials recover their properties after sustaining damage thanks to reversible chemical bonds. Hence, only a suitable external stimulus is required to trigger the mending action, permitting multiple healing in the same damage site.

In this area of interest, the Diels-Alder is particularly suitable for coating application, because both its products and intermediates obtained during the healing treatment are stable to aggressive environments, such as the major oxidation agents, air and water [96].

To demonstrate the capability of the system to heal severe damages, samples were scratched and then restored by a thermal treatment in order to promote reverse and direct DA reactions.

Steel substrates have been coated with 2Ph2Epo65 epoxy resin by means of solvent casting with a final thickness of 120 μm. Two homogeneous set of samples, each made by 3 different specimens, were severely mechanically damaged (30 mm long cut through the whole thickness) in order to make the metal susceptible to corrosion. A set of samples was exposed to the corrosive environment to investigate the corrosion kinetics, while the other set was restored by thermal treatments and then exposed to the saline solution. The protection capability has been evaluated by exposure in a water saline solution. The salt solution has been prepared by dissolving 5 ± 1 parts by mass of sodium chloride in 95 parts of water, reproducing the conditions set out in Test Method ASTM B117 – 16. The pH of the solution has been corrected in the range between 6.5 and 7.2 at 23 ± 3°C, using diluted reagent grade hydrochloric acid (HCl) or reagent grade sodium hydroxide (NaOH). Figure 5-1 shows the severe test to which the samples were subjected.

Figure 5-1. Test condition environment

The damaged samples without remedial treatment revealed rusty spots after 3 hours of exposure in the saline solution, and further blistering and delamination were observed at the cut edges after 92 hours (Figure 5-2 left side). On the contrary, the restored samples did not show any corrosion damage after 92 hours, as reported in Figure 5-2 (right hand side).

Figure 5-2. DA epoxy coating: in the middle the damaged film; on the left-hand side the "not healed" coating; on the right-hand side the healed coating

A complete recovery of morphological damage at 120°C allows the restoration of the corrosion protection capability, while the further annealing at 90°C was applied to recover the crosslinking density, affecting thermo-mechanical properties. The full morphological damage recovery is confirmed also by careful microscopic analysis. The faint scratches observed in the right-hand side picture of Figure 5-2 correspond to the damage in the metal substrate surface, produced during the coating cutting, and still visible through the transparent healed epoxy coating.

Even if salt spray and different cyclic exposure tests are widely used in the coating industry, these tests yield essentially qualitative information, but they are not suitable for a quantitative evaluation of healing efficiency. More detailed information can be pursued by the analysis of water content uptake into the coating film during immersion in a saline solution.

Electrochemical impedance spectroscopy (EIS) is a powerful tool to study the performance of high resistance coatings and has been extensively used to measure the corrosion protection properties of organic coatings on metal surfaces [97].

Each system is identified with a specific impedance, $Z(\omega)$, defined by the following equation 5-1 in the electrochemical convention:

$$Z(\omega) = Z' - iZ'' \tag{5-1}$$

where $Z' = ZM \cos(\omega t)$

$Z'' = - ZM \, \text{sen}(\omega t)$

The impedance can be represented as a vector in the complex plane, whose module is reported in 5-2:

$$|Z| = \sqrt{(Z')^2 + (Z'')^2} \tag{5-2}$$

with the angle ϕ with the real axis (5-3)

$$\phi = \tan^{-1}\left(-\frac{Z''}{Z'}\right) \tag{5-3}$$

where Z" is the real (resistive) component, and Z' is the imaginary (reactive) part. In this work, the degradation of as prepared coating system, and the same coating recovered by self-healing treatment were investigated by EIS. Equivalent circuit (EC) models were proposed to interpret the electrochemical impedance data for the coating systems.

The study of the interface is of interest because the electrolyte solution can penetrate the coating defects, resulting in an electrical continuity with the metal substrate. The polarization phenomena that occur at the SC/EI interface involve

the formation of a space charge layer in the semiconductor (C_{sc}) and probably also a surface charge layer, intrinsic or due to adsorption phenomena. While, in the electrolyte a compact double electric layer and a diffused charge layer are formed (R_{ct}). The simplified equivalent circuit is shown schematically in Figure 5-3.
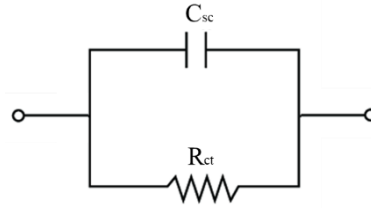
Figure 5-3. Simplified equivalent circuit for the interface SC/EI

The polymeric coating can be simply modeled with a capacitor with C_r capacity, if it is assumed that the system has a flat geometry and high resistance. The defects of the coating through the thickness represent an area whose resistivity is sufficiently lower than that of the coating to allow the passage of a conduction current. The defects are schematized by a resistance R_p in the equivalent circuit of the polymeric layer, shown in Figure 5-4.
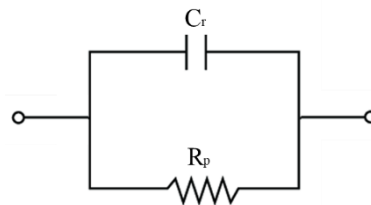
Figure 5-4. Simplified equivalent circuit for protective coating

In the complete equivalent circuit, it is necessary to consider the capacity C_r of the coating and the resistance R_p of its defects. The equivalent circuit of the coating-metal interface is in series respect to R_p, inasmuch as the passage of conduction current can only occur through the defects. The resulting circuit is shown in the Figure 5-5, where R_w is the resistance of the electrolytic solution between the counterelectrode/reference electrode and the coating.
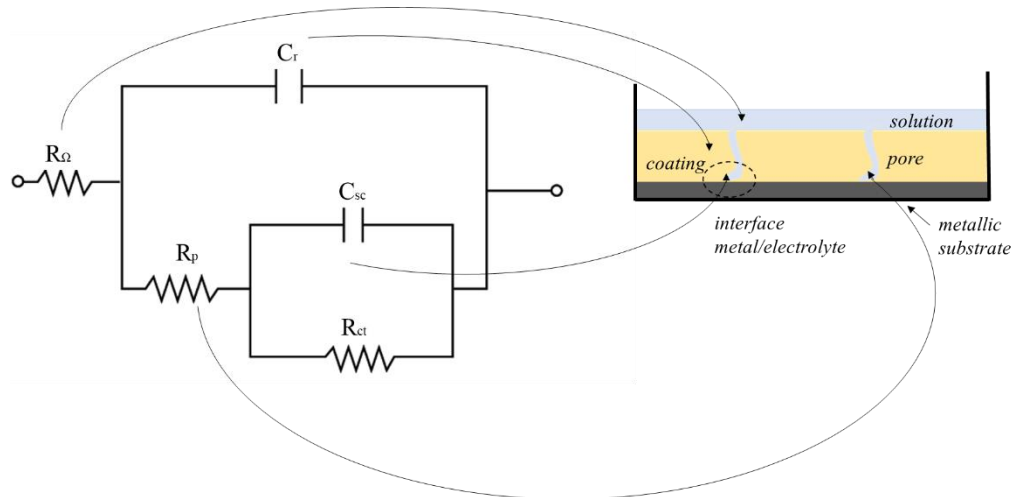
Figure 5-5. Equivalent circuit for the complete system

The kinetics of water absorption in the protective coating can be studied by monitoring the capacity. These measurements are carried out by contacting the coating and an electrolyte solution and recording over time the variation of the system impedance.

If the coating is intact, no degradation occurs, and if the measurement frequency is high enough, the real part Z" can be neglected: the imaginary part of Z coincides with the impedance of the polymer capacity C_r. When the water is absorbed by the coating, since its dielectric constant is much greater than that of the dry polymer ($\varepsilon_{H_2O} \sim 78$ while $\varepsilon_r = 3 \div 10$), there is a gradual increase in ε_r, therefore in C_r. Usually, the capacitance increases monotonically from the initial value C_0 to the saturation value C_∞.

To obtain information on the water absorption kinetics from the capacity curves, two models are needed: the first relates the C capacity of the polymer to the water content, and the second describes how the water content varies over time. These models have been integrated into the "Continuous Model", that defines each infinitesimal layer of the polymeric matrix as a parallel RC elementary circuit, whose electrical characteristics depend on the coating matrix and on the concentration of penetrant absorbed. For high frequency impedance measurements, only the capacitive component of the model is considered. The

data obtained from the capacity measurements are represented with diagrams C', the real part of the complex capacity C, vs √t. The capacity curve is also related to the loss angle δ as a function of √t, where δ is the phase shift between the voltage phasor and the current phasor.

In an ideal capacitor, the polarization of the dielectric is instantaneous and therefore the capacitive current is 90° out of phase with respect to the voltage, *i.e.* the complex impedance is purely imaginary. In a real capacitor, the polarization phenomena occur in a finite time, characteristic of the dielectric and the capacitive current also has a component in phase with the voltage, due to the dissipation of part of the electrical energy as heat: δ is lower than 90°. Since the coating has the dielectric properties of an insulator, it should behave like a capacitor: its insulating properties are the better the more δ it is close to 90°. During the capacity test, if the water absorption causes corrosion or delamination reactions, with a consequent increase in the resistive component of the system impedance, the value of δ decreases.

The protective properties of the coatings were evaluated and analyzed by electrochemical specific parameters of coating. The result was offered for a comparison of the protective properties of the same coating system, as prepared and after self-healing treatment.

Steel substrates was cut into the size of 50 mm × 50 mm × 2 mm, then specimens were polished using sandpaper up to 1200 grit and extensively cleaned with acetone and ethanol successively. Finally, metal substrates have been coated with 2Ph2Epo65 epoxy resin by means of solvent casting with a final thickness of 120 µm and cured for 24 hours at 90°C. Two homogeneous set of samples, each made by 3 different specimens, were analyzed: a set was tested as prepared, while the other was first damaged and restored by thermal treatments and then tested.

In the mechanically damaged set of samples, the polymeric coating was scratched with the pointed round tip. A compass pin, with a defined applied weight (mass 50 g), was used as indenter in order to obtain a controlled depth and to avoid shavings stack on scratch edges (Figure 5-6).

a) b)
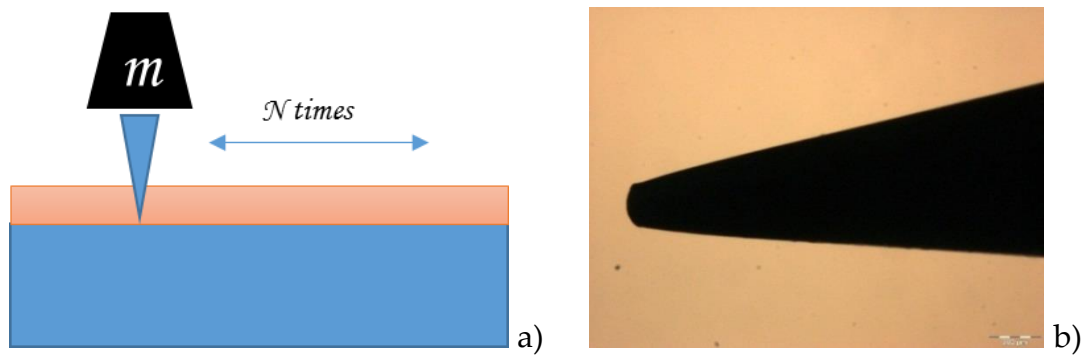
Figure 5-6. a) Indentation set-up; b) compass pin (magnification 20X)

Each scratched sample was morphologically analyzed to evaluate the width and the depth of the cut before performing the self-healing cycle. In fact, the recovery treatment would be ineffective if the scratch had completely removed the polymeric layer, preventing the material interdiffusion.

Samples were visualized by Leica's dual-core 3-D microscope. A Leica Microsystems' map surface imaging and metrology software, Map DCM 3D, was used to visualize and quantify features of measured surfaces and to characterize 3-D surface texture and geometry (Figure 5-7).
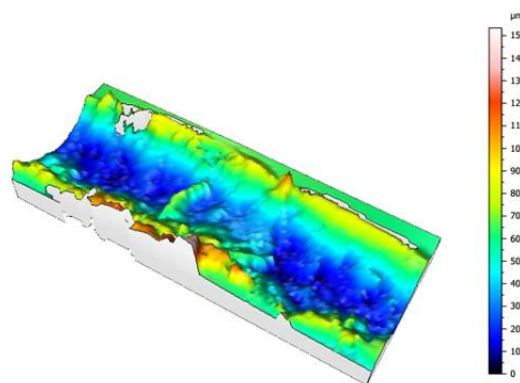
Figure 5-7. Map surface imaging: 3-D surface texture

The Figure 5-7 e Figure 5-8 are an example of cut morphological analysis: the width (340 μm) and depth (~50 μm) are compatible with a potentially successful recovery treatment.
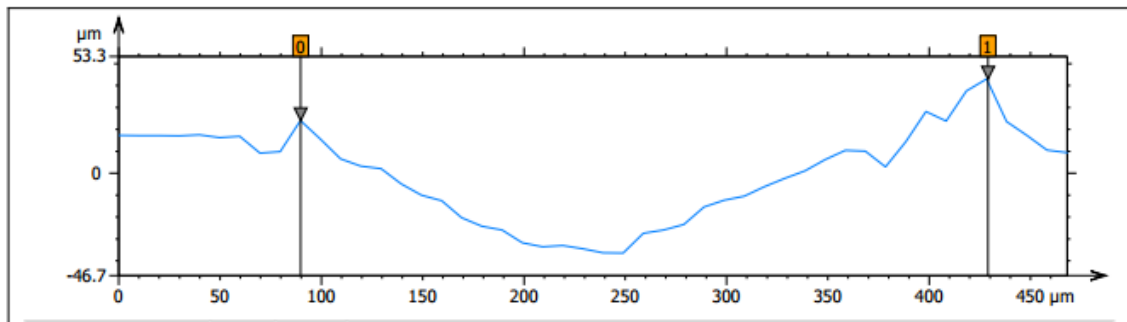
Figure 5-8. Cut morphological analysis

EIS measurements were carried out in aqueous aerated chloride solution (0.6 M NaCl), pH 7, at 25°C. In Figure 5-9 was reported the experimental cell set-up. The three electrodes electrochemical cell was made by sealing a glass cylinder onto each sample (working electrode) by an O-ring, which left an exposed sample surface area of 3.14 cm²; the reference and counter electrodes were respectively one of Ag/AgCl and a platinum mesh. All the electrochemical potential values are indicated with reference to the Saturated Calomel Electrode (SCE).
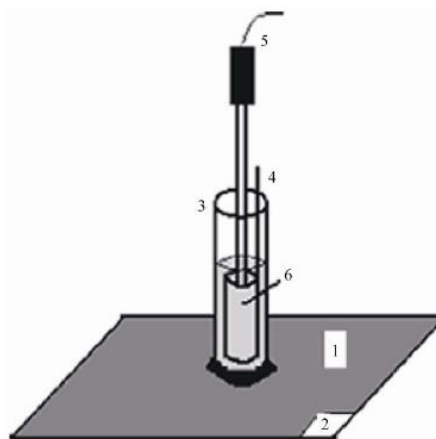
Figure 5-9. Experimental cell setup: 1) coated substrate, 2) coated removed area for making working electrode contact, 3) glass tube, 4) platinum mesh counter electrode, 5) SCE reference electrode, and 6) test electrolyte

EIS measurements were performed in the frequency range between $10^{-2} \div 10^{5}$ Hz using a Solartron 1255 Frequency Response Analyzer (FRA) coupled to a Solartron 1296 dielectric interface, and a sinusoidal voltage signal of 50 mV. The

experimental spectra were interpreted on the basis of equivalent electrical circuit models obtained from the Zview fitting software.

The Capacitance Fast Transient Technique (CFTT), based upon the coating capacitance evolution, can estimate the amount of water contained within an organic coating. The CFTT tests were carried out at a frequency of 10^4 Hz using an electrochemical interface Solartron 1287. All the measurements were performed at room temperature and with the electrochemical cell inside a Faraday cage to reduce external interferences as much as possible.

Many authors reported changes of the capacitance and resistance during immersion in water solution [98]. The water uptake can be estimated by the empirical Brasher – Kingsbury equation 5-4 [99]:

$$\phi = \frac{log\left(\frac{C_t}{C_0}\right)}{log \ \varepsilon_{H_2O}} \qquad \text{5-4}$$

Where C_t is the coating capacitance at time t, C_0 the capacitance of the "dry" coating and ε_{H_2O} is the water dielectric constant.

Comparison between the neat sample and a sample scratched and then thermally treated (20 min at 120°C and annealed at 90°C for 12 h) for inducing the healing is reported in the above diagram. Both the systems experienced similar trends with phase angles very close to 90° and beginning saturation after 25 hours of exposition. The two samples have got very similar slope in the initial stage confirming that healing treatment stitched the engraved area (no changes in water uptake rates and time to reach saturation), leading to the complete recovery of the coating functionality.

The initial ramp observed in the coating capacitance diagram ($C \, vs \, \sqrt{t}$, Figure 5-10) is proportional to the diffusion coefficient: the plot exhibits an initial linear trend, associated to a Fickian absorption model [100]. A deviation from the linear behavior is observed at the incipient saturation after 25 hours (300 s½).
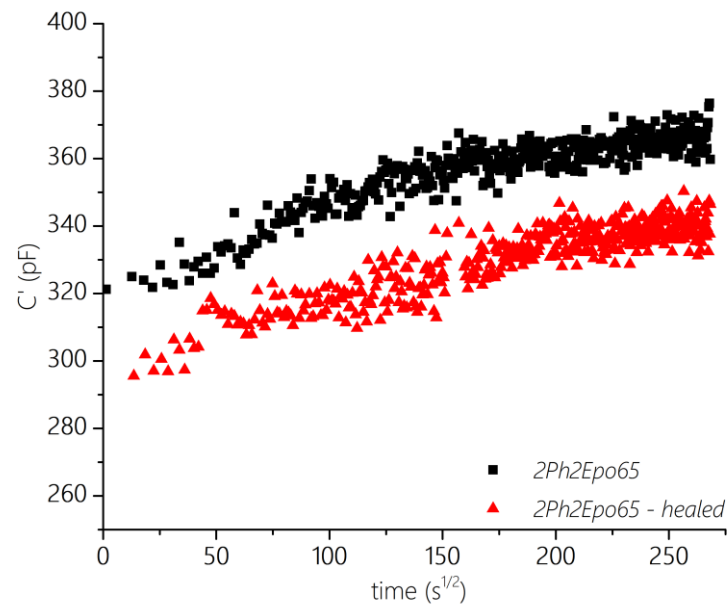
Figure 5-10. Capacitance behavior during immersion

Protective coatings are chiefly physical barrier to prevent contact between metal and aggressive environment. Nevertheless, even in the case of intact and continuous coating layer, diffusion of water, oxygen and chlorine ions through the barrier could have a detrimental effect on metal endurance to corrosion. A comparison between mechanical properties, in the pristine condition and after healing and further exposure to saline solution, is used as an overall landmark of structural and functional properties of barrier coating. Nanoindentation tests have been performed in order to evaluate the elastic modulus and hardness of thin DA epoxy resin casted on metal substrates. Material conditions have been evaluated and compared between the pristine as prepared sample, and the sample after incremental treatments, including morphological healing, structural healing and additional exposure to saline solution. Mechanical features of samples are reported in Table 5-1.

Table 5-1. Reduced modulus [GPa] and hardness [GPa] of self-heling coating

Specimen Type	Hardness, H [GPa]	Reduced Modulus, E_r [GPa]
As prepared	0.224±0.03	3.80±0.03
Morphological healing 20' at 120°C	0.179±0.05	2.54±0.05
Structural healing 20' at 120°C + 12h at 90°C	0.232±0.03	3.56±0.05
After healing and additional exposure to saline environment	0.206±0.07	3.44±0.07

The effects of healing on structural properties, such as modulus and hardness, can be related to changes in the crosslinking density observed as result of DA and r-DA reactions. After heating at 120°C required to promote the morphological recombination of cut edges, the modulus and hardness drop down by a factor of 2. In fact, the occurrence of r-DA reaction induces the cleavage of specific covalent bonds and reduces the crosslinking density. However, the effect is not permanent. The pristine properties can be recovered by prolonged annealing at 90°C, where DA reaction can lead to the restoration of network. This trend is shown by mechanical data obtained by nanoindentation, consistent with published result [101].

5.2. Self-healing composites

The self-healing epoxy 2Ph2Epo65 has been considered for manufacturing a composite plate with the aim to investigate the fracture behavior and to assess the healing efficiency of the composite system.

The plane geometry allowed to identify the effect of the presence of carbon fibers in the healing potential of the developed epoxy resin. Figure 5-11 shows the main steps in the manufacturing of a laminate: a) a dry unidirectional preform was cut and lied in a mould, with a polyimide film put in the intermediate plane to induce delamination; (b) dry fibers are impregnated with uncured 2Ph2Epo65; (c) the material is crosslinked under the vacuum bag for 24 hours at 90°C; (d) reversible fiber composite hardened with the polyimide film is ready. A total of 12 unidirectional layers were laminated to a final thickness of 3 mm.
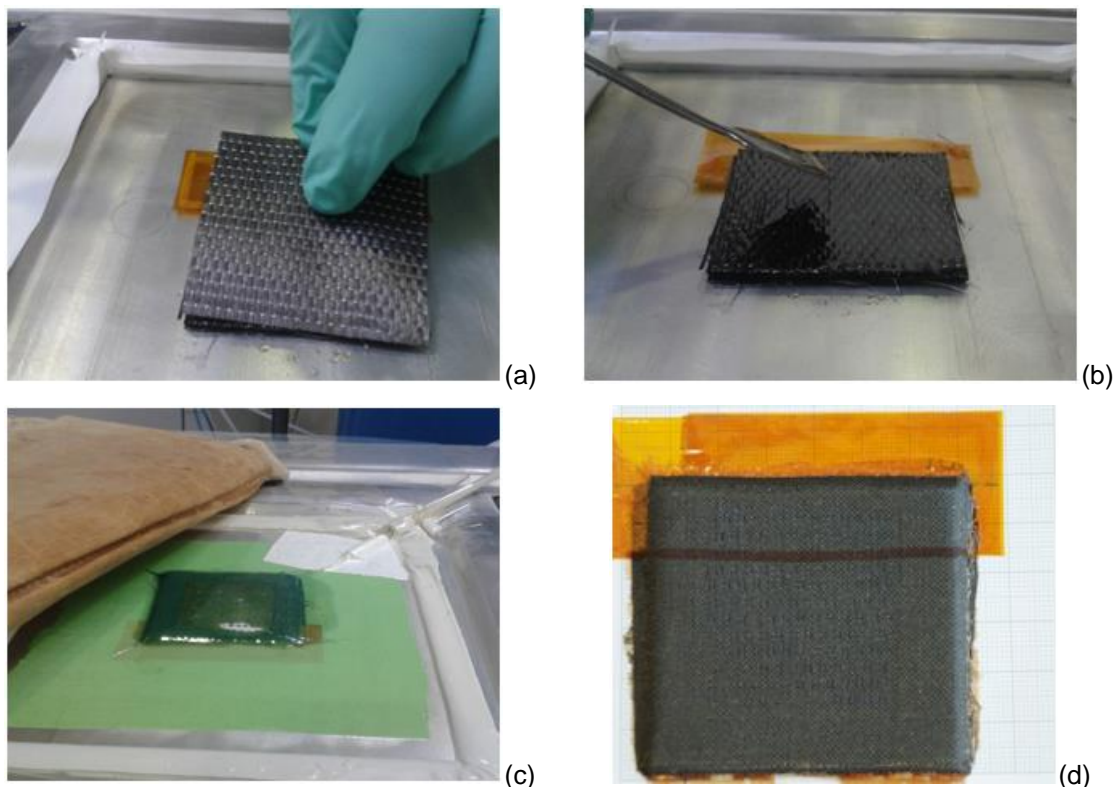
Figure 5-11. Manufacturing stages of the composite laminate: (a) dry preforms with polyimide film in the mid-plane; (b) reversible polymer addition; (c) vacuum for composite consolidation; (d) final coupon

Figure 5-12 reports two optical micrographs recorded on different sections of the composite to evaluate the coupon quality after the infusion process. Images show a uniform composite, without bubbles trapped between layers, with no fiber distortions.
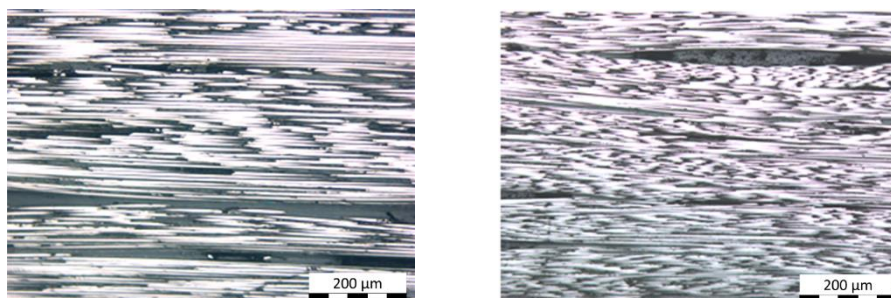
Figure 5-12. Optical micrographs on a plate section containing fibers and reversible resin, 5X magnification

Figure 5-13 shows the thermogravigram of the manufactured coupon, recorded by TGA 500 of TA Instruments in High Resolution mode, at 50°C/min up to 600°C in nitrogen flow, and up to a 1000°C in air flow.

TGA High Resolution is an extension of conventional TGA whereby the heating rate is varied as a function of the rate of sample weight loss. This TGA technique, with, double step is the useful procedure to determine the composition of the polymer/Carbon Fiber blend sample, because it allows the reduction of the heating rate during a weight loss transition, yielding to improved separation of overlapping or poorly defined weight loss events.

The epoxy resin decomposition is well resolved from the carbon fiber decomposition before the switch to an air purge to burn off the carbon.
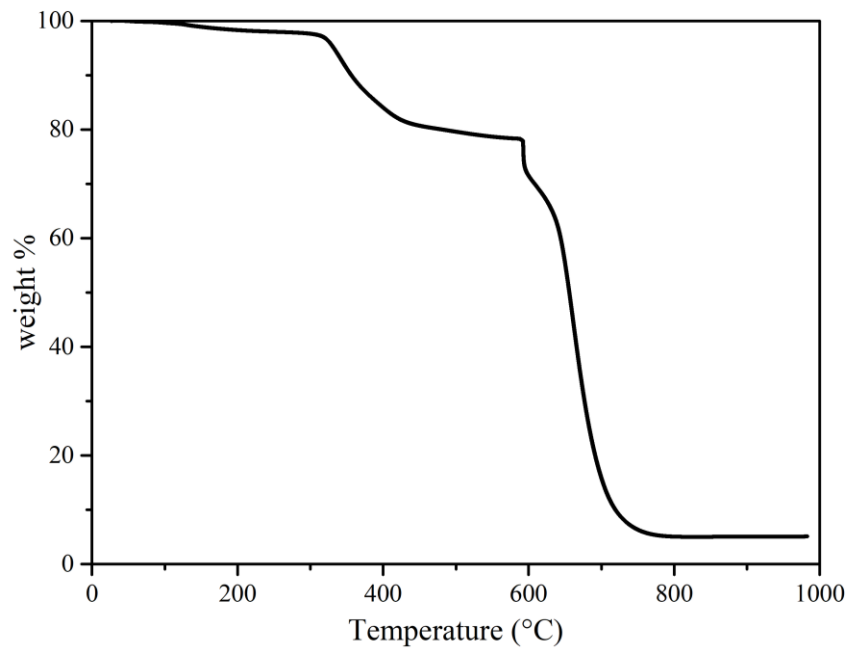
Figure 5-13. TGA thermogram of carbon reinforced composite sample: in nitrogen flow up to 600°C and in air flow up to 1000°C

About 25% of the sample is made up of a matrix, that degrade in nitrogen flow up to 600°C, and the remaining 75% of carbon reinforcing fibers which are consumed by pyrolysis in air flow up to 800°C.

Interlaminar behavior of the CFRP (composite fiber-reinforced plastic) has been studied by means of shear strength of the laminate. Shear tests can be conducted on composite laminates following different experimental approaches, depending on the mode of fracture that needs to be assessed. The ability to recover damages after a cohesive failure has been investigated by interlaminar shear strength (ILSS): mode II fracture loading has been studied by performing the End Notch Failure (ENF), while the interlaminar critical strength by Short Beam Shear tests (SBS).

The experimental comparison between the loading capacity of intact and healed material, indicating the healing efficiency, can be evaluated as the ability of sample to recover the initial interlaminar strength (equation 5-5):

$$\eta(\%) = \frac{ILSS_{healed}}{ILSS_{pristine}} \cdot 100 \qquad\qquad 5\text{-}5$$

The composite plate manufactured by liquid moulding process under vacuum bag was tested. All tests are performed on multiple samples and reported results are the calculated average values of single measured sample.

The presence of a Kapton layer in ENF bending test leads to the mutual sliding of separated parts promoting a mode II failure (shear mode 3), according to ASTM D7905. In Figure 5-14, the sample dimensions and the parameters of the ENF tests (a), and load versus displacement curves during ENF tests (b) are reported.
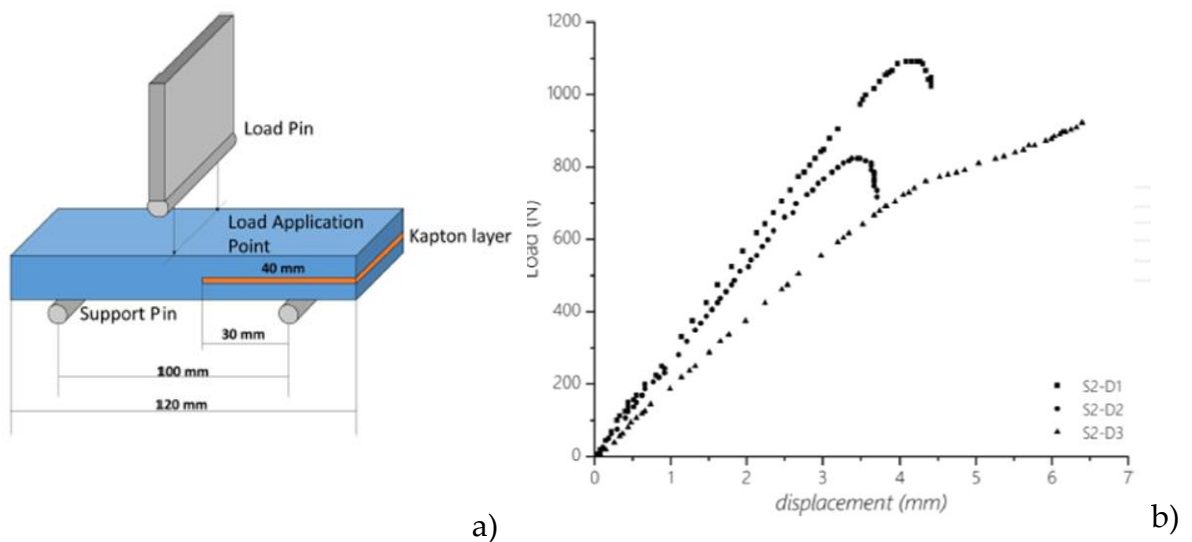
Figure 5-14. End notch failure (ENF) test experimental setup (a); End Notched Failure test (b)

Load versus displacement curves showed an initial linear behavior up to the critical load (nonlinearity load, NL). Above this point, delaminations start and steadily propagate until the maximum load is achieved. Afterwards, unstable delamination growth leads to load decrease.

The first healing treatment allowed to recover the pristine stiffness, with a sample strength decrease. However, during the third load cycle (*i.e.*, after the second healing), a significant stiffness loss is experienced.

Different behavior between neat polymer and laminate should be related to specific composite features. Delaminations could occur both as effect of a matrix failure and as interface debonding. Moreover, any damage incurring to the reinforcing fibers would reduce material stiffness without chance of recovery. The critical strain energy release rate should be evaluated as function of the NL load. Fracture toughness was determined using (equation 5-6):

$$G_{IIc} = \frac{3mP^2\,a^2}{2B}$$
<div align="right">5-6</div>

where m is the calibration compliance, P is the critical load, a is the critical length, and B is the specimen width.

Composite healing efficiencies were also determined by conducting Short Beam tests, according to ASTM D2344. The delamination is achieved by flexing a sample of the composite until breakage and a self-repair thermal treatment is carried out after each test, according to the schematic procedure showed in Figure 5-15.
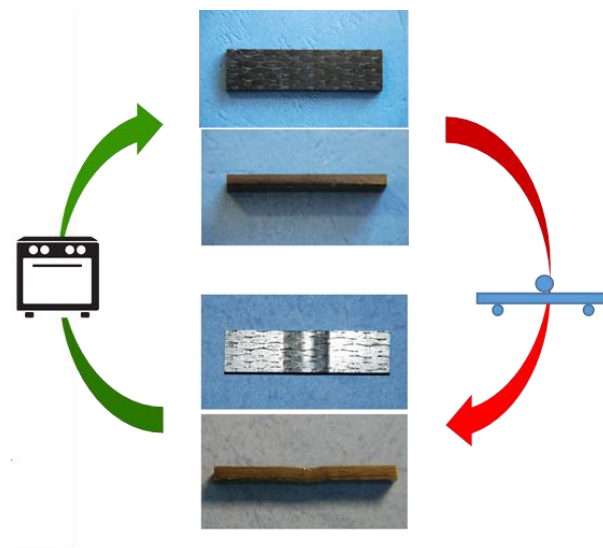
Figure 5-15. Schematic procedure for multiple Self-Healing assessment in CFRP: self-repair thermal treatment is carried out after each test

After mechanical test the sample resulted completely deformed in the nose area (Figure 5-16 a,b). Thus, specimen has been thermally treated for 20 minutes at

120°C and 24 hours at 90°C, according to the recovery treatment, before a second ILSS test was carried out. The sample, after recovering the initial geometry (Figure 5 10 c,d), through the healing cycle, was re-tested, resulting again in a similar deformation (Figure 5 10 e,f).
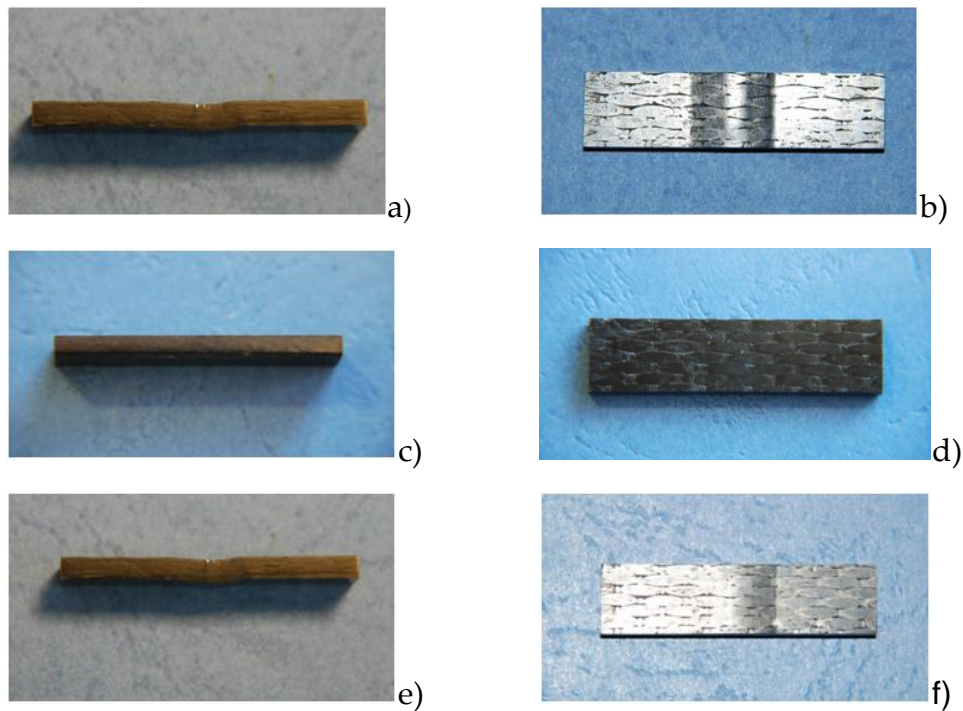
Figure 5-16. ILSS sample: as prepared (a and b); after the healing treatment (c and d); healed sample after ILSS test (e and f)

In Figure 5-17 are reported test scheme for samples of size 20 x 10 x 3.2 mm^3 (a) and an example of load versus displacement curves during SBS tests (b).
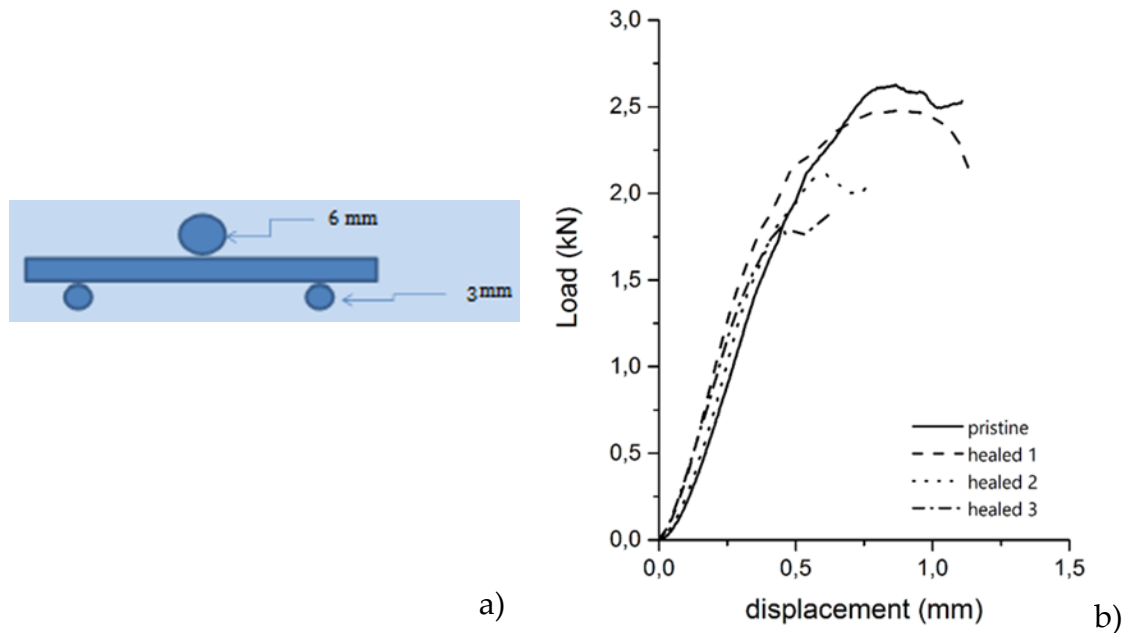
Figure 5-17 Short Beam Shear (SBS) test experimental setup (a); SBS test on composite samples (b)

Table 5-2 reports the recovery efficiencies measured as interlaminar critical strength and as critical energy for mode II delaminations. Fracture toughness showed a less effective recovery ability of 52.4% compared to static interlaminar strength recovery of 89.7%.

Table 5-2. Strength recovery after failures

Cycle	ILSS [MPa]	η [%]	G_{IIc} [J/m²]	η [%]
0	54.1±1.1	100	650±20	100
1	51.4±5.1	95.1	683±13	89.7
2	44.2±4.9	81.7	341±32	52.4

Finally, it has been used a method that focus on the evaluation of pulse/echo responses through the thickness of the tested medium to determine damage: the computed tomography scan (CT-scan). It is a non-destructive analysis, therefore it should be a perfect completion of the self-healing ability of the material, in order to extend the life cycle of the product through non-invasive monitoring and maintenance. The water tank C-scan uses a single element piezoelectric transducer to transmit and capture signal responses: it has been already

employed by several authors to evaluate crack self-healing performance [102,103].

Figure 5-18 below shows the CT-scan layout for the undamaged (green) and damaged (red) scanned areas. The whole undamaged sample was scanned in order to assess the presence of damage in the samples: the red solid line on the sample indicates the end of the Kapton layer (40 mm in length).
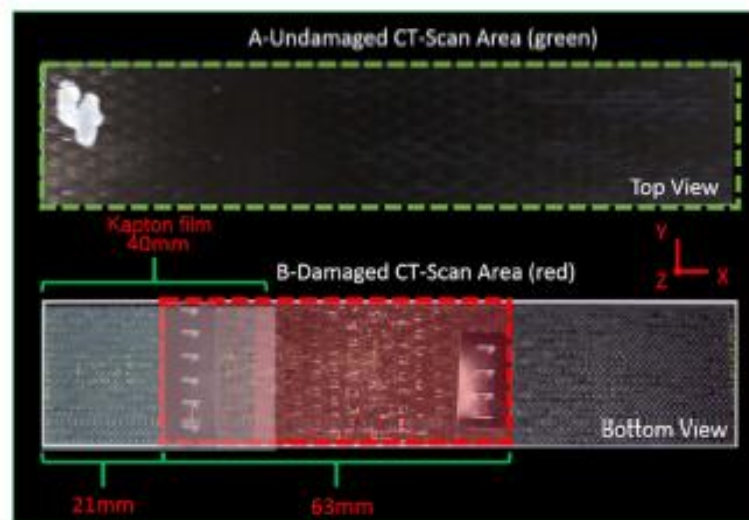
Figure 5-18. CT-scan: A) Undamaged CT-scan area; B) Damaged CT-scan area

Figure 5-19 shows the CT-scan results for the X -axis plane of a sample. After the first mechanical test, there is a clear evidence of an extension in the fracture propagating from the Kapton film through the middle section between undamaged (UD) and damaged first time (D1), *i.e.* the black line extending down from the top middle of the sample. After the first healing cycle (H1) the crack extension has considerably reduced back to the Kapton layer. While the first damage and healing cycle show remarkable recovery, the healing between second damage (D2) and second mending treatment (H2) has reduced. In fact, after H2 there is a decrease in the damage region, but this reduction is not consistent over the whole length, leaving areas where damage persists. The final damage event shows that failure has grown to the middle of the sample and is evident along the section.
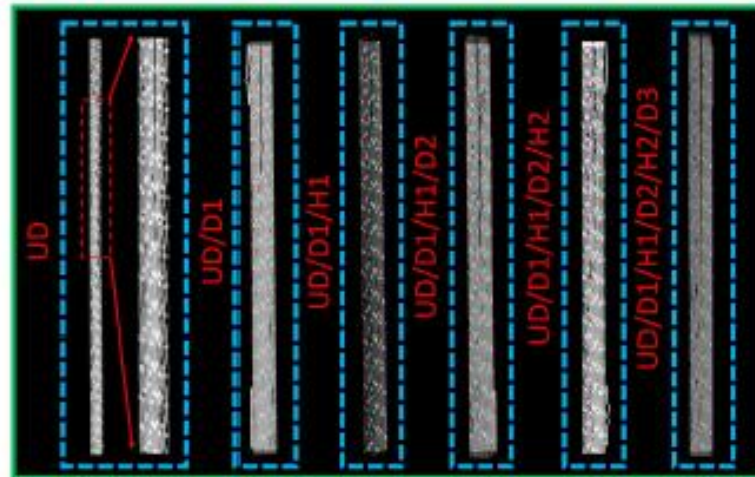
Figure 5-19. X-axis plane results

Using the X-axis CT-scan information it is possible to evaluate the extent of damage and recovery for each damage state. Figure 5-20 shows the total length of delamination, starting from the undamaged state, which includes the 40 mm Kapton layer.
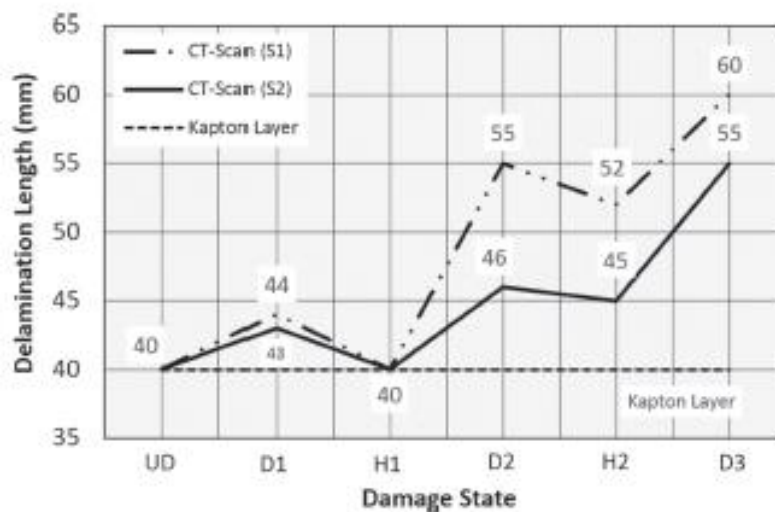
Figure 5-20. Damage progression and recession for each damage state, for S1 and S2 samples

The diagram clearly shows the recovery of the delamination after each healing cycle; although recovery does occur, the structure weakens after each damage/recovery cycle.

6. A Comprehensive approach for self-healing composites

The interphase plays a key role in determining the mechanical interfacial properties of composite materials, so engineers constantly pay attention to novel coupling agents that can improve mechanical performance or introduce new interesting features for FRP [104–106]. The interphase supports the transfer of stress between the matrix and the reinforcement and attenuates the mismatch of the mechanical properties between the matrix and the reinforcing fibers. Marked differences in mechanical properties lead to stress concentrations, with the consequent micro-crack formation and propagation up to failure. These cracks are usually unpredictable and difficult to repair. Therefore, preventing or repairing interphase damage could be a new strategy for the design of high-performance composites.

In recent years, self-healing composites have attracted the scientific world attention thanks to their ability to recover damage [107–109]. However, FRP composites based on intrinsic self-healing epoxy can only recover the damages related to the cohesive failure of hosting matrix. The delamination between matrix and reinforcement would not benefit from the reversible reaction to restore the pristine condition, due to the lack of reversible functional groups grafted onto the fibers. An alternative approach to intrinsic healing of the hosting

matrix is to allow the reversible Diels-Alder reaction even at the interface between functionalized reinforcements and furan functionalized epoxy amine thermoset matrix [66,110,111].

A comprehensive approach, schematized in the Figure 6-1, aims to promote a mixed-mode recovery strategy for cohesive failures within the hosting matrix and adhesive at the interfaces between polymer and reinforcement.
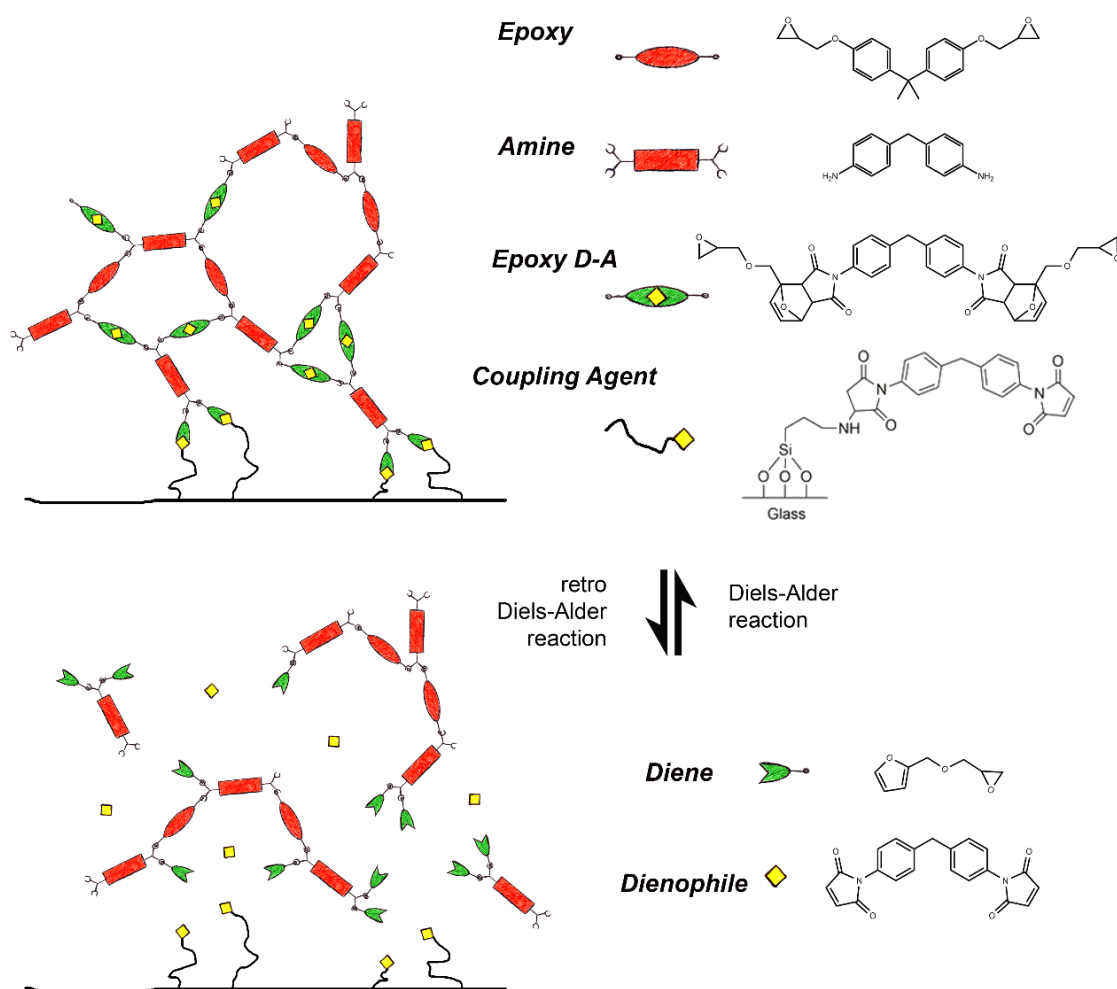
Figure 6-1. Hybrid network sheme with Diels-Alder interface

In this work a coupling agent based on Diels-Alder chemistry, with reversible bonds compliant to the self-healing epoxy previously formulated, has been developed to integrate the recovery ability at the interface.

The methodology implemented for the functionalization of commercial dry preform has promoted superior adhesion between matrix and reinforcement. The micro-droplet pull-out tests performed on commercial and self-healing resin revealed the increase in interfacial shear strength (IFSS) for both commercial DGEBA (+31%) and for a self-healing epoxy 2Ph2Epo65 (+ 92%) systems. Furthermore, additional micro-droplet pull-out tests carried out on virgin and healed samples, to verify the healing capability at the interface, resulted in an effective mending ability, with a retain of 37% in IFSS after one test/SH cycle and 15% after two cycles.

6.1. Reinforcement decoration

The performance of the composites takes advantage of the stiffness and strength of high-performance fibers by dispersing them in a matrix, which transfers forces to the fibers across the fiber-matrix interface. Strong adhesion between the reinforcing fibers and the hosting matrix is achieved by combining the contribution of mechanical friction and chemical bonding.

The common practice in the composite science is to apply an appropriate chemical treatment on the fiber surface to improve the wettability during processing and adhesion after resin setting [104,105].

To integrate the recovery ability and to enable a reversible [4 + 2] cycloaddition within the interphase, the reinforcement can be functionalized with a diene, such as a furan derivative [112], or a dienophile, such as maleimide [66,68,113,114].

Glass fibers, the most common reinforcement fibers for polymer matrix composites, for its low cost, high tensile strength, high chemical resistance and excellent insulating properties, were explored.

With the aim of introducing at the interface the same pendant DA dienophile present in the matrix, in this work, a glass fiber was first activated with an aminosilane and then reacted with bismaleimide through Michael's addition reaction.

6.1.1. Coupling agent deposition route

In order to promote reversible bonding at the interface between polymer and substrate, a two-step route was carried out to graft BMI onto the surface. The functionalization was performed according to the following scheme:

- Immersion in a solution of 1% w/w 3-aminopropyltriethoxysilane (APTES) in ethanol and water (25:75 by weight ratio) at boiling temperature for 2 hours allowed the introduction of the primary amino group (Figure 6-2a);

- Immersion of substrates in N,N-Dimethylformamide (DMF) solution with 5% w/w of BMI at 80°C for 2 hours led to Michael's addition of BMI onto surfaces (Figure 6-2b).
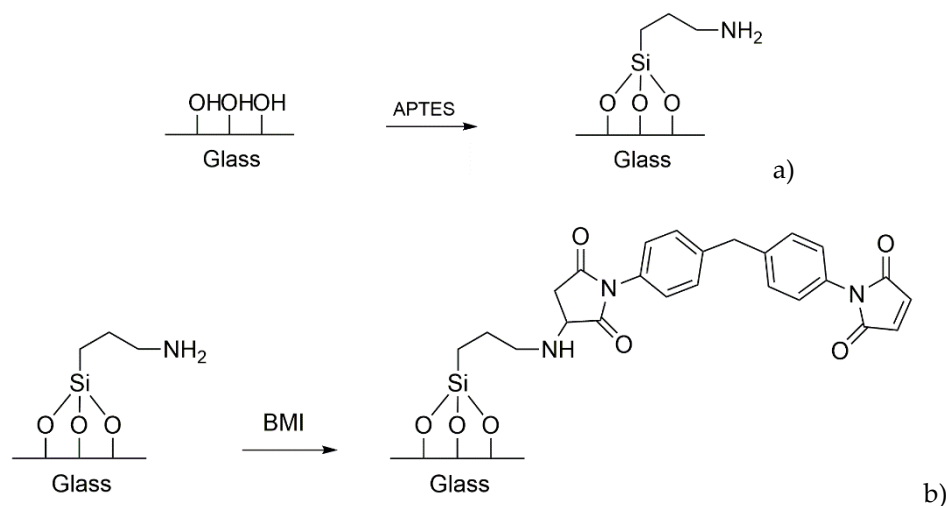
Figure 6-2. Glass surface functionalization scheme: a) amination; b) decoration with maleimide

6.1.2. Evaluation of functionalization

Contact angle

The contact angle was measured through sessile-drop technique using Dataphysics OCA-20. Water and diiodomethane drops (1 μL volume) were dispensed at rate of 0.5 μL/s in order to establish the tangent angle of the drop of liquid with respect to the flat solid surface. The Owens, Wendt, Rabeland Kaelble (OWRK) method [116] was used for calculation of the surface free energy of the solid.

In fact, the study of surface energy by measuring the contact angle is one of the most used methods to evaluate the wettability of solid fibers and propensity to bind with the matrix. Nonetheless, contact angles on fibers with diameter ranging between 7 and 12 microns, for carbon and glass fibers respectively, cannot directly be measured due to geometrical constraints. In the case of glass reinforcement, surface interactions can be evaluated using a plane model

geometry. The treatment features were assessed on a flat glass slide and then reproduced onto reinforcement fibers.

Owens and Wendt hypothesized that the total surface tension could be expressed, according to equation 6-1, as the sum of two surface tension components, each of which derived from a specific type of interaction: the dispersive surface tension component γ^d, and the polar one γ^p, related to hydrogen and dipole-dipole bonding.

$$\gamma = \gamma_S + \gamma_L - 2\sqrt{\gamma_S^d \gamma_L^d} - 2\sqrt{\gamma_S^p \gamma_L^p} \qquad 6\text{-}1$$

Assuming that the solid surface tension is constant for a solid surface, the value of the experimental contact angle, in combination with Young equation 6-2, determines the solid surface tensions (equation 6-3):

$$\gamma_{L,V} \cos\theta = \gamma_{S,V} - \gamma_{S,L} \qquad 6\text{-}2$$

$$\gamma_L(1 + \cos\theta) = 2\sqrt{\gamma_S^d \gamma_L^d} + 2\sqrt{\gamma_S^p \gamma_L^p} \qquad 6\text{-}3$$

The contact angles were measured by depositing a drop of two liquids with very different properties, such as water and diiodomethane, on the glass surface, before and after the surface treatments above described.

The plain glass surface and its amino-functionalized and BMI-decorated analogues are compared in Table 6-1, where the contact angles of water and diiodomethane are reported, as well as the polar, dispersive and total surface tensions.

Table 6-1 Water and diiodomethane contact angles and surface energy parameters

Owens–Wendt method	water (degree) [°]	diiodomethane (degree) [°]	Superficial Free Energy [mJ m^{-2}]		
			γ_s^p	γ_s^d	γ
Plain glass	49.16	52.70	28.68	22.00	50.68
NH$_2$ functionalized glass	72.50	57.00	12.18	22.85	35.03
BMI grafted glass	88.66	45.20	2.23	32.01	34.24

The images of the contact angle measurements, performed using the sessile-drop technique, are shown in Figure 6-3.
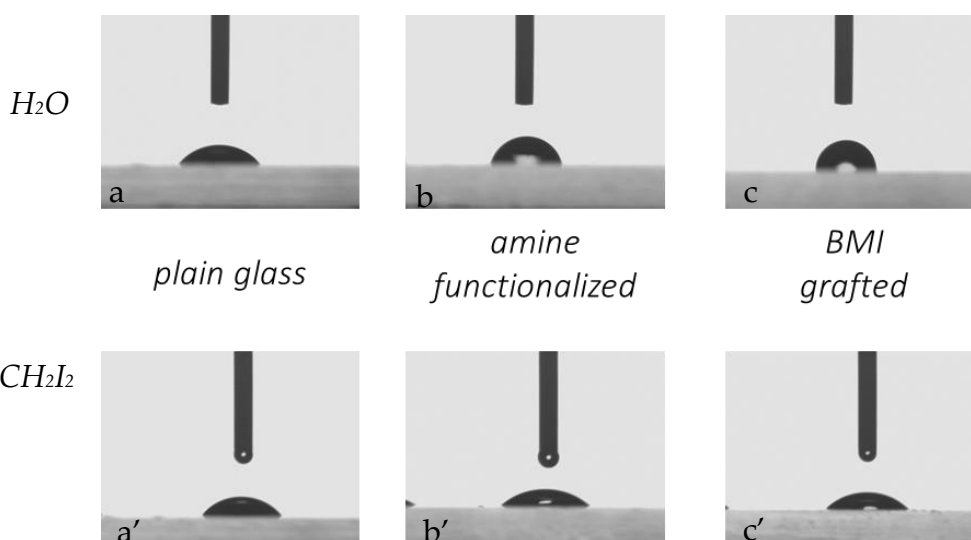
Figure 6-3. Contact angle measurement through sessile-drop technique with water and diiodomethane, respectively: a, a') plain glass; b, b') amine functionalized glass; c, c') BMI grafted glass

The results confirm the modification of the surface after the amino-silane and the following BMI treatments. The contact angle with the water increases, indicating a strong reduction in the polar component of the surface tension related to decrease of surface-water interactions. The trend is clearly highlighted in Table 6-1. The diiodomethane contact angles do not follow a defined path.

However, the analysis of experimental result using the Owens and Wendt method leads to interesting results: both surface treatments induce a similar reduction in total surface tension. This means that the wettability of the epoxy resin on organo-modified surfaces increases with respect to plain glass slide.

Therefore, the further BMI treatment is effective in modifying the nature of chemical interactions with the cross-linking resin, favouring reversible interactions through the Diels-Alder reaction rather than irreversible covalent bonds through the amino-epoxy addition.

The contact angle verified that the surface treatment had taken place; to define the chemical nature of the grafted groups, the ninhydrin test was carried out.

Ninhydrin test

Ninhydrin is a chromogenic reagent, chemically 2,2-dihydroxyindane-1,3dione, widely used in colorimetric estimation of substances containing free amino groups. In fact, ninhydrin can detect ammonia as well as amines (primary and secondary), because once reacted with these chemicals, it produces a deep blue or purple colour, popularly known as Ruhemann's purple.

Ninhydrin tautomerizes to 1,2,3-indane trione which forms a Schiff base when react with amine group. Condensation of this intermediate amine with another molecule of ninhydrin follows to form the expected chromophore Ruhemann's purple (Figure 6-4).
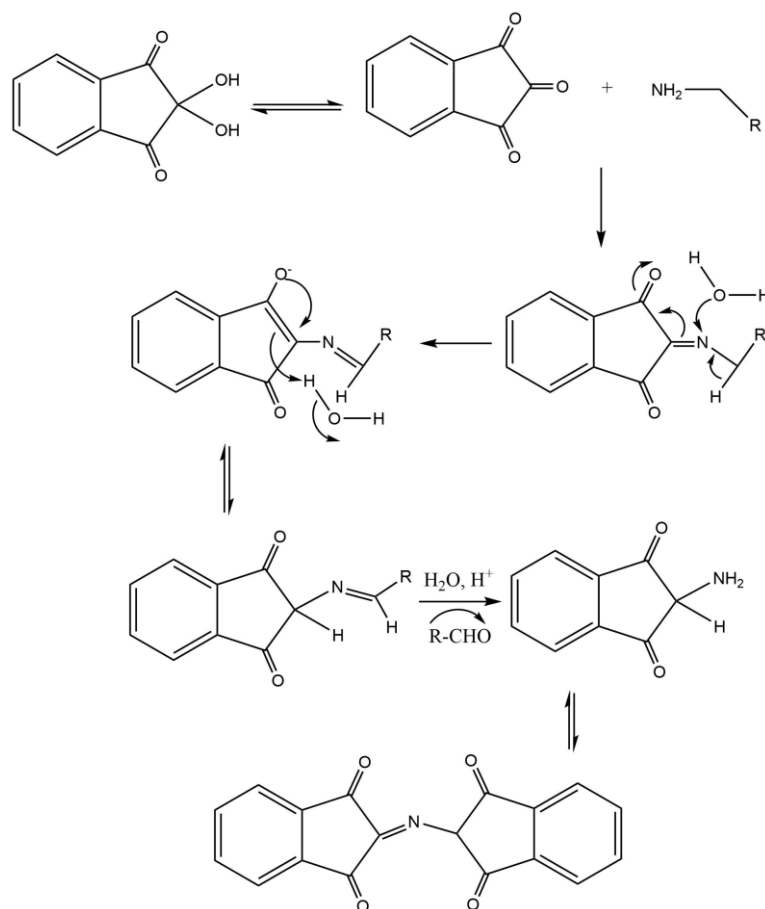
Figure 6-4. Chromophore Ruhemann's purple formation

Ninhydrin reagent was prepared dissolving 0.2 g of ninhydrin in 50 mL of distilled water. A few drops of this solution were poured onto the treated supports, plane and fiber.

The effectiveness of the decoration with aminosilane is highlighted by the deep purple colour; the subsequent functionalization with BMI is demonstrated by the absence of colouring.

*Scanning electron microscopy (*SEM)

For an effective implementation of the healing capacity at the interface between polymeric matrix and reinforcement, it is necessary that both the functionalization with aminosilane and the decoration with BMI have been successful on the whole surface. Morphological analysis was performed by scanning electron microscopy (SEM XL30, FEI Company, The Netherlands) on

samples obtained by mounting portions of the substrates on stubs and coating with a thin carbon film deposited by sputtering. SEM pictures of the reinforcement surface, taken after each treatment (Figure 6-5), highlight the effectiveness of surface treatments. SEM analysis showed a flat surface for plain glass, and a uniform texture for the surfaces after treatment: jagged after functionalization with aminosilane and smoother after subsequent BMI grafting.
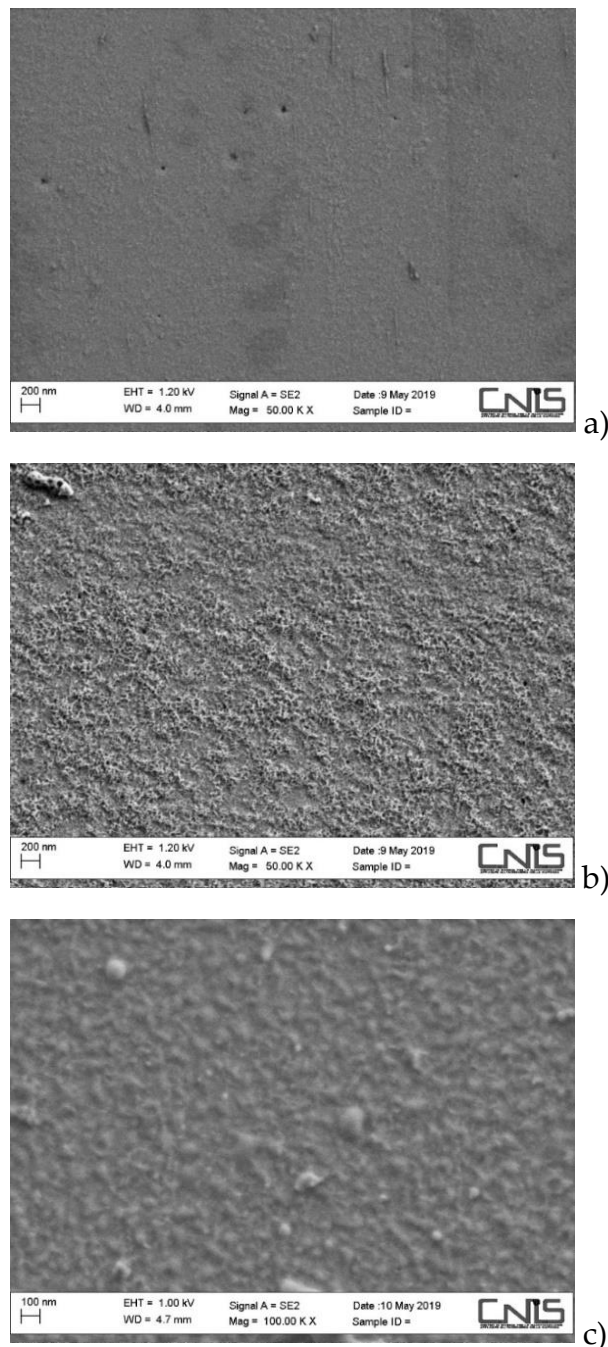
Figure 6-5. SEM pictures: a) glass; b) aminosilane functionalized glass; c) BMI decorated glass

6.2.   Characterization of interfacial debonding and fiber pull out

The glass fibers were extracted from commercial dry preform for composite manufacturing, supplied by GURIT and prepared following the same protocol described for flat glass substrates. Resin droplets with an average diameter of $100 \div 150$ μm were dispensed on individual glass fibers and cured at 90°C for 24 hours before testing.

Micro droplets single fiber pull-out tests were carried out using a TA Instruments thermo-mechanical analyser TMA 2940 at room temperature, applying a linear force increase of 0.1 N/min.

The micro-droplet pull-out test consists in dabbing a small amount of liquid resin onto the fiber surface. After the resin droplets are cured, they form concentric elliptical micro droplets around the fiber. The fiber specimen is suspended at one end from a load cell of a mechanical testing machine and the micro-droplet is gripped by micro-vice jaw [117,118]. The shearing force at the interface is transferred to the fiber through the fiber-matrix interfacial bond and is recorded by the load cell. The interfacial shear strength between glass fiber and epoxy matrix can be calculated according to the following equation 6-4, which is based on the assumption of a constant IFSS between the fiber and its surrounding matrix.

$$\tau_i = \frac{F}{(\pi D L)} \qquad \qquad 6\text{-}4$$

where F is the maximum fiber axial force recorded at the onset of microdroplet debonding, D is the fiber diameter, L is the embedded fiber length and πDL is the embedded area. Therefore, we designate the value τi as the effective IFSS.

The experimental set-up requires a small device to hold a single glass fiber (12 μm in diameter) and the application of a controlled and small axial force. After a preliminary trial and error test, the appropriate size range of the micro-

drops was selected in order to avoid fiber breakage due to excessive load transfer. Figure 6-6 illustrates the experimental setup based on the TA Instruments TMA 2940, along a schematic diagram of the sample geometry. The embedding length of the micro-drop is limited to the range between 100 and 150 microns. Samples with a good interface require a smaller droplet in order to avoid fiber breakage due to excessive loading.
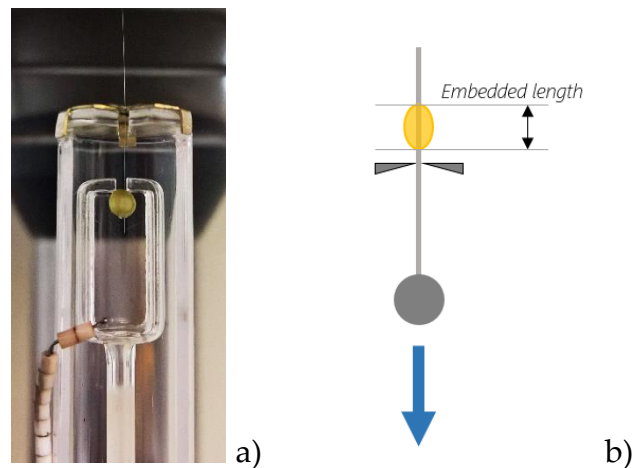
Figure 6-6 Single fiber pull-out test: a) actual fixture; b) load schematic

The set-up was validated by analyzing the interface behavior for the commercial epoxy/commercial fiberglass pair. The interfacial strength estimated with the modified equipment was in conformity with the data available in literature for such systems [119].

Although this test is very easy to perform, there are still several concerns that users should be aware of. These include stress concentration during sample loading, uneven shear stress distribution along the fiber-matrix interface, resin droplet geometry, strain rate and the effect of loading points on shearing plate in contact with the resin droplet. All this would significantly affect the test results and the dispersion in the test data.

Table 6-2 shows the droplet pull-out test carried out. According to the preliminary configuration of the apparatus, the average size of the droplet wetting area on the fiber surface was set to about 120 microns. Tests were carried

out on commercial DGEBA droplets and self-healing epoxy, namely 2Ph2Epo65 dropped on pristine fiber and fiber treated by the BMI coupling agent.

Table 6-2. Micro droplet pull-out test results on pristine and BMI decorated fibers

Description	Droplet length (μm)	IFSS (MPa)	Δ
DGEBA – GF	125	57.8 ± 7.54	-
DGEBA – GF(BMI)	118	75.6 ± 6.25	+31 %
2Ph2Epo65 – GF	127	38.6 ± 7.51	-
2Ph2Epo65 – GF(BMI)	125	74.4 ± 7.05	+92 %

The developed coupling agent led to strengthening the interface: +31% for DGEBA and +92% for 2Ph2Epo65, if compared with bare glass fiber.

Further tests were carried out on pristine fiber and fiber treated by the BMI coupling agent, also following recovery treatments, in order to verify the healing ability at the interface. As reported in Table 6-3, an effective self-healing was detected, with a retain of 37% in IFSS after one test/SH cycle and 15% after two cycles.

Table 6-3. Micro droplet pull-out test results on pristine and Self-healed specimens

Description	Droplet length (μm)	IFSS (MPa)	IFSS (%)
2Ph2Epo65 – GF(BMI)	125	74.36 ± 14.12	-
2Ph2Epo65 – GF(BMI)-SH1	105	27.53 ± 11.33	37
2Ph2Epo65 – GF(BMI)-SH2	101	11.5 ± 3.50	15

The debonding occurred during test at the interface between fiber and matrix was investigated by optical microscopy, carried out before and after the mechanical test, by means of optical microscope Olympus BX 51. The images were captured using a 20X magnification in bright field and polarized light. Figure 6-7 shows a sample before (a, a') and after (b, b') the test.
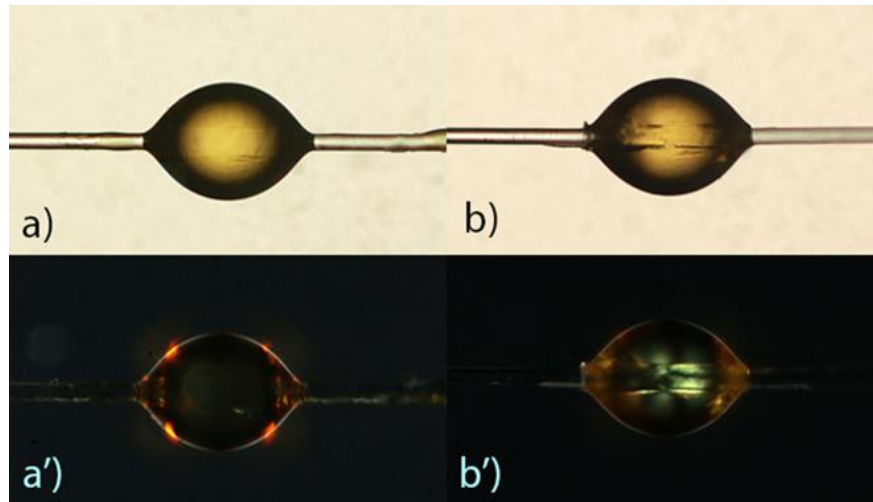
Figure 6-7. Resin drops onto fiber (20X magnification), in bright and polarized light, respectively, before (a, a') and after the mechanical test (b, b')

The droplet has the shape of an ellipsoid with a slightly pronounced meniscus at the interface with fiber. After the test, the droplet has lost its far ends and the leftwise slipping direction can be recognized by the resin stack on the fiber right side. Polarized light microscopy shows a slight presence of residual stresses related to the polymerization stages (Figure 6-7a'), while the image taken after the test shows the complete release of shear stresses and the loss of chemical bonding is clearly detectable from a small penny-shaped crack [120] (Figure 6-7b') that propagates along the entire interface.

In Figure 6-8 are reported SEM analysis of two different droplets, before and after healing treatment. The specimens were examined with a Cambridge type SEM microscope S630: they were prepared for observation by placing on an aluminum stub, on a double-sided graphite disc, and observed after a process of graphitization.
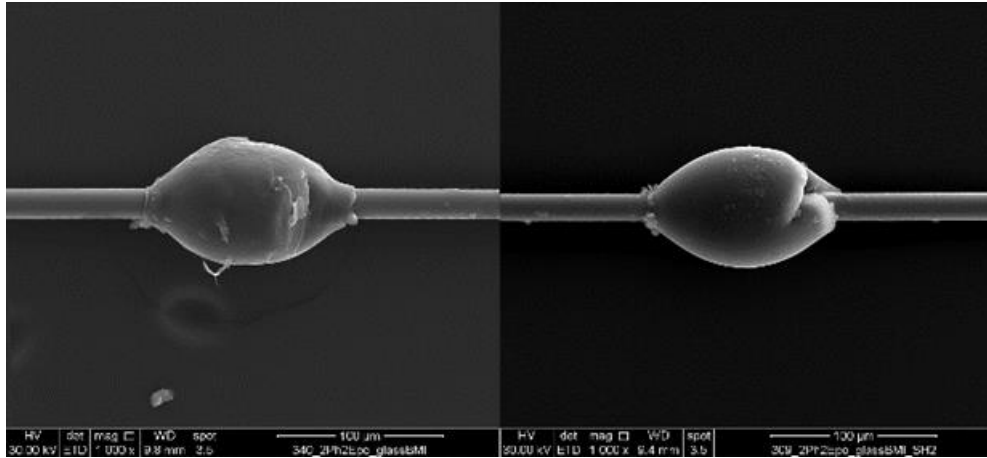
Figure 6-8. SEM analysis of two different droplets: before and after healing treatment

The overall ellipsoidal shape is retained after healing. The cropped extremity partially recovers original shape (right image) due to limited viscous flow.

7. Conclusion and future work

Self-healing polymers are a class of smart materials able to recover after sustaining damage.

A family of thermosetting epoxy resins, containing Diels-Alder adducts in the epoxy precursor backbone, has been prepared and characterized. The DA adducts can be reversibly cleaved and reformed under the appropriate thermal conditions, and this feature has been exploited to produce intrinsically self-repairing materials.

The possibility to tailor the properties of "dynamic" epoxy resins containing Diels-Alder bonds would allow the development of novel materials, such as reengineered FRP combining the ease of processability typical of thermosets with reworking/recycling capability at the end of life typical of thermoplastics, as an effort to improve environmental sustainability of advanced materials.

7.1. Remarks

In the first part, this thesis focuses on the effects of different structural features, such as average number of crosslinking functionality and molecular mobility of epoxy precursors, on the efficiency of healing process. High cross-linking density and molecular stiffness improve mechanical performances, such as elastic modulus and glass transition temperature, and allow fabrication of self-healing fiber-reinforced composites, presented in the second part, by conventional manufacturing technologies.

Thus, the molecular design, the preparation, and the evaluation of properties of self-healing epoxy and its composites have been discussed.

The most remarkable aspect of this system is its inherent ability to undergo self-healing process. Indeed, after a complete cycle of fracture and healing, the same stiffness (2.75 GPa) is recorded.

Also, the requirements of easy and efficient self-healing were compromised with development of material properties compliant with structural and semi-structural applications. In particular, the possibility to tailor the properties of dynamic epoxy resins containing Diels-Alder bonds has allowed the development of novel smart materials, such as active coatings and FRP materials with self-healing ability.

The capability of a self-healing epoxy system, namely 2Ph2Epo65, to acts as a corrosion-protection coating have been evaluated. The barrier features of the coating have been verified after recovery of severe damages and the further exposure to corrosive environment. A complete self-healing cycle, including a first heating at 120°C to achieve a uniform morphological healing, followed by annealing at 90°C for full restoration of mechanical properties, resulted in re-establishment of coating protective efficiency against saline solution corrosion. Spectroscopic, mechanical and Electrochemical Impedance Spectroscopic

investigations confirmed the self-healing via recombination of Diels-Alder adducts and the following crosslinking restoration.

Regarding the use of resin as a composite matrix, the ability to recover damages after a cohesive failure has been investigated by interlaminar shear strength (ILSS): mode II fracture loading has been studied by performing the End Notch Failure (ENF), while the interlaminar critical strength by Short Beam Shear (SBS) tests. The efficiency, measured as interlaminar critical strength and as critical energy for mode II delaminations, is in both cases about 90%.

Finally, a smart interface was implemented, in order to obtain a composite material able to recover delaminations and debonding, by exploiting Diels-Alder bonds present in the resin bulk and at fiber interface.

The procedure to measure the fiber-matrix interface strength and self-healing efficiency, based on a thermo-mechanical analysis (micro-droplet pull-out test), revealed the increase in IFSS for the pristine system (+92%) and an effective self-healing, retaining 37% in IFSS after one test/SH cycle and 15% after two cycles.

7.2. Perspectives

The synthesized materials show self-regeneration functionality and robust reprocessing capacity guided by molecular interconnections based on dynamic bonds.

This would allow the development of reengineered FRP, also carbon fiber composites, combining the ease of processability typical of thermosetting materials with the reworking / recycling capacity typical of thermoplastics.

By modulating the composition of the hybrid system, an effective separation of the matrix and the reinforcement phase would be possible, and the fillers and monomers could be reused, thus leading to good environmental sustainability.

Furthermore, by transferring the same concept to other systems, such as nano-composite materials, a similar molecular interconnection would allow sustainable nanocomposite technology to find applications, such as systems of damage-resistant materials, in the fields of flexible electronics, micro -devices and intelligent structures.

Literature

[1] C.B. Bucknall, I.C. Drinkwater, G.R. Smith, Hot plate welding of plastics: Factors affecting weld strength, Polym. Eng. Sci. 20 (1980) 432–440. https://doi.org/10.1002/pen.760200609.

[2] D. Liu, C.Y. Lee, X. Lu, Repairability of Impact-Induced Damage in SMC Composites, J. Compos. Mater. 27 (1993) 1257–1271. https://doi.org/10.1177/002199839302701302.

[3] M. Meo, F. Achard, M. Grassi, Finite element modelling of bridging micro-mechanics in through-thickness reinforced composite laminates, Compos. Struct. 71 (2005) 383–387. https://doi.org/10.1016/J.COMPSTRUCT.2005.09.025.

[4] S.R. White, N.R. Sottos, P.H. Geubelle, J.S. Moore, M.R. Kessler, S.R. Sriram, E.N. Brown, S. Viswanathan, Autonomic healing of polymer composites., Nature. 409 (2001) 794–7. https://doi.org/10.1038/35057232.

[5] S.J. Garcia, Effect of polymer architecture on the intrinsic self-healing character of polymers, Eur. Polym. J. 53 (2014) 118–125. https://doi.org/10.1016/J.EURPOLYMJ.2014.01.026.

[6] D.G. Bekas, K. Tsirka, D. Baltzis, A.S. Paipetis, Self-healing materials: A review of advances in materials, evaluation, characterization and monitoring techniques, Compos. Part B Eng. 87 (2016) 92–119. https://doi.org/10.1016/J.COMPOSITESB.2015.09.057.

[7] M.J. Kryger, M.T. Ong, S.A. Odom, N.R. Sottos, S.R. White, T.J. Martinez, J.S.

Moore, Masked Cyanoacrylates Unveiled by Mechanical Force, J. Am. Chem. Soc. 132 (2010) 4558–4559. https://doi.org/10.1021/ja1008932.

[8]   *,† Chan-Moon Chung, † Young-Suk Roh, † and Sung-Youl Cho, J.-G. Kim‡, Crack Healing in Polymeric Materials via Photochemical [2+2] Cycloaddition, (2004). https://doi.org/10.1021/CM049394+.

[9]   D.A. Davis, A. Hamilton, J. Yang, L.D. Cremar, D. Van Gough, S.L. Potisek, M.T. Ong, P. V. Braun, T.J. Martínez, S.R. White, J.S. Moore, N.R. Sottos, Force-induced activation of covalent bonds in mechanoresponsive polymeric materials, Nature. 459 (2009) 68–72. https://doi.org/10.1038/nature07970.

[10]   S. Karthikeyan, R.P. Sijbesma, Forcing a molecule's hand, Nat. Chem. 2 (2010) 436–437. https://doi.org/10.1038/nchem.677.

[11]   J.D. Rule, E.N. Brown, N.R. Sottos, S.R. White, J.S. Moore, Wax-Protected Catalyst Microspheres for Efficient Self-Healing Materials, Adv. Mater. 17 (2005) 205–208. https://doi.org/10.1002/adma.200400607.

[12]   U.S. Chung, J.H. Min, P.-C. Lee, W.-G. Koh, Polyurethane matrix incorporating PDMS-based self-healing microcapsules with enhanced mechanical and thermal stability, Colloids Surfaces A Physicochem. Eng. Asp. 518 (2017) 173–180. https://doi.org/10.1016/J.COLSURFA.2017.01.044.

[13]   N.W. Khun, D.W. Sun, M.X. Huang, J.L. Yang, C.Y. Yue, Wear resistant epoxy composites with diisocyanate-based self-healing functionality, Wear. 313 (2014) 19–28. https://doi.org/10.1016/J.WEAR.2014.02.011.

[14]   Q. Li, A.K. Mishra, N.H. Kim, T. Kuila, K. Lau, J.H. Lee, Effects of processing conditions of poly(methylmethacrylate) encapsulated liquid curing agent on the properties of self-healing composites, Compos. Part B Eng. 49 (2013) 6–15. https://doi.org/10.1016/J.COMPOSITESB.2013.01.011.

[15]   S.H. Cho, H.M. Andersson, S.R. White, N.R. Sottos, P.V. Braun, Polydimethylsiloxane-Based Self-Healing Materials, Adv. Mater. 18 (2006) 997–1000. https://doi.org/10.1002/adma.200501814.

[16]   N.I. Khan, S. Halder, M.S. Goyat, Influence of dual-component microcapsules on self-healing efficiency and performance of metal-epoxy composite-lap joints, J. Adhes. 93 (2017) 949–963. https://doi.org/10.1080/00218464.2016.1193806.

[17]   S. Bleay, C. Loader, … V.H.-C.P.A., undefined 2001, A smart repair system for polymer matrix composites, Elsevier. (n.d.). https://www.sciencedirect.com/science/article/pii/S1359835X01000203 (accessed December 11, 2019).

[18]   B.A.R. Hamilton, N.R. Sottos, S.R. White, Self-Healing of Internal Damage in Synthetic Vascular Materials, 61801 (2010) 5159–5163. https://doi.org/10.1002/adma.201002561.

[19]   K.S. Toohey, N.R. Sottos, J.A. Lewis, J.S. Moore, S.R. White, Self-healing materials with microvascular networks, Nat. Mater. 6 (2007) 581–585. https://doi.org/10.1038/nmat1934.

[20]   H.R. Williams, R.S. Trask, I.P. Bond, Self-healing composite sandwich structures, Smart Mater. Struct. 16 (2007) 1198–1207. https://doi.org/10.1088/0964-1726/16/4/031.

[21]   J.W.C. Pang, I.P. Bond, 'Bleeding composites'—damage detection and self-repair using a biomimetic approach, Compos. Part A Appl. Sci. Manuf. 36 (2005) 183–188. https://doi.org/10.1016/j.compositesa.2004.06.016.

[22]   Y.C. Yuan, T. Yin, M.Z. Rong, M.Q. Zhang, Self healing in polymers and polymer composites. Concepts, realization and outlook: A review, EXPRESS Polym. Lett. 2 (2008) 238–250. https://doi.org/10.3144/expresspolymlett.2008.29.

[23]   P. Cordier, F. Tournilhac, C. Soulié-Ziakovic, L. Leibler, Self-healing and thermoreversible rubber from supramolecular assembly, Nature. 451 (2008) 977–980. https://doi.org/10.1038/nature06669.

[24]   K. Haraguchi, K. Uyama, H. Tanimoto, Self-healing in Nanocomposite Hydrogels, Macromol. Rapid Commun. 32 (2011) 1253–1258. https://doi.org/10.1002/marc.201100248.

[25]   A.B. South, L.A. Lyon, Autonomic Self-Healing of Hydrogel Thin Films, Angew. Chemie Int. Ed. 49 (2010) 767–771. https://doi.org/10.1002/anie.200906040.

[26]   M. Burnworth, L. Tang, J.R. Kumpfer, A.J. Duncan, F.L. Beyer, G.L. Fiore, S.J. Rowan, C. Weder, Optically healable supramolecular polymers, Nature. 472 (2011) 334–337. https://doi.org/10.1038/nature09963.

[27]   J.D. Fox, S.J. Rowan, Supramolecular Polymerizations and Main-Chain

Supramolecular Polymers, Macromolecules. 42 (2009) 6823–6835. https://doi.org/10.1021/ma901144t.

[28] Y.H. Kim, R.P. Wool, A theory of healing at a polymer-polymer interface, Macromolecules. 16 (1983) 1115–1120. https://doi.org/10.1021/ma00241a013.

[29] G.O. Wilson, M.M. Caruso, S.R. Schelkopf, N.R. Sottos, S.R. White, J.S. Moore, Adhesion Promotion via Noncovalent Interactions in Self-Healing Polymers, ACS Appl. Mater. Interfaces. 3 (2011) 3072–3077. https://doi.org/10.1021/am200584z.

[30] J. Fox, J.J. Wie, B.W. Greenland, S. Burattini, W. Hayes, H.M. Colquhoun, M.E. Mackay, S.J. Rowan, High-Strength, Healable, Supramolecular Polymer Nanocomposites, J. Am. Chem. Soc. 134 (2012) 5362–5368. https://doi.org/10.1021/ja300050x.

[31] M. V. Biyani, E.J. Foster, C. Weder, Light-Healable Supramolecular Nanocomposites Based on Modified Cellulose Nanocrystals, ACS Macro Lett. 2 (2013) 236–240. https://doi.org/10.1021/mz400059w.

[32] S. Burattini, B.W. Greenland, D.H. Merino, W. Weng, J. Seppala, H.M. Colquhoun, W. Hayes, M.E. Mackay, I.W. Hamley, S.J. Rowan, A Healable Supramolecular Polymer Blend Based on Aromatic π−π Stacking and Hydrogen-Bonding Interactions, J. Am. Chem. Soc. 132 (2010) 12051–12058. https://doi.org/10.1021/ja104446r.

[33] J.M. Vega, A.M. Grande, S. van der Zwaag, S.J. Garcia, On the role of free carboxylic groups and cluster conformation on the surface scratch healing behaviour of ionomers, Eur. Polym. J. 57 (2014) 121–126. https://doi.org/10.1016/j.eurpolymj.2014.05.005.

[34] R.K. Bose, N. Hohlbein, S.J. Garcia, A.M. Schmidt, S. van der Zwaag, Connecting supramolecular bond lifetime and network mobility for scratch healing in poly(butyl acrylate) ionomers containing sodium, zinc and cobalt., Phys. Chem. Chem. Phys. 17 (2015) 1697–704. https://doi.org/10.1039/c4cp04015e.

[35] J.-M. Lehn, Dynamers: From Supramolecular Polymers to Adaptive Dynamic Polymers, in: Springer, Cham, 2013: pp. 155–172. https://doi.org/10.1007/12_2013_267.

[36] Y. Amamoto, H. Otsuka, A. Takahara, K. Matyjaszewski, Self-Healing of

Covalently Cross-Linked Polymers by Reshuffling Thiuram Disulfide Moieties in Air under Visible Light, Adv. Mater. 24 (2012) 3975–3980. https://doi.org/10.1002/adma.201201928.

[37] S.Y. An, S.M. Noh, J.H. Nam, J.K. Oh, Dual Sulfide-Disulfide Crosslinked Networks with Rapid and Room Temperature Self-Healability, Macromol. Rapid Commun. 36 (2015) 1255–1260. https://doi.org/10.1002/marc.201500123.

[38] Z. Fang, N. Zheng, Q. Zhao, T. Xie, Healable, Reconfigurable, Reprocessable Thermoset Shape Memory Polymer with Highly Tunable Topological Rearrangement Kinetics, ACS Appl. Mater. Interfaces. 9 (2017) 22077–22082. https://doi.org/10.1021/acsami.7b05713.

[39] S. Telitel, Y. Amamoto, J. Poly, F. Morlet-Savary, O. Soppera, J. Lalevée, K. Matyjaszewski, Introduction of self-healing properties into covalent polymer networks via the photodissociation of alkoxyamine junctions, Polym. Chem. 5 (2014) 921–930. https://doi.org/10.1039/C3PY01162C.

[40] D. Montarnal, M. Capelot, F. Tournilhac, L. Leibler, Silica-like malleable materials from permanent organic networks., Science. 334 (2011) 965–8. https://doi.org/10.1126/science.1212648.

[41] B. Rickborn, The Retro-Diels-Alder Reaction Part I. C-C Dienophiles, in: Org. React., John Wiley & Sons, Inc., Hoboken, NJ, USA, 1998: pp. 1–393. https://doi.org/10.1002/0471264180.or052.01.

[42] B. Rickborn, The Retro-Diels-Alder Reaction Part II. Dienophiles with One or More Heteroatom, in: Org. React., John Wiley & Sons, Inc., Hoboken, NJ, USA, 1998: pp. 223–629. https://doi.org/10.1002/0471264180.or053.02.

[43] Y.-L. Liu, T.-W. Chuo, Self-healing polymers based on thermally reversible Diels–Alder chemistry, Polym. Chem. 4 (2013) 2194. https://doi.org/10.1039/c2py20957h.

[44] M. Grigoras, G. Colotin, Copolymerization of a bisanthracene compound with bismaleimides by Diels-Alder cycloaddition, Polym. Int. 50 (2001) 1375–1378. https://doi.org/10.1002/pi.792.

[45] † Jeffrey R. Jones, † Charles L. Liotta, *,† and David M. Collard, D.A. Schiraldi‡, Cross-Linking and Modification of Poly(ethylene terephthalate-co-2,6-anthracenedicarboxylate) by Diels−Alder Reactions with Maleimides, (1999).

https://doi.org/10.1021/MA990638Z.

[46]   Y.-L. Liu, T.-W. Chuo, Self-healing polymers based on thermally reversible Diels–Alder chemistry, Polym. Chem. 4 (2013) 2194. https://doi.org/10.1039/c2py20957h.

[47]   X. Chen, M. a Dam, K. Ono, A. Mal, H. Shen, S.R. Nutt, K. Sheran, F. Wudl, A thermally re-mendable cross-linked polymeric material., Science. 295 (2002) 1698–1702. https://doi.org/10.1126/science.1065879.

[48]   X. Chen, F. Wudl, A.K. Mal, H. Shen, S.R. Nutt, New Thermally Remendable Highly Cross-Linked Polymeric Materials, Macromolecules. 36 (2003) 1802–1807. https://doi.org/10.1021/ma0210675.

[49]   T. Plaisted, S.N.-N.-A. Materialia, undefined 2007, Quantitative evaluation of fracture, healing and re-healing of a reversibly cross-linked polymer, Elsevier. (n.d.). https://www.sciencedirect.com/science/article/pii/S1359645407003862 (accessed December 15, 2019).

[50]   Rana Gheneim, and Catalina Perez-Berumen, A. Gandini*, Diels–Alder Reactions with Novel Polymeric Dienes and Dienophiles: Synthesis of Reversibly Cross-Linked Elastomers, (2002). https://doi.org/10.1021/MA020343C.

[51]   A. Amalin Kavitha, N.K. Singha, A tailor-made polymethacrylate bearing a reactive diene in reversible diels-alder reaction, J. Polym. Sci. Part A Polym. Chem. 45 (2007) 4441–4449. https://doi.org/10.1002/pola.22195.

[52]   Y. Zhang, A.A. Broekhuis, F. Picchioni, Thermally Self-Healing Polymeric Materials : The Next Step to Recycling Thermoset Polymers ?, Macromolecules. 42 (2009) 1906–1912.

[53]   Q. Tian, Y.C. Yuan, M.Z. Rong, M.Q. Zhang, A thermally remendable epoxy resin, J. Mater. Chem. 19 (2009) 1289. https://doi.org/10.1039/b811938d.

[54]   E.B. Murphy, E. Bolanos, C. Schaffner-Hamann, F. Wudl, S.R. Nutt, M.L. Auad, Synthesis and characterization of a single-component thermally remendable polymer network: Staudinger and stille revisited, Macromolecules. (2008). https://doi.org/10.1021/ma800432g.

[55]   A.M. Peterson, R.E. Jensen, G.R. Palmese, Reversibly cross-linked polymer gels as healing agents for epoxy-amine thermosets, ACS Appl. Mater. Interfaces. 1 (2009) 992–995. https://doi.org/10.1021/am900104w.

[56]   A.M. Peterson, R.E. Jensen, G.R. Palmese, Room-Temperature Healing of a Thermosetting Polymer Using the Diels–Alder Reaction, ACS Appl. Mater. Interfaces. 2 (2010) 1141–1149. https://doi.org/10.1021/am9009378.

[57]   P.A. Pratama, A.M. Peterson, G.R. Palmese, The role of maleimide structure in the healing of furan-functionalized epoxy-amine thermosets, Polym. Chem. (2013). https://doi.org/10.1039/c3py00084b.

[58]   J.S. Park, H.S. Kim, H. Thomas Hahn, Healing behavior of a matrix crack on a carbon fiber/mendomer composite, Compos. Sci. Technol. 69 (2009) 1082–1087. https://doi.org/10.1016/j.compscitech.2009.01.031.

[59]   F. Ghezzo, D.R. Smith, T.N. Starr, T. Perram, A.F. Starr, T.K. Darlington, R.K. Baldwin, S.J. Oldenburg, Development and characterization of healable carbon fiber composites with a reversibly cross linked polymer, J. Compos. Mater. (2010). https://doi.org/10.1177/0021998310363165.

[60]   Y. Zhang, A.A. Broekhuis, F. Picchioni, Thermally Self-Healing Polymeric Materials: The Next Step to Recycling Thermoset Polymers?, Macromolecules. 42 (2009) 1906–1912. https://doi.org/10.1021/ma8027672.

[61]   C. Toncelli, D.C. De Reus, F. Picchioni, A.A. Broekhuis, Properties of Reversible Diels-Alder Furan/Maleimide Polymer Networks as Function of Crosslink Density, Macromol. Chem. Phys. 213 (2012) 157–165. https://doi.org/10.1002/macp.201100405.

[62]   A. Gandini, M.N. Belgacem, Furans in polymer chemistry, Prog. Polym. Sci. (1997). https://doi.org/10.1016/S0079-6700(97)00004-X.

[63]   M. Choura, N.M. Belgacem, A. Gandini, Acid-catalyzed polycondensation of furfuryl alcohol: Mechanisms of chromophore formation and cross-linking, Macromolecules. (1996). https://doi.org/10.1021/ma951522f.

[64]   D.H. Turkenburg, H.R. Fischer, Diels-Alder based, thermo-reversible cross-linked epoxies for use in self-healing composites, Polymer (Guildf). 79 (2015) 187–194. https://doi.org/10.1016/J.POLYMER.2015.10.031.

[65]   A.M. Peterson, R.E. Jensen, G.R. Palmese, Thermoreversible and remendable glass–polymer interface for fiber-reinforced composites, Compos. Sci. Technol. 71 (2011) 586–592. https://doi.org/10.1016/j.compscitech.2010.11.022.

[66] A.M. Peterson, R.E. Jensen, G.R. Palmese, Kinetic considerations for strength recovery at the fiber-matrix interface based on the Diels-Alder reaction, ACS Appl. Mater. Interfaces. 5 (2013) 815–821. https://doi.org/10.1021/am302383v.

[67] W. Zhang, J. Duchet, J.F. Gérard, Self-healable interfaces based on thermo-reversible Diels-Alder reactions in carbon fiber reinforced composites, J. Colloid Interface Sci. 430 (2014) 61–68. https://doi.org/10.1016/j.jcis.2014.05.007.

[68] W. Zhang, J. Duchet, J.F. Gérard, RSC Advances healing ability of thermo-reversible interfaces a carbon fi ber / epoxy microcomposite, (2016) 114235–114243. https://doi.org/10.1039/C6RA23246A.

[69] O. Diels, K. Alder, Synthesen in der hydroaromatischen Reihe, Justus Liebig's Ann. Der Chemie. 460 (1928) 98–122. https://doi.org/10.1002/jlac.19284600106.

[70] M.A. Tasdelen, Diels–Alder "click" reactions: recent applications in polymer and material science, Polym. Chem. 2 (2011) 2133. https://doi.org/10.1039/c1py00041a.

[71] A. Sanyal, Diels-Alder Cycloaddition-Cycloreversion: A Powerful Combo in Materials Design, Macromol. Chem. Phys. 211 (2010) 1417–1425. https://doi.org/10.1002/macp.201000108.

[72] D.L. Reger, S.R. Goode, D.W. Ball, Chemistry: Principles and Practice., Brooks/Cole Pub Co, 2009.

[73] Y.-L. Liu, C.-Y. Hsieh, Crosslinked epoxy materials exhibiting thermal remendablility and removability from multifunctional maleimide and furan compounds, J. Polym. Sci. Part A Polym. Chem. 44 (2006) 905–913. https://doi.org/10.1002/pola.21184.

[74] X. Kuang, G. Liu, X. Dong, X. Liu, J. Xu, D. Wang, Facile fabrication of fast recyclable and multiple self-healing epoxy materials through diels-alder adduct cross-linker, J. Polym. Sci. Part A Polym. Chem. 53 (2015) 2094–2103. https://doi.org/10.1002/pola.27655.

[75] S. Dello Iacono, A. Martone, A. Pastore, G. Filippone, D. Acierno, M. Zarrelli, M. Giordano, Thermally Activated Multiple Self-Healing Diels-Alder Epoxy System, (2017) 1–6. https://doi.org/10.1002/pen.

[76] C.G. de Almeida, S.G. Reis, A.M. de Almeida, C.G. Diniz, V.L. da Silva, M. Le Hyaric, Synthesis and antibacterial activity of aromatic and heteroaromatic amino

alcohols., Chem. Biol. Drug Des. 78 (2011) 876–80. https://doi.org/10.1111/j.1747-0285.2011.01231.x.

[77] W.C. Oliver, G.M. Pharr, An improved technique for determining hardness and elastic modulus using load and displacement sensing indentation experiments, J. Mater. Res. 7 (2011) 1564–1583. https://doi.org/10.1557/JMR.1992.1564.

[78] G. Scheltjens, M.M. Diaz, J. Brancart, G. Van Assche, B. Van Mele, A self-healing polymer network based on reversible covalent bonding, React. Funct. Polym. 73 (2013) 413–420. https://doi.org/10.1016/J.REACTFUNCTPOLYM.2012.06.017.

[79] V. Froidevaux, M. Borne, E. Laborbe, R. Auvergne, A. Gandini, B. Boutevin, Study of the diels-alder and retro-diels-alder reaction between furan derivatives and maleimide for the creation of new materials, RSC Adv. 5 (2015) 37742–37754. https://doi.org/10.1039/c5ra01185j.

[80] A.A. Kavitha, N.K. Singha, "Click Chemistry" in Tailor-Made Polymethacrylates Bearing Reactive Furfuryl Functionality: A New Class of Self-Healing Polymeric Material, ACS Appl. Mater. Interfaces. 1 (2009) 1427–1436. https://doi.org/10.1021/am900124c.

[81] A. Gandini, A.J.D. Silvestre, D. Coelho, Reversible click chemistry at the service of macromolecular materials. 2. Thermoreversible polymers based on the Diels-Alder reaction of an A-B furan/maleimide monomer, J. Polym. Sci. Part A Polym. Chem. 48 (2010) 2053–2056. https://doi.org/10.1002/pola.23957.

[82] P. Cassagnau, J.P. Montfort, G. Marin, P. Monge, Rheology of polydisperse polymers: relationship between intermolecular interactions and molecular weight distribution, Rheol. Acta. 32 (1993) 156–167. https://doi.org/10.1007/BF00366679.

[83] Y. Heo, H.A. Sodano, Self-Healing Polyurethanes with Shape Recovery, Adv. Funct. Mater. 24 (2014) 5261–5268. https://doi.org/10.1002/adfm.201400299.

[84] R. Geitner, J. Kötteritzsch, M. Siegmann, R. Fritzsch, T.W. Bocklitz, M.D. Hager, U.S. Schubert, S. Gräfe, B. Dietzek, M. Schmitt, J. Popp, Molecular self-healing mechanisms between C_{60}-fullerene and anthracene unveiled by Raman and two-dimensional correlation spectroscopy, Phys. Chem. Chem. Phys. 18 (2016) 17973–17982. https://doi.org/10.1039/C6CP03464K.

[85] R. Geitner, J. Kötteritzsch, M. Siegmann, T.W. Bocklitz, M.D. Hager, U.S. Schubert,

S. Gräfe, B. Dietzek, M. Schmitt, J. Popp, Two-dimensional Raman correlation spectroscopy reveals molecular structural changes during temperature-induced self-healing in polymers based on the Diels–Alder reaction, Phys. Chem. Chem. Phys. 17 (2015) 22587–22595. https://doi.org/10.1039/C5CP02151K.

[86] L. Strandman-long, Furfuryl alcohol-III . Infrared , matrix infrared and Raman spectra and ab initio and normal coordinate calculations, 31 (1981) 643–653.

[87] S. Zheng, I.A. Ashcroft, A depth sensing indentation study of the hardness and modulus of adhesives, Int. J. Adhes. Adhes. 25 (2005) 67–76. https://doi.org/10.1016/j.ijadhadh.2004.02.004.

[88] E.N. Brown, N.R. Sottos, S.R. White, Fracture testing of a self-healing polymer composite, Exp. Mech. 42 (2002) 372–379. https://doi.org/10.1007/BF02412141.

[89] J. Canadell, H. Goossens, B. Klumperman, Self-Healing Materials Based on Disulfide Links, Macromolecules. 44 (2011) 2536–2541. https://doi.org/10.1021/ma2001492.

[90] H. Zhang, H. Xia, Y. Zhao, Poly(vinyl alcohol) Hydrogel Can Autonomously Self-Heal, ACS Macro Lett. 1 (2012) 1233–1236. https://doi.org/10.1021/mz300451r.

[91] P. Pedeferri, Cathodic protection and cathodic prevention, Constr. Build. Mater. 10 (1996) 391–402. https://doi.org/10.1016/0950-0618(95)00017-8.

[92] D.W. DeBerry, Modification of the Electrochemical and Corrosion Behavior of Stainless Steels with an Electroactive Coating, J. Electrochem. Soc. 132 (1985) 1022. https://doi.org/10.1149/1.2114008.

[93] M.J. Gimeno, S. Chamorro, R. March, E. Oró, P. Pérez, J. Gracenea, J. Suay, Anticorrosive properties enhancement by means of phosphate pigments in an epoxy 2k coating. Assessment by NSS and ACET, Prog. Org. Coatings. 77 (2014) 2024–2030. https://doi.org/10.1016/j.porgcoat.2014.04.004.

[94] S.K. Ghosh, John Wiley & Sons., Functional coatings : by polymer microencapsulation, Wiley-VCH, 2006. https://books.google.it/books?hl=it&lr=&id=wTvOFzwOvEIC&oi=fnd&pg=PR11 &dq=S.K.+Ghosh,+Functional+Coatings,+Wiley-VCH,+Weinheim,+2006.&ots=sK4FOplfdb&sig=ekUOpOL9QMthHerKG1kEHp Zxs4g#v=onepage&q&f=false (accessed February 9, 2018).

[95] Patil S; Sainkar S.R.;Patil P.P., Poly(o-anisidine) coatings on copper: synthesis, characterization and evaluation of corrosion protection performance, Appl. Surf. Sci. 225 (2004) 204–216. https://doi.org/10.1016/J.APSUSC.2003.10.050.

[96] S.H. Cho, S.R. White, P. V. Braun, Self-Healing Polymer Coatings, Adv. Mater. 21 (2009) 645–649. https://doi.org/10.1002/adma.200802008.

[97] R.B. Ningshen S., Mudali U.K., Electrochemical impedance spectroscopy and its applications, Electrochem. Impedance Spectrosc. Its Appl. 27 (2009) 493–531. https://doi.org/10.1007/978-1-4614-8933-7.

[98] M. Del Grosso Destreri, J. Vogelsang, L. Fedrizzi, F. Deflorian, Water up-take evaluation of new waterborne and high solid epoxy coatings. Part II: Electrochemical impedance spectroscopy, Prog. Org. Coatings. 37 (1999) 69–81. https://doi.org/10.1016/S0300-9440(99)00056-9.

[99] D.M. Brasher, A.H. Kingsbury, Electrical measurements in the study of immersed paint coatings on metal. I. Comparison between capacitance and gravimetric methods of estimating water-uptake, J. Appl. Chem. 4 (2007) 62–72. https://doi.org/10.1002/jctb.5010040202.

[100] F. Galliano, D. Landolt, Evaluation of corrosion protection properties of additives for waterborne epoxy coatings on steel, Prog. Org. Coatings. 44 (2002) 217–225. https://doi.org/10.1016/S0300-9440(02)00016-4.

[101] X. Li, H. Gao, W.A. Scrivens, D. Fei, X. Xu, M.A. Sutton, A.P. Reynolds, M.L. Myrick, Nanomechanical characterization of single-walled carbon nanotube nforced epoxy composites, Nanotechnology. 15 (2004) 1416–1423. https://doi.org/10.1088/0957-4484/15/11/005.

[102] G. Li, M. John, A self-healing smart syntactic foam under multiple impacts, Compos. Sci. Technol. 68 (2008) 3337–3343. https://doi.org/10.1016/j.compscitech.2008.09.009.

[103] M. John, G. Li, Self-healing of sandwich structures with a grid stiffened shape memory polymer syntactic foam core, Smart Mater. Struct. 19 (2010). https://doi.org/10.1088/0964-1726/19/7/075013.

[104] J. Karger-kocsis, H. Mahmood, A. Pegoretti, Progress in Materials Science Recent advances in fiber / matrix interphase engineering for polymer composites, 73

(2015) 1–43. https://doi.org/10.1016/j.pmatsci.2015.02.003.

[105] M. Jing, J. Che, S. Xu, Z. Liu, Q. Fu, SC, Appl. Surf. Sci. (2017). https://doi.org/10.1016/j.apsusc.2017.11.134.

[106] S. Park, J. Jin, Effect of Silane Coupling Agent on Interphase and Performance of Glass Fibers / Unsaturated Polyester Composites, 179 (2001) 174–179. https://doi.org/10.1006/jcis.2001.7788.

[107] V.A. Online, Polymer Chemistry Synthesis of a diamine cross-linker containing Diels – Alder adducts to produce self-healing thermosetting epoxy polymer from a widely used epoxy monomer †, (2013) 724–730. https://doi.org/10.1039/c2py20611k.

[108] D. Therriault, E. Haddad, W. Jamroz, Self-Healing Materials Systems : Overview of Major, 2012 (2012). https://doi.org/10.1155/2012/854203.

[109] A. Gandini, Progress in Polymer Science The furan / maleimide Diels – Alder reaction : A versatile click – unclick tool in macromolecular synthesis, Prog. Polym. Sci. 38 (2013) 1–29. https://doi.org/10.1016/j.progpolymsci.2012.04.002.

[110] B. Gacal, H. Durmaz, M.A. Tasdelen, G. Hizal, U. Tunca, Y. Yagci, A.L. Demirel, Anthracene–Maleimide-Based Diels–Alder "Click Chemistry" as a Novel Route to Graft Copolymers, Macromolecules. 39 (2006) 5330–5336. https://doi.org/10.1021/ma060690c.

[111] B. Liu, Z. Liu, X. Wang, G. Zhang, S. Long, J. Yang, Interfacial shear strength of carbon fiber reinforced polyphenylene sulfide measured by the microbond test, Polym. Test. 32 (2013) 724–730. https://doi.org/10.1016/J.POLYMERTESTING.2013.03.020.

[112] C. Tarducci, J.P.S. Badyal, S.A. Brewer, C. Willis, Diels-Alder chemistry at furan ring functionalized solid surfaces, Chem. Commun. (2005) 406–408. https://doi.org/10.1039/b412906g.

[113] T. Engel, G. Kickelbick, Thermoreversible Reactions on Inorganic Nanoparticle Surfaces: Diels – Alder Reactions on Sterically Crowded Surfaces, (2012).

[114] W. Zhang, J. Duchet, J.F. Gérard, Journal of Colloid and Interface Science Self-healable interfaces based on thermo-reversible Diels – Alder reactions in carbon fiber reinforced composites, J. Colloid Interface Sci. 430 (2014) 61–68.

https://doi.org/10.1016/j.jcis.2014.05.007.

[115] A.M. Peterson, R.E. Jensen, G.R. Palmese, Thermoreversible and remendable glass – polymer interface for fiber-reinforced composites, Compos. Sci. Technol. 71 (2011) 586–592. https://doi.org/10.1016/j.compscitech.2010.11.022.

[116] D.K. Owens, R.C. Wendt, Estimation of the surface free energy of polymers, J. Appl. Polym. Sci. (1969). https://doi.org/10.1002/app.1969.070130815.

[117] U. Gaur, B. Miller, Microbond method for determination of the shear strength of a fiber/resin interface: Evaluation of experimental parameters, Compos. Sci. Technol. 34 (1989) 35–51. https://doi.org/10.1016/0266-3538(89)90076-6.

[118] H.F. Wu, C.M. Claypool, An analytical approach of the microbond test method used in characterizing the fibre-matrix interface, J. Mater. Sci. Lett. 10 (1991) 260–262. https://doi.org/10.1007/BF00735651.

[119] A. Godara, L. Gorbatikh, G. Kalinka, A. Warrier, O. Rochez, L. Mezzo, F. Luizi, A.W. van Vuure, S. V. Lomov, I. Verpoest, Interfacial shear strength of a glass fiber/epoxy bonding in composites modified with carbon nanotubes, Compos. Sci. Technol. 70 (2010) 1346–1352. https://doi.org/10.1016/j.compscitech.2010.04.010.

[120] A.N. Netravali, P. Schwartz, S.L. Phoenix, Study of interfaces of high-performance glass fibers and DGEBA-based epoxy resins using single-fiber-composite test, Polym. Compos. 10 (1989) 385–388. https://doi.org/10.1002/pc.750100602.

Publications and Presentations

Scientific Publications

1. S. Dello Iacono, A. Martone, A. Pastore, G. Filippone, D. Acierno, M. Zarrelli, M. Giordano, E. Amendola, "Thermally Activated Multiple Self-Healing Diels-Alder Epoxy System". Polymer Engineering & Science 2017 - DOI: 10.1002/pen.24570.

2. A. Martone, S. Dello Iacono, A. Pastore, and E. Amendola "Fabricating nature-inspired self-healing polymers", Society of Plastics Engineers (SPE), 2017.

3. G. Malfense Fierro, F. Pinto, S. Dello Iacono, A. Martone, E. Amendola, M. Meo. "Monitoring of self-healing composites: a nonlinear ultrasound approach". Smart Materials and Structures. 2017, 26, 1-17 - doi.org/10.1088/1361-665X/aa89a8.

4. S. Dello Iacono, E. Amendola, and A. Martone. "BMI-based coupling agent to improve adhesion in self-healing composites". Macromolecular Symposia, 2020, 389, 1900107 - https://doi.org/10.1002/masy.201900107.

Books

1. S. Dello Iacono, A. Martone, E. Amendola. "Diels-Alder chemistry to develop self-healing epoxy resins and composites thereof". Chapter in IntechOpen book "Paint and Coatings Industry" - ISBN 978-953-51-6154-7; doi: 10.5772/intechopen.81360.

Proceedings

2. S. Dello Iacono, A. Martone, E. Amendola. "Corrosion-resistant self-healing coatings". AIP Conference Proceedings 1990, 020010 (2018); doi: 10.1063/1.5047764.

3. A. Martone, S. Dello Iacono, S. Xiao, F. Xu, E. Amendola. "An integrated strategy to promote self-healing at interface in composites based on Diels-Alder epoxy". AIP Conference Proceedings 1981, 020046 (2018); doi: 10.1063/1.5045908.

4. A. Martone, S. Dello Iacono, A. Zamani, M. Lepore, L. Sanguigno, A. Maligno and E. Amendola. "Modelling of the Micro-bond test for Mechanical Analysis of the Fibre/Matrix Interphase in Fibre Reinforced Plastics". AIP Conference Proceedings 2196, 020041 (2019); https://doi.org/10.1063/1.5140314.

Communications to national and international Conferences

1. A. Pastore, S. Dello Iacono, A. Martone, E. Amendola, "Corrosion-Resistant Self-Healing Coatings", Smart Materials & Surfaces - SMS EUROPE 2017, 16.

2. A. Martone, S. Dello Iacono, G. P. Malfense Fierro, F. Pinto, M. Meo, E. Amendola, "Intrinsic Healing of Delaminations In Diels-Alder Epoxy Carbon Fiber Composites". 25th Annual International Conference on Composites and Nano Engineering 2017.

3. S. Dello Iacono, A. Martone, A. Pastore, V. Marzocchi, A. Squillace, E. Amendola, "Mendable Diels-Alder Epoxies As Corrosion-Protective Coatings". ICCE-25, 25th Annual International Conference on Composites and Nano Engineering 2017; POSTER.

4. A. Martone, S. Dello Iacono, S. Xiao, F. Xu, E. Amendola. "An integrated strategy to promote self-heling at inteface in composites based on Diels-Alder epoxy", 8th International Conference on Times of Polymers (TOP) and Composites 2018.

5. S. Dello Iacono, A. Martone, E. Amendola, "A comprehensive approach to induce self-healing feature in epoxy composites". Nano Innovation 2018.

6. S. Dello Iacono, A. Martone and E. Amendola, "Insights on Diels-Alder coupling agent for the interfacial adhesion recovery in FRP and nanocomposites". Nanoinnovation 2019; POSTER.

7. E. Amendola, A. Martone, S. Dello Iacono, A. Zamani, M. Lepore, L. Sanguigno, A. Maligno "Micro-bond test for Mechanical Analysis of the Fibre/Matrix Interphase in Self-Healing Composites". 9th International Conference on Structural Analysis of Advanced Materials – ICSAAM2019

8. S. Dello Iacono, E. Amendola and A. Martone, "BMI-based coupling agent to improve adhesion in self-healing composites". International Conference on Design and Technologies for Polymeric and Composite Products – Polcom 2019.

9. S. Dello Iacono, A. Martone, F. Mura, M. Rossi and E. Amendola "Adhesion promotion via Diels-Alder covalent bonds in self-healing composites". Polychar27 - World Forum on Advanced Materials 2019

Communication to international Conferences unrelated to the thesis work

1. S. Dello Iacono, R. Carcione, F. Limosani, A. Santoni and F. Antolini, "Study of the CdS QDs formation in film by thermal and laser treatment". SuperFox 2020.